

Software and Modeling Development for Wax Deposition Phenomenon

by
Arya Shahdi

A Dissertation

In

Petroleum Engineering

Submitted to the Graduate Faculty
of Texas Tech University in
Partial Fulfillment of
the Requirements for
the Degree of

Doctor of Philosophy

Approved by

Dr. Ekarit Pancharoensawad
Chair of Committee

Dr. Sheldon Gorell

Dr. Amin Ettehadtavakkol

Dr. James Sheng

Dr. Mark A. Sheridan
Dean of Graduate School

June 2019

This work is licensed under a Creative Commons Attribution-NonCommercial 4.0
International License by Arya Shahdi
<https://bit.ly/19xWvud>

Dedicated to
my loving my parents, Atosa and Bahram

ACKNOWLEDGMENTS

This thesis could have never been completed without the great deal of support and assistance from my adviser. I would like to thank Dr. E. Panacharoensawad, whose invaluable knowledge about this research topic guided me throughout my Ph.D. I am blessed to work with such a great scholar and an amazing person.

I thank my dissertation committee members, Drs. Amin E. Tavakkol, Sheldon Gorell and, James Sheng. I also want to thank research groupmates Dr. Raymond Eghorieta and Ms. Moldir Yermekova for very interesting research collaborations.

I also thank other amazing faculty members of petroleum engineering department at Texas Tech University. I had the honor to take classes and work with them as the teaching assistant during my Ph.D. They made my academic journey at TTU a memorable era.

Finally, I would like to thank my beloved family for supporting me in every step of my life through their endless love and care. I also thank my aunt Azita and uncle-in-law Amir. I spend one year living with their beautiful family and learned a lot from them.

TABLE OF CONTENT

ACKNOWLEDGMENTS.....	ii
ABSTRACT	vi
LIST OF TABLES.....	viii
LIST OF FIGURES.....	x
INTRODUCTION	1
1.1 Background.....	3
2. LITERATURE REVIEW	6
2.1 Thermodynamics of paraffin.....	6
2.2 Wax deposition phenomenon in pipelines	9
THEORETICAL FRAMEWORK.....	17
3.1 SP-Wax thermodynamic model	17
2.1.1 Liquid phase non-ideality.....	18
2.1.2 Solid phase non-ideality.....	19
2.1.3 Thermo-physical properties.....	21
2.1.4 Molar volume.....	22
2.1.5 Van der Waals volume	24
2.2 SP-Depo wax deposition modeling software	24
2.2.1 Definition of wax and MinC concept.....	25
2.2.2 Thermodynamically calculated parameters	27
2.2.3 Wax deposition theory.....	30
2.2.4 Aging term.....	31
2.2.5 Buildup term	32
2.2.6 Laminar Flow Formulation	35
SOFTWARE DEVELOPMENT AND IMPLEMENTATION	38
2.3 SP-Wax software	38
2.3.1 SPWaxInt.exe	41
2.3.2 SPWaxFn (.cpp & header)	42
2.3.3 SPWaxBinary (.exe & .cpp).....	45
2.3.4 SPWaxInitialization (.exe & .cpp)	47
2.3.5 SPWaxPrecipitation (.exe & .cpp)	48
2.3.6 SPWaxOneTemperatureCase (.exe & .cpp)	50
2.3.7 SPWaxCCN (.exe & .cpp)	51

2.4	SP-Depo software	52
2.4.1	Primary programming path.....	54
2.4.2	Main_caller.h and Main_caller.cpp	61
2.4.3	Solid_properties.h and Solid_properties.cpp	63
2.4.4	pipe_geometry.h and pipe_geometry.cpp	63
2.4.5	inlet_condition.h and inlet_condition.cpp	64
2.4.6	coolant_condition.h and coolant_condition.cpp.....	64
2.4.7	fluid_properties.h and fluid_properties.cpp	65
2.4.8	simulation_options.h and simulation_options.cpp	65
2.4.9	SP_Wax_Functions.h and SP_Wax_Functions.cpp	68
2.4.10	SP_Wax_Main.h and SP_Wax_Main.cpp.....	68
2.4.11	deposit_properties.h and deposit_properties.cpp.....	69
2.4.12	temperature_profile.h and temperature_profile.cpp	70
2.4.13	velocity_profile.h and velocity_profile.cpp	76
2.4.14	concentraion_profile.h and concentration_profile.cpp	77
2.4.15	single_phase_deposition.h and single_phase_deposition.cpp	79
2.4.16	fitting_search.h and fitting_search.cpp	80
2.4.17	linear_regression.h and linear_regression.cpp.....	81
2.4.18	user_numerical_method.h and user_numerical_method.cpp.....	83
2.4.19	user_equation_format.h and user_equation_format.cpp	85
	RESULTS AND DISCUSSION.....	88
2.5	SP-Wax thermodynamic model and software.....	88
2.5.1	Validation of empirical correlations.....	89
2.5.2	Experimental dataset	93
2.5.3	Binary System Model Validation.....	97
2.5.4	Multicomponent System Model Validation.....	98
2.5.5	Thermodynamic Verification of CCN and Aging Process	104
2.6	Wax Deposition in Laminar Flow.....	107
2.7	SP-Depo Wax Deposition Model and Software.....	112
2.7.1	Minimum depositable carbon number (MinC)	114
2.7.2	Thickness and solid wax fraction predictions	116
2.7.3	Deposit's solid phase composition	124
2.7.4	Sensitivity analysis	132

CONCLUSIONS.....	153
NOMENCLATURE	155
BIBLIOGRAPHY.....	159

ABSTRACT

Wax deposition is an inevitable phenomenon which mainly occurs in subsea pipelines where surrounding temperature is well below the Wax Appearance Temperature (WAT). Formation of waxy deposit is extremely problematic because it can result in reduction of cross-sectional area of pipe, potential blockage of production stream, elevated pressure-drop, increased risk of production shutdowns, etc. There are two equally important aspects of wax deposition phenomenon. The first one is related to the thermodynamics of paraffin. Through thermodynamic models, it can be understood how carbon number components precipitate upon temperature and pressure change. The second aspect is to address the hydrodynamic, heat-transfer and mass-transfer of the flow during the wax deposition phenomenon. In this study, the both aspects have been investigated through newly developed SP-Wax and SP-Depo modeling software. Within both software, core calculation is coded in C++ and the OpenMp parallel programming technique is incorporated to improve the performance. Also, a C# Windows Forms user interface is created for maximum reusability for technical and non-technical users.

SP-Wax is our first software which has been developed to predict different SLE thermodynamic characteristics of the paraffinic solutions. In SP-Wax, the precipitation curve, Wax Appearance Temperature (WAT), equilibrium constants, relative concentration gradients, liquid-phase composition, solid phase's Average Carbon Number (ACN) and Carbon Number Distribution (CND) are predicted as a function of temperature in the equilibrium condition. SP-Wax predictions are validated by experimental data of five binary and seven multicomponent systems. For the first time, diffusion and counter-diffusion concepts in the aging process are thermodynamically proven using the SP-Wax software. It is also shown that SP-Wax can be used as a quick tool to predict the solid phase composition of the waxy deposits with a reasonable accuracy.

For our second simulation tool, SP-Depo is developed which is equipped with a new thermodynamically-coupled wax deposition model. SP-Depo is coded in an object-oriented format (containing more than 40 classes and 350 methods) and incorporates the SP-Wax thermodynamic model for the solid phase composition prediction. In SP-Depo, Levenberg-Marquardt optimization tool is coded to tune the model using the fitting parameters.

Through our analysis, it is shown that the newly developed wax deposition model can successfully predict 1) thickness, 2) solidified wax fraction, 3) solid phase Average Carbon Number (ACN) and Carbon Number Distribution (CND). In addition, the physics behind the wax deposition phenomenon was further elucidated by comparing the SP-Depo simulation results to the experimental data of more than 12 flow-loop experiments.

LIST OF TABLES

Table 3-3-1: Coefficient table of Extension of Pitzer CSP models	22
Table 3-2: Coefficients of DIPPR correlations for molar volume calculation	23
Table 3-3: GCVOL Coefficients.....	24
Table 3-4: Van der Waals volume	24
Table 5-1: Binary system experimental data [30][75]	94
Table 5-2: Supplementary data from Garden Banks and South Pelto oil case experiments [10] [38]	95
Table 5-3: Experimental precipitation data for Garden Banks [38], Fleming et al. [29], and Zheng et al. [6]	96
Table 5-4: Correction factor coefficients of different oil systems from Dauphin et al. [77]	101
Table 5-5: Temperatures data at the end of experiments for five tests plus experimental data [10], [38] and predictions of Average Carbon Number (ACN), Mode, and Critical Carbon Number (CCN). South Pelto and Garden Banks are the names of oil samples that have been used by Panacharoensawad [10] and Ritirong [38], respectively.....	106
Table 5-6: Estimated relative error of the SP-Wax prediction for precipitation curves (Figure 4) of multicomponent systems.	107
Table 5-7: Temperature differences between predicted and experimental WAT parameter of five binary systems.	107
Table 5-8: Operating conditions of Singh et al. wax deposition tests [3].....	108
Table 5-9: $k\alpha$ values for different testing flow conditions	110
Table 5-10: Test conditions of the used experiments [10].....	112
Table 5-11: Experimental data of deposit's thickness, Fw and ACN.....	113
Table 5-12: Determined fitting parameters in Eq.3-62 and Eq.3-63 by LM algorithm in SP-Depo	124
Table 5-13: Adjusted msr1 and msr2 for two n-alkane compositions	136
Table 5-14: Original and new testing conditions for case 1. Every other parameter is the same	137
Table 5-15: Original and new testing conditions for case 2. Other parameters are the same	139

Table 5-16: Original and changed parameters for upscaled sensitivity case analysis 141

LIST OF FIGURES

Figure 2-1: Branching progression with increased molecular weight	6
Figure 2-2: SP-Depo simulation: temperature profile within the flowing fluid in the pipe at t=0 for test #28 [10]	12
Figure 2-3: SP-Depo simulation: concentration profile within the flowing fluid in the pipe at t=0 for test #28 [10]. MinC is set to be 30	13
Figure 2-4: SP-Depo simulation: Chilton-Colburn analogy (scenario A), partial precipitation (C) and the solubility method (scenario B) for wax mass flux consideration in wax deposition modeling	14
Figure 3-1: SP-Depo simulation: thermodynamically calculated $\partial C \partial T$ versus carbon number for different temperatures. Smoothened input South Pelto composition have been used. $\textcolor{red}{X}$ is the smallest depositable carbon number component at $T = 10.5^\circ\text{C}$	26
Figure 3-2: Minimum depositable carbon number versus temperature based on smoothened input South Pelto oil composition. The red points represent the lowest temperatures where MinC is shifted and the solid lines show the MinC within a temperature range.....	27
Figure 3-3: Diffusivity versus carbon number at three different temperatures	30
Figure 3-4: Incoming and diffusive wax mass flux at the waxy deposit's interface	33
Figure 4-1: SP-Wax flowchart for calculation of the precipitation curve	39
Figure 4-2: SP-Wax run-time at different temperatures	40
Figure 4-3: Source and executable files in SP-Wax (Computations of SLE model).....	41
Figure 4-4: The header and cpp files in SP-Wax software	42
Figure 4-5: Function in SP-Wax software	42
Figure 4-6: Solid phase activity coefficient function used in SP-Wax	44
Figure 4-7: The created input files for the binary system option.....	45
Figure 4-8: A snapshot of SPWaxbinary.cpp	47
Figure 4-9: General required inputs for the multicomponent system option.....	49
Figure 4-10: SP-Wax interface for multicomponent systems with various functionalities. The inputs are given through different textboxes on the left of the screen and the plots are created. In [1] the predicted and experimental precipitation curves can be plotted, in [2] the solid phase composition can be plotted for the given temperature range using a	

trackbar, in [3] different SLE characteristics can be plotted (as desired) for the provided temperature point and, in [4] the relative concentration gradient is plotted for CCN determination	52
Figure 4-11: An example of SP-Depo's diagnostic session during LM run.	53
Figure 4-12: C++ header-files of SP-Depo.....	54
Figure 4-13: SP-Depo.cpp and Deposition1PMain.Run(program_path).....	55
Figure 4-14: main_caller.cpp and deposition1.Calculate().....	56
Figure 4-15: single_phase_deposition.h and Dorman-Prince method	58
Figure 4-16: Main method to calculate the RHS of the governing ODEs	59
Figure 4-17: two functions for calculation of ODEs	60
Figure 4-18: Input calling header-files (section “A”)	61
Figure 4-19: Created input files by C# which will be used by CPP files based on the provided input information by the user.....	61
Figure 4-20: A screenshot of SP-Depo user-interface. Different tabs acquire different input information	62
Figure 4-21: Class, and methods which are included in Main_caller.h.....	63
Figure 4-22: Class, and methods which are included in solid_properties.h	63
Figure 4-23:Pipe’s input properties.	64
Figure 4-24: Class, and methods which are included in pipe_geometry.h	64
Figure 4-25: Class, and methods which are included in inlet_condition.h.....	64
Figure 4-26: Class, and methods which are included in coolant_condition.h	64
Figure 4-27: “Liquid properties” section of SP-Depo which takes the equations of rheological properties of the oil phase	65
Figure 4-28: Class, and methods which are included in fluid_properties.h.....	65
Figure 4-29: Simulation Option section in SP-Depo GUI	66
Figure 4-30: class, and methods which are included in simulation_options.h	67
Figure 4-31: SP-Wax thermodynamic model tab in SP-Depo GUI.....	68
Figure 4-32 : Class, and methods which are included in SP_Wax_Functions.h	68
Figure 4-33: Class, and methods which are included in SP_Wax_Main.h.....	69
Figure 4-34: SP-Depo header-files about wax deposition and transport equations.....	69
Figure 4-35: Class, and methods which are included in deposit_properties.h.....	70

Figure 4-36: radial temperature profile in the pipe for different axial locations	74
Figure 4-37: Deposit's interface temperature color map for different time and z locations	75
Figure 4-38: Deposit's interface temperature	76
Figure 4-39: Class, and methods which are included in temperature_profile.h	76
Figure 4-40:Class, and methods which are included in velocity_profile.h.....	77
Figure 4-41: Class, and methods which are included in concentration_profile.h.....	79
Figure 4-42: Class, and methods which are included in single_phase_deposition.h.....	79
Figure 4-43: Class, and methods which are included in fitting_search.h	80
Figure 4-44: $dCdT$ versus temperature for C46H94. The data points are generated by the SP-Wax thermodynamic model and the solid lines are generated by the fitted three-zone regression equations.....	82
Figure 4-45: SP-Depo simulation: dC/dT curves for carbon numbers C 46-51	82
Figure 4-46: concentration, $dCdT$ and Dwo versus temperature. The data points are generated by the SP-Wax thermodynamic model and the lines are from the fitted regression equations.....	83
Figure 4-47: Class, and methods which are included in linear_regression.h.....	83
Figure 4-48: Class, and methods which are included in linear_regression.h.....	83
Figure 4-49: Header files in section "D"	84
Figure 4-50: Liquid Properties input tab in SP-Depo	85
Figure 4-51: Equation insertion tab where user can provide the equation for non-constant variables including the fluid properties.....	86
Figure 4-52: Equation Description manual	86
Figure 4-53: Big Equation Creation Guidelines	87
Figure 4-54: Operator List assignment	87
Figure 4-55: Available equation types	88
Figure 5-1: Molar volume comparison between experimental data [34] and correlations from DIPPR and GCVOL models at $T=288.15^{\circ}\text{K}$	89
Figure 5-2: Molar volume comparison between experimental data [34] and correlations from DIPPR and GCVOL models at $T=298.15^{\circ}\text{K}$	90

Figure 5-3:SP-Wax Enthalpy of fusion prediction using Coutinho et al. model correlation versus experimental data of Broadhurst	91
Figure 5-4: SP-Wax Temperature of fusion prediction using Coutinho et al. model correlation versus experimental data of Broadhurst.....	91
Figure 5-5: SP-Wax Enthalpy of solid phase transition prediction using Coutinho et al. model correlation versus experimental data of Broadhurst.....	92
Figure 5-6: SP-Wax Temperature of solid phase transition prediction using Coutinho et al. model correlation versus experimental data of Broadhurst.....	92
Figure 5-7: CSP model prediction of vaporization enthalpy for different carbon numbers at T=25°C versus experimental data (Morawetz and Chickos et al. [73], [74])......	93
Figure 5-8:Compositional input data of n-alkanes for oil cases of Garden Banks and South Pelto and exponentially fitted lines	97
Figure 5-9: SP-Wax predictions and experimental data [30], [75] (symbol) of solid solubilities for five binary system at 1 bar (Table 5-1).....	98
Figure 5-10: SP-Wax precipitation curve validation against Fleming et al.(a) [29], Rittirong(b) [38], and Zheng et al.(c) [6].....	100
Figure 5-11: SP-Wax predictions versus precipitation data of Dauphin et al. [77]	101
Figure 5-12: Solid phase CND data of paraffin deposit. SP-Wax predictions versus CND experimental data of Ritirrong [38] and Panacharoensawad [10] at average deposit temperature $T_{avg} = 0.5(T_{int} + T_{wall})$ at the end of each test	103
Figure 5-13: SP-Wax relative concentration gradient predictions for five tests of Ritirrong [38] and Panacharoensawad [10]. Associated CCN values are annotated in the graph for each test. Blue and red highlighted sections are referred to carbon number components that diffuse in and out of the deposit, respectively.	105
Figure 5-14: Deposit's thickness versus solid wax fraction. Points represent the experimental data and the solid lines are created by our developed simulation	108
Figure 5-15: Simulation results versus experimental data for solid wax fraction and effective pipe's radius parameters. Colored lines are generated by our simulation and the rest are experimental data [3].....	109
Figure 5-16: LM adjusted $k\alpha$ versus volumetric flow rate	110
Figure 5-17: $k\alpha$ versus ambient temperature for Qoil = 1 gal/min	111

Figure 5-18: Derived crystal aspect ratio versus solid wax fraction for five operating conditions.....	111
Figure 5-19: Normalized mole composition of South Pelto oil (used in Panacharoensawad [10]).....	113
Figure 5-20: Deposit's raw HTGC data for Test #29 where CCN=33 is determined by red	115
Figure 5-21: SP-Wax simulation: deposit's solid phase CND at coolant temperature (T=28.77°C).....	115
Figure 5-22: HTGC data with separated liquid and solid compositions.....	116
Figure 5-23: Concentration calculated from the SP-Wax thermodynamic model with fitted regression curve for South Pelto oil case	117
Figure 5-24: $\partial C / \partial T$ calculated from the SP-Wax thermodynamic model with fitted regression curve for South Pelto oil case	117
Figure 5-25: D_{wo} calculated from the SP-Wax thermodynamic model with fitted regression curve for South Pelto oil case	118
Figure 5-26: Deposit's thickness axial profile for Test #21 ($Voil = 1.19 \text{ m/s}$)	119
Figure 5-27: Deposit's solid wax fraction axial profile for Test #21 ($Voil = 1.19 \text{ m/s}$)	119
Figure 5-28: Average deposit's and solid wax fraction predictions versus experimental data for $Voil = 2.24 \text{ m/s}$	121
Figure 5-29: Average deposit's and solid wax fraction predictions versus experimental data for $Voil = 1.83 \text{ m/s}$	122
Figure 5-30: Average deposit's thickness and solid wax fraction predictions versus experimental data for $Voil = 1.19 \text{ m/s}$	123
Figure 5-31: The deposit's surrounding temperatures	124
Figure 5-32: Pipe's inner wall temperature (T_{wh}) for Test #21	125
Figure 5-33: The deposit's interface temperature (T_i) for Test #21	126
Figure 5-34: Predicted solid phase ACN in axial direction for test #21	127
Figure 5-35: Experimental CND versus SP-Depo predictions at interface, average and wall temperatures, respectively for Test #32	128

Figure 5-36: ACN prediction at T_{wh} , T_{dep} and T_i versus experimental data. ACN was adjusted and updated after subtracting the oil composition from the raw HTGC data for $Voil = 1.83 \text{ m/s}$	129
Figure 5-37: Predicted and experimental ACN for three oil velocities	130
Figure 5-38: Effect of shear stress on the deposit. As oil velocity increases, shorter n-alkanes will be removed by the flow because of their low yield stress and ACN will increase ($\text{ACN}_3 > \text{ACN}_2 > \text{ACN}_1$)	131
Figure 5-39: solid mass of grouped components versus time.....	132
Figure 5-40: Average deposit's and solid wax fraction predictions from Bruno and Weatherford n-alkane compositions for $Voil = 2.24 \text{ m/s}$	133
Figure 5-41: Average deposit's and solid wax fraction predictions from Bruno and Weatherford n-alkane compositions for $Voil = 1.83 \text{ m/s}$	134
Figure 5-42: Average deposit's and solid wax fraction predictions from Bruno and Weatherford n-alkane compositions for $Voil = 1.19 \text{ m/s}$	135
Figure 5-43: ACN predictions using Bruno and Weatherford n-alkane compositions... ..	136
Figure 5-44: Simulation result comparison for case 1 sensitivity analysis with pipe's size variation	138
Figure 5-45: Simulation result comparison for case 2 sensitivity analysis with ambient temperature variation	140
Figure 5-46: Inner pipe's wall temperature versus axial sections	142
Figure 5-47: Pipe's inner wall temperature versus time.....	143
Figure 5-48: Deposit's interface temperature versus axial locations for different times ..	143
Figure 5-49: Deposit's interface temperature map (z vs time)	144
Figure 5-50: Radial temperature profile within the pipe at $t = 0 \text{ hr}$	145
Figure 5-51: Radial temperature profile within the pipe at $t = 48 \text{ hr}$	145
Figure 5-52:Radial concentration profile within the pipe at $t = 0 \text{ [hr]}$	146
Figure 5-53: Radial temperature profile within the pipe at $t = 48 \text{ hr}$	147
Figure 5-54: Axial solid wax fraction profile for different times	148
Figure 5-55: Solid wax fraction map (z vs time)	149
Figure 5-56: Average solid wax fraction versus time	149
Figure 5-57: Axial deposit's thickness profile for different times	150

Figure 5-58: Deposit's thickness map (z vs time)	150
Figure 5-59: Average deposit's thickness versus time	151
Figure 5-60: Deposit's solid phase ACN versus time at wall, deposit and interface temperature	151
Figure 5-61: Deposit's solid phase carbon number distribution at wall, deposit and interface temperatures	152

CHAPTER 1

INTRODUCTION

Energy is an important element for economic development. When energy is not adequately supplied, it can hinder the economic growth [1]. Although the universal demand for energy continuously increases, fossil fuel remains the main source of energy. In recent years, on average, the daily oil production rate has been above ninety million barrels per day. By considering the remained conventional oil reserves of 1.64 trillion barrels [2] and assuming that the oil production rate stays constant, oil can be produced for approximately 50 more years. These numbers show the limitation of current conventional oil reserves. That is why new efforts should be made to look into harsher and more difficult environments to find other potential oil reserves. Seventy percent of our planet's surface is covered by the ocean and, there is a great possibility to find new hydrocarbon reserves in the middle of the ocean hundred miles away from the shoreline. In such conditions, the transportation of oil becomes a critical issue. Scales and flow assurance problems are among the main challenges during the transportation of oil. In the subsea condition, the hydrocarbon is exposed to a very cold environment ($T = 4^{\circ}\text{C}$) where wax molecules start precipitating out of oil and stick to the inner wall of the pipe. Accordingly, periodic remedial actions are needed to maintain the production by discharging the deposit from the pipeline. Therefore, a complete understanding of the paraffin deposition phenomenon is crucial in planning effective treatments in the most optimal and cost-efficient way possible. In one instance , due to paraffin deposition problem and flow assurance mismanagement, the financial loss was reported to be as high as \$100 million while the main part of it was due to production shutdown for several days [3]. There are two general approaches in treating wax deposition problem. The first method is to mechanically remove the deposit from the inner surface of the pipe using a device called "pig". The pig is placed inside the pipe and moved by the production stream to scratch the deposit. The second treatment method is to use appropriate chemicals to prevent or remove the waxy deposit chemically. Some of the common chemical products are solvents, paraffin inhibitors and dispersants [4].

Both mentioned remedial methods are expensive and require detailed planning. Aside from the operating costs associated with pigging and chemical treatment, deferring production

is extremely costly [5] which leads to the loss of tens of millions of dollars. Lu [5] investigated the cost of pigging with different frequencies for a twenty-nine km long line. Seven days pigging frequency led to twenty-five million dollars while pigging every ninety days costed less than five million dollars per year. This emphasizes the importance of flow assurance management and planning.

There are two equally important aspects associated with wax deposition phenomenon. The first one is related to the thermodynamics of paraffin and the second one is to address the hydrodynamic, heat transfer and mass transfer of the flow during the deposition phenomenon. In my Ph.D., both aspects have thoroughly beeninvestigated and two modeling software (SP-Wax and SP-Depo) have been developed for further influential contribution.

In general, wax deposition can be characterized by thickness, solid wax fraction and carbon number distribution. For an optimal paraffin deposition treatment design, the mentioned characteristics need to be predicted accurately by a reliable wax deposition model [6]–[8]. The available wax deposition models usually consider wax as a single-component [3], [9]–[12] however, there are several n-alkane components that individually contribute to the deposition with different precipitation rates [6], [13]. The popular single-component modeling approach has some major flaws which are listed below.

Firstly, crude oil usually contains a wide range of n-alkane components starting from C5 to C₆₀₊ with different melting temperatures. Although, some n-alkane components could precipitate at a certain temperature, they might remain dissolved at another temperature. Therefore, it is impossible to refer to a certain range of carbon number components as wax at different temperatures. Therefore, the definition of wax from the single-component modeling approach is inconsistent.

Second, in wax deposition models, solubility of wax is an important parameter which is required in the calculations. In the single-component approach, only one lumped solubility curve is used, and it is assumed to be constant during the wax deposition phenomenon. However, due to inconsistent precipitation rate of different carbon number components,

the lumped solubility also changes as precipitation occurs. In the single-component approach, this important effect is not considered and could lead to errors.

Lastly, In the single-component approach, the deposit's solid phase Carbon Number Distribution (CND) cannot be predicted. CND prediction plays an important role in planning chemical and pigging treatments.

In this study, our main objective was to develop a compositional wax deposition model to predict the deposit's solid phase composition in addition to thickness and solid wax fraction in paraffin deposition phenomenon. For this purpose, we needed to develop two reliable models for thermodynamic and wax deposition predictions. SP-Wax is our first software which is developed based on the thermodynamic model of Coutinho et al. [14]–[21] and other literature [22]–[35]. For our second simulation tool, we developed SP-Depo software with a new thermodynamically-coupled wax deposition model to predict the composition of the waxy deposits along with other deposition characteristics. In our model, the depositable carbon number components are determined at given operating conditions and, then, they are grouped into one pseudo-single-component for the wax deposition calculation. The depositible carbon number components are referred to those n-alkanes that participate in deposition process at certain flow conditions. In this study, we have developed a consistent thermodynamic methodology to determine the minimum depositable carbon number component as a function of temperature. Next, the thermodynamic properties of the pseudo-single-component will be calculated based on the properties of all carbon numbers. By choosing this approach, unlike Zheng et al. [6], we only need to solve the PDE (for calculation of concentration profile) once, which results in performance enhancement and improved simulation speed.

1.1 Background

The primary deposition characteristics, which are responsible in determining the frequency of wax deposition treatments, are thickness, solid wax fraction [8] and deposit's solid phase carbon number distribution (CND) [9]. A systematic modeling procedure based on heat and mass transport needs to be developed to approximate the mentioned properties [3], [9]. Among the three deposit's properties, carbon number distribution of the deposit is

exclusively related to the thermodynamics of wax. Coutinho proposed a thermodynamic model which can deal with the nonideality of waxy solutions [20]. The model only uses the properties of pure components and can predict the phase behavior of liquid and solid as well as their compositions. He validated his model with various experimental data. This model was a huge improvement since, unlike the other models, it was capable of dealing with more than one solid phase in waxy solutions. This used to be the primary limitations of SLE modeling approaches. For liquid phase non-ideality, it is proven that ideal and regular solution models, Flory-Huggins activity coefficient approach and improved UNIFAC do not work in paraffinic systems [21]. Instead, it is shown that the improved Entropic free-volume and Flory free-volume models are suitable for accounting liquid phase non-ideality in paraffin systems.

On the other hand, for wax deposition phenomenon in pipe, some conditions need to be satisfied for n-alkanes to precipitate and form a stable deposit. For example, heavy components should be present in the oil sample [36] and the ambient temperature should be less than WAT for wax molecules to precipitate out of the oil. Finally, the wax crystals need to have an adequate attraction to stick to the wall and within their networks.

Mechanisms that are likely to be involved in paraffin deposition process include molecular diffusion, gravity settlement, co-crystallization of n-alkanes, Brownian diffusion, aging, shear or turbulent effect, shear dispersion [37], [38]. Molecular diffusion mechanism is characterized by radial concentration gradient inside the pipe. Many studies have suggested that the molecular diffusion is the dominant driving force for wax deposition [3], [39]–[41]. Also it is suggested that the Brownian diffusion mechanism can safely be neglected since it is a very slow process [40]. For shear dispersion effect, it is believed that the suspended precipitated wax particles might settle down toward the pipe's wall due to the differences in fluid particle velocities. However, it is not considered to be very significant [39]. Gravity settling is another process which causes the particles to settle due to their higher density than liquid.

Increasing in solidified wax content of the deposit with time is called aging and it is related to the hardness of the deposit[3]. Shear effect is included in several wax deposition models

[10], [13], [42] to account for additional wax mass flux and deposition thickness reduction[3], [42]–[44]. The other requirement of forming wax crystals is co-crystallization process which includes bounding of several n-alkanes. This implies that thicker deposit is not, necessarily, expected when more soluble wax is present in the oil sample [45].

CHAPTER 2

2. LITERATURE REVIEW

For investigating the physics behind the wax deposition phenomenon, it is necessary to analyze the thermodynamics of paraffin in equilibrium condition as well as the wax deposition models in flowing conditions. Accordingly, complete literature reviews about both aspects are presented in this chapter.

2.1 Thermodynamics of paraffin

Normal and slightly branched alkanes are considered as wax particles. These components are predominantly present in carbon number range of $C_{20} - C_{50}$ [37]. Due to higher degree of branching, heavier carbon number components (larger than C_{50}) are not usually considered as wax. The following graph is an example of a general branching progression of alkanes with increase of carbon number.

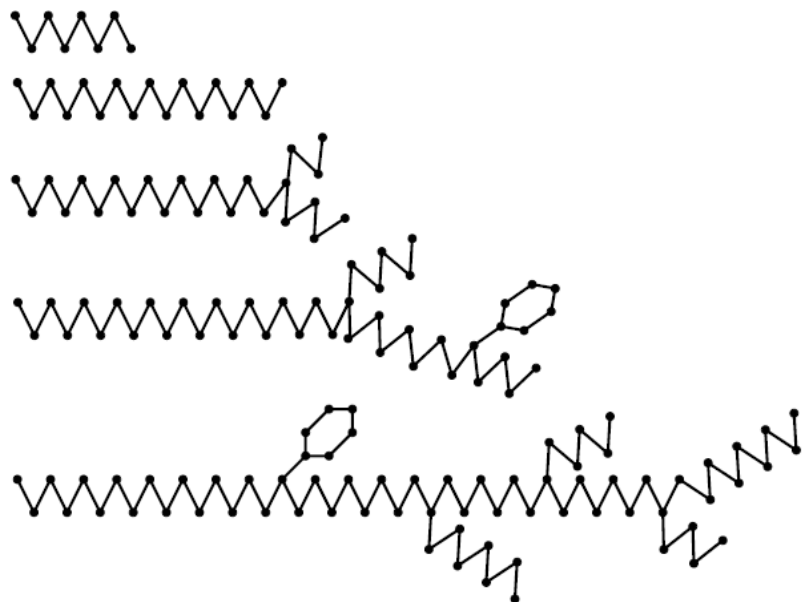


Figure 2-1: Branching progression with increased molecular weight

From the above figure, it can be seen that the normal n-alkanes are mainly present within lighter carbon number components. However, due to their low melting points, they do not largely participate in solidification.

In paraffinic solutions, correctly accounting for solid and liquid phase's non-idealities are in great importance. Won [46] was the first researcher who related the fugacity terms using the activity coefficients of each carbon number in both phases. He incorporated the regular solution theory to express activity coefficients. In his modeling, the pressure effect on fugacities was neglected and the specific heat capacity of each component for two phases were assumed to be the same ($\Delta C_p = 0$). He later found his first assumption to be invalid and considered the specific heat transfer coefficient differences in his new approach [47]. Won's model did not use an independent expression for describing each phase's fugacity. This method was later analyzed by Pederson for calculating WATs of several oil samples and it was discovered that the model is largely overpredicting the WATs [27]. The observed behavior was an indication of less thermodynamic favorability of solid phase in compare to what was predicted by the model. Accordingly, further attempts were carried to make the solid phase less thermodynamically favorable in compare to the liquid phase. This objective was followed by Hansen et al. [48]. In their modeling, polymer solution theory was used to calculate activity coefficient of liquid phase while the solid phase was assumed to be ideal ($\gamma_s = 1.0$). Pedersen et al. [49] made several suggestions which caused the solid phase's fugacity coefficients to increase. Their model was similar to Won however, iso-alkanes were also considered as participants in precipitation. Their lower heat of melting was the main cause of increase in solid phase fugacities. Ruffier et al. [50] proposed a thermodynamically consistent methodology to calculate the solid phase activity coefficients independent of the liquid phase. Erickson et al. [51] emphasized the importance of distinguishing between components which are responsible for wax formation and those which are not. Therefore, more realistic melting temperature and heat of fusion values were chosen to use in the governing equations. The enthalpy of fusion was the main factor to determine the tendency of a compound to precipitate below its melting temperature. Increase in ΔH^f affects the fugacity of the solid phase to rise exponentially. Rønning sen et al. [52] modified the wax formation model which was proposed by Pederson. The model assumed that just C_{7+} components and only normal alkanes contribute to wax formation. The following formula was used to determine the mole fraction of wax forming compounds for a specific carbon number,

$$Z_i^s = Z_i^{tot} \left(1 - (A + B * M_i) \left(\frac{\rho_i - \rho_i^p}{\rho_i^p} \right)^c \right) \quad (2-1)$$

where M_i , ρ_i , ρ_i^p and Z_i^{tot} are molecular weight, average density, density of a normal paraffin of the same molecular weight as carbon number fraction i, and total mole fraction of carbon number fraction i respectively. A, B and C are fitting parameters obtained based on experimental data.

Won [46] calculated the liquid phase fugacity from Soave–Redlich–Kwong equation as follows:

$$f_i^{\circ L} = \phi_i^{\circ L}(P)P \quad (2-2)$$

where $\phi_i^{\circ L}$ is the fugacity coefficient of pure component i in a liquid phase.

For C_{7+} fraction, the EOS inputs (ω , T_c and P_c) can be calculated using proposed procedure by Pederson [36]. For the critical pressure of C_{20+} , separate correlations were proposed for participating and non-participating components. Rønning et al. [52] showed the importance of such distinction in critical pressure parameter formulas for n-alkanes and non-wax-forming components to match the experimental data. The WAT experiments were conducted using NMR spectroscopy. Several experimental studies were conducted by Hansen et al. [53] and it was revealed that the solidified paraffin contains more than one phase. A model, later, was proposed based on a multi-solid phase assumption. The solid phase was assumed to contain several pseudo-components where each one consists of either one single pure component or multiple carbon number compounds [54]. After grouping, each pseudo-component's pure solid fugacity was compared to its f_i^v and f_i^L and if $f_i^{\circ s}$ was the lowest, that pseudo-component was considered to be in the solid phase. However, this method is, massively, dependent on grouping variations. Ideally, it is expected that grouping should be done to a level where further subgrouping does not make

much difference on the results. But this behavior was not seen in the proposed model of Lira-Galeana et al.[54]. Further modification of multi-solid phase modeling approach was done by Pan et al.[55] although the existence of a robust pseudo-component grouping procedure remained unfulfilled.

For the solid phase, predictive Wilson methodology is proven to be an appropriate model for accounting its non-ideality while ideal solution models are believed to describe liquid phase behavior adequately accurate in wax precipitation occurrence [56]. Ghanaei computed the Poynting correction term via melting properties of pure components at reference pressure and fusion temperature at high pressure. Modified Racket equation [57] was used to calculate the molar volume of the liquid phase. Won [46], [47] and Nichita's correlations [58] were chosen to calculate melting temperature and molar volume of the solid phase respectively. An extended UNIQUAC model was applied for solid phase by Coutinho et al. for non-ideal solid-liquid equilibria [20]. He then presented a work of wax precipitation prediction in jet and diesel fuel [59]. In that work, modified UNIFAC and UNIQUAC equations were used for liquid and solid phases, respectively. Vafaie et al. used the previously described multi-solid phase model developed by Lira-Galeanaetal while Peng–Robinson EOS was applied for liquid and gas phases [60]. Different activity coefficient models were studied by Esmaeilzadeh et al. [61] and it was reported that predictive Wilson method is suitable for describing a non-ideal solid phase. Ji et al. predicted WDT in binary and multicomponent systems using UNIQUAC model [62]. In their study, initially, they predicted the thermodynamic characteristics of n-alkanes to calculate different parameters in the fugacity equation. In our study, we developed a predictive thermodynamic software primarily based on the Coutinho model to estimate various SLE characteristics of paraffinic solutions.

2.2 Wax deposition phenomenon in pipelines

In the previous section, the thermodynamic aspect of the wax deposition was investigated in the solid-liquid equilibrium condition. However, wax deposition occurs in the pipeline and in the flowing condition. Therefore, it is crucial to simulate the hydrodynamic, heat-transfer and mass-transfer of the flow within the modeling of wax deposition phenomenon.

In the following section, an overview about the history of the wax deposition research is provided.

Crude oil contains a variety of complex hydrocarbon mixtures including high molecular weight long-chain saturated organic compounds known as paraffins. During transportation, such components are responsible for the formation of waxy deposits on the inner side of the pipe when they are exposed to a cold environment. In the reservoir condition, due to high temperature and pressure, the solubility of paraffins is high enough to be fully dissolved in the crude oil. However, when crude oil reaches to the subsea pipeline, it will be exposed to a cold environment (around 4°C) where heavy organic components precipitate out of the solution due to their limited solubility. There are several proposed mechanisms for wax deposition occurrence. Burger et al. [40] analyzed the wax deposition in the Trans Alaska Pipeline and concluded that molecular diffusion, Brownian diffusion and shear dispersion are primary mechanisms in the formation of waxy deposits. They concluded that molecular diffusion and shear dispersion are dominantly responsible for the deposition at higher and lower temperatures, respectively. Singh et al. [3] later showed that the only responsible mechanism is the molecular diffusion for the deposition of waxy components. In their study, they conducted experiments with different operating conditions to quantify the effect of other potential responsible mechanisms. Among all, only the shear effect was appeared to have some minor impacts on the deposition even though, the Reynolds number was within the range of the laminar flow. Singh et al. [3] also showed that the deposit's solid fraction increases with time through a counter-diffusion process where carbon number components larger than CCN diffuse toward the deposit and smaller n-alkanes move away from it. This process was verified thermodynamically by Shahdi and Panacharoensawad [63]. In the pipe, there is a radial temperature gradient within the flowing fluid where the highest temperature is at the center (e.g., Figure 2-2). Paraffin concentration is a great function of temperature which expectedly varies in the radial direction along with the temperature change. In Figure 2-3, an example of the concentration profile is presented which is approximated by SP-Depo software. Notably, heavy n-alkanes have higher concentrations at the bulk in compare to the deposit's interface. Such concentration gradient derives heavy paraffin components to move toward the waxy deposit from the center of the pipe. Within the deposit, a similar concentration gradient

exists where concentration is lower near the wall. Such gradient results in further diffusion of heavy n-alkanes toward the wall where they will be solidified. Along this process, due to an existing temperature gradient within the deposit, some n-alkanes start solidifying before reaching to the wall. This results in a complicated morphological structure of waxy deposits [64].

Convective wax mass flux due to the existence of concentration gradient has been addressed differently in the literature. The following three wax mass flux theories are mainly used in wax deposition models:

- A. No precipitation at the bulk – Singh et al. [3]
- B. Instantaneous precipitation (solubility method) – Venkatesan [11]
- C. Partial precipitation – Lee [12]

First scenario is to assume that waxy components will not precipitation until they reach to the deposit's interface [3]. Second method however considers an instantaneous precipitation for paraffinic components dictated only by the thermodynamic [11]. These two approaches result in an upper and lower bound for wax mass flux. In 2008, Lee [12] proposed a new wax mass flux model (C) which lays between the two limiting bounds by considering a partial precipitation.

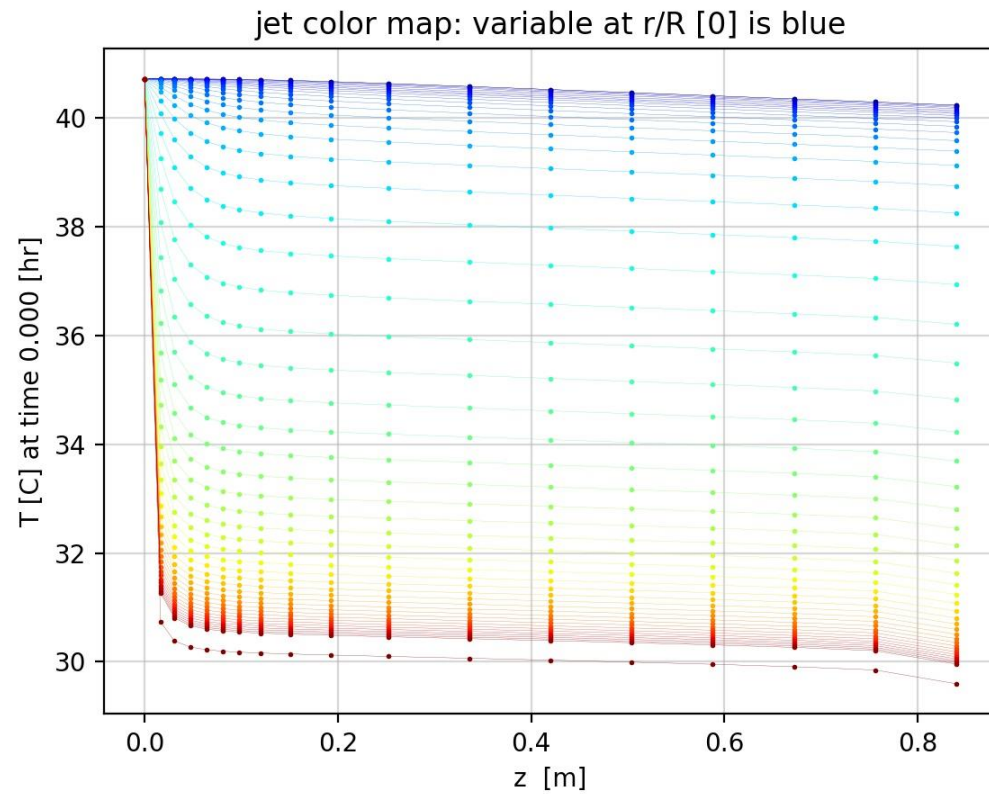


Figure 2-2: SP-Depo simulation: temperature profile within the flowing fluid in the pipe at $t=0$ for test #28 [10]

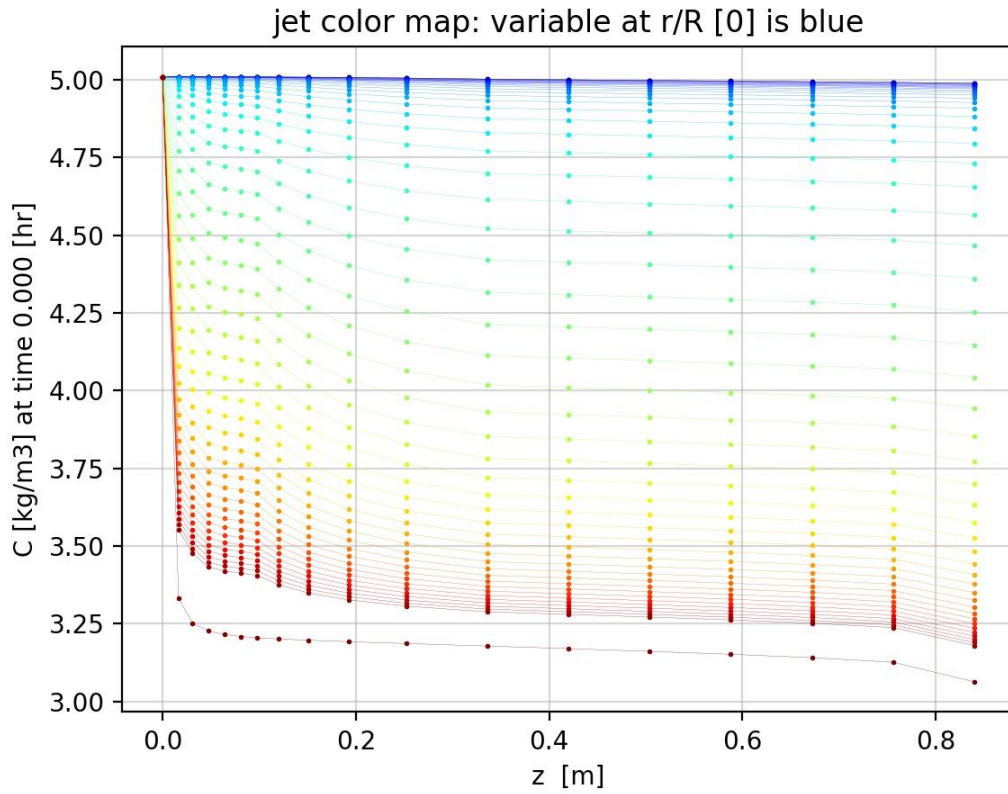


Figure 2-3: SP-Depo simulation: concentration profile within the flowing fluid in the pipe at $t=0$ for test #28 [10]. MinC is set to be 30

Further attempts were taken to develop a mathematical model for predicting the deposit's thickness, solid wax fraction and solid phase carbon number distribution. Previously, the existing wax deposition models assumed a constant value for solid wax fraction and used the deposit's oil content as an adjustment parameter to tune the model. This approach was disproven by several experimental studies [3], [5], [10], [12], [65]. Increase in solid wax fraction is very important because it results in an increased deposit's thermal conductivity and decreased wax molecular diffusivity. Singh et al. [3] developed a mass transfer model to account for the growth and aging process of wax deposition phenomenon under the laminar flow. In that study, decoupled correlations for heat and mass transfer calculations were used and satisfactory results were obtained. Singh et al. method is based on the first wax mass flux scenario (A) where no precipitation in the bulk was assumed. Although scenario (A) worked adequately well for the laminar flow, it was not well-adopted for the case where turbulent flow was present. Venkatesan and Fogler [42] showed that

precipitation is significant in turbulent flow condition and cannot be neglected. In that study, it was shown that even though the precipitated particles do not directly contribute to the deposition, the paraffin solubility decreases due to decreased dissolved mass. Accordingly, a new concentration profile will be formed similar to Figure 2-3. The resulted concentration gradient contributes to the molecular diffusion in wax deposition phenomenon. Lee [12] further compared the two wax mass flux scenarios and showed that, in reality, true wax mass flux falls between the (A) and (B) scenarios in the turbulent flow conditions. In his modeling, he accounted for the kinetics of the paraffin precipitation in the oil phase. From SP-Depo software, the following graph (Figure 2-4) was generated which perfectly illustrates all three scenarios for wax mass flux where the light blue curve represents the upper bound or the maximum theoretical limit for the wax mass flux (scenario A) and the black line represents the scenario B where the lowest wax mass flux is expected.

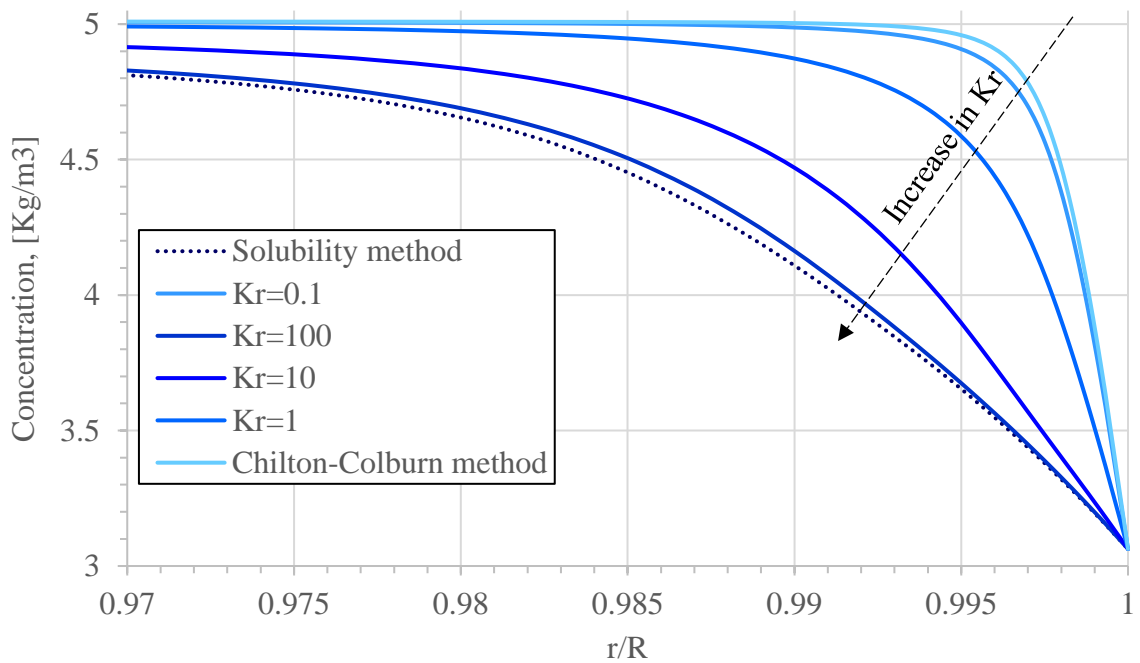


Figure 2-4: SP-Depo simulation: Chilton-Colburn analogy (scenario A), partial precipitation (C) and the solubility method (scenario B) for wax mass flux consideration in wax deposition modeling

In the previously mentioned models, the impact of shear effect was not included. Panacharoensawad [10] proposed a new wax deposition model which considered scenario (A) for wax mass flux. He then introduced two fitting parameters to include the shear effect and the initial deposit's growth in the modeling. In that study, the model successfully predicted different characteristics of the wax deposition phenomenon under single-phase and two-phase water-in-oil flow conditions. Later on, panacharoensawad et al. [9] broadened the application of the previously developed wax deposition model to two-phase gas-oil slug flow conditions. In SP-Depo, we made it possible for user to choose any of the above modeling procedures as desired.

Up to this point, all proposed wax deposition models were only capable of estimating the deposit's thickness (δ) and the solid wax fraction (\bar{F}_w). Then, Zheng et al. [6] solved the transport equations for all precipitable carbon number components separately rather than treating the paraffin as a pseudo-component (similar to the previous models). In this modeling approach, he accounted for each component's mass flux individually and was able to predict deposit's solid phase carbon number distribution. Zheng et al. [6] used Coutinho's thermodynamic model to predict SLE properties of waxy components including their solubilities. In the proposed model, the concentration profile was determined for all precipitable carbon number components. Zheng et al. [6] was a pioneering study in estimation of deposit's CND however, there are some serious issues associated with the proposed modeling which are elaborated as follow:

- Simulation run-time. In SP-Depo, we found that concentration profile calculation is one of the slowest steps in our program even though we only solved it once for one lumped component. Therefore, in a multi-mile subsea pipeline, it is not practical to solve the concentration profile for all precipitable carbon number components at each axial section.
- No selective depletion consideration. In a long subsea pipeline, it will be more likely for heavier components to precipitate sooner than lighter n-alkanes. Therefore, there will be less dissolved heavy n-alkanes in the oil to precipitate. In other word, in reality, oil composition will be updated as precipitation continues.

- Used temperature for deposit's solid phase composition estimation requires more investigation. In that study, there is not a clear explanation for using the appropriate temperature for solid phase composition prediction to account for the complex morphological structure of the deposit. In addition, average carbon number analysis of the deposit's solid phase is not included.
- No shear effect investigation. Even though, the importance of shear stress effect on wax deposition occurrence has been well-established, it is not included in Zheng et al. study.

In our study, we address the above issues and introduce a new thermodynamically-coupled wax deposition model (SP-Compo model). In our developed model, we only assume one pseudo-single-component (explained in later sections) and solve the transport equations accordingly. Concentration, $\frac{dc}{dt}$ and diffusivity terms are calculated directly from the thermodynamic characteristic of individual precipitable carbon number components. For example, in SP-Compo model, the concentration is the summation of each precipitable carbon number concentration in the oil. Within our model, concentration, $\frac{dc}{dT}$ and diffusivity terms are called thousands of times. Since our thermodynamic model takes about 0.2 - 0.5 seconds to run at each temperature, it was not practical to directly use the thermodynamic model to obtain these parameters. Instead, we fitted sets of regression equations to the thermodynamic data and used them throughout our calculations. So, the thermodynamic model is required to be called only once (at each time step). Then, the thermodynamically calculated data are fitted to sets of regression equations. In the next chapter, the detailed theoretical framework of our developed model will be provided.

CHAPTER 3

THEORETICAL FRAMEWORK

In this chapter, the theoretical framework and technical aspects of our two developed software (SP-Wax and SP-Depo) will be thoroughly presented.

3.1 SP-Wax thermodynamic model

In this section the mathematical framework of the developed thermodynamic model in SP-Wax is presented. SP-Wax is based on the thermodynamic model of Coutinho et al. [14]–[21] and other literature [22]–[35]. From SP-Wax, solidified weight fraction values ($S_f \left[\frac{w}{w} \right]$) at different temperatures are calculated and plotted. The generated curve from the plotted S_F values is called precipitation curve and it varies with input oil composition. Therefore, the n-alkane composition of the system (z_i) should be provided. In the software, the input composition should be in mole fraction. Please note that SP-Wax can only predict characteristics of the n-alkane system. Therefore, composition of the total fluid is not required. User should only provide the weight percentage of n-alkanes in the total fluid (W_{NA}). For example, if in one-kilogram solution, there is 250 grams of soluble wax, W_{NA} will be 25%.

SP-Wax can predict SLE thermodynamic properties of the solution at any temperature below WAT. However, convergence problem might be encountered near WAT. To overcome this problem, a set of initial values for equilibrium constants are generated at various temperatures. These K values are then used as initial guesses of equilibrium constant parameters when SP-Wax is called. By this solution, the mentioned convergence problem has been eliminated.

In SP-Wax, Coutinho thermodynamic model was chosen because it can express the non-ideality of the liquid and solid phases accurately. In SP-Wax, governing equations [33] are solved for non-ideal paraffinic solutions and different SLE characteristics are reported. The following governing equation relates each carbon number component's equilibrium constant (K_i) to its thermo-physical properties using activity coefficients (γ_i^L, γ_i^S).

$$K_i = \frac{\gamma_i^L}{\gamma_i^S} \exp \left(\frac{\Delta H_i^f}{RT_i^f} \left(\frac{T_i^f}{T} - 1 \right) + \frac{\Delta H_i^{tr}}{RT_i^{tr}} \left(\frac{T_i^{tr}}{T} - 1 \right) - \frac{\Delta_s^l C_{p_i}}{R} * \left(\frac{T_i^f}{T} - \ln \left(\frac{T_i^f}{T} \right) - 1 \right) \right) \quad (0-1)$$

where $\Delta H_i^f, T_i^f, \Delta H_i^{tr}, T_i^{tr}$ and $\Delta_s^l C_{p_i}$ are thermo-physical properties and are expressed through empirical correlations (discussed later). Newly calculated K values are then compared to the previous equilibrium constants (K^C) through the following relation. If the calculated error is not less than a certain threshold, the calculation continues. The error is calculated as:

$$\epsilon = \frac{\sum |K_i^C - K_i|}{\sum K_i^C} \quad (0-2)$$

The mole fraction of the precipitated phase in n-alkane system (n_s) is determined from the following equation as follows:

$$\sum_{i=1}^{i=N} \left(z_i * \frac{K_i - 1}{1 + n_s * (K_i - 1)} \right) = 0 \quad (0-3)$$

Finally, the liquid and solid phase compositions (x_i^L, x_i^S) are calculated from

$$x_i^L = \frac{z_i}{1 + n_s * (K_i - 1)} \quad (0-4)$$

$$x_i^S = \frac{z_i * K_i}{1 + n_s * (K_i - 1)} \quad (0-5)$$

2.1.1 Liquid phase non-ideality

In SP-Wax, liquid-phase non-ideality [21] is expressed by:

$$\ln \gamma_i^L = \ln \frac{\phi_i}{x_i} + 1 - \frac{\phi_i}{x_i} \quad (0-6)$$

where ϕ_i is the composition fraction,

$$\phi_i = \frac{x_i S_i}{\sum x_j S_j} \quad (0-7)$$

The main difference between all models is the way element "S" has been defined. In SP-Wax Entropic Free-Volume model has been used and "S" is defined as:

$$S_i(\text{Entropic}) = (V_{m,i} - V_{w,i})^{2/3} \quad (0-8)$$

2.1.2 Solid phase non-ideality

In SP-Wax, solid phase activity coefficients are calculated using Wilson method [16] as follows:

$$\ln(\gamma_i^s) = -\ln(\sum_j \Lambda_{ij} x_j) + 1 - \sum_j \frac{\Lambda_{ji} x_j}{\sum_k \Lambda_{jk} x_k} \quad (0-9)$$

where

$$\Lambda_{ij} = \exp\left(-\frac{\lambda_{ij} - \lambda_{ii}}{RT}\right) \quad (0-10)$$

$$\Lambda_{ij} = \exp\left(-\frac{\lambda_{ij} - \lambda_{ii}}{RT}\right) \quad (0-11)$$

$$\lambda_{ii} = -\frac{1}{3}(\Delta H_i^{\text{sub}} - RT) \quad (0-12)$$

$$\Delta^{\text{sub}}H = \Delta^{\text{vap}}H + \Delta^{\text{f}}H + \Delta^{\text{tr}}H \quad (0-13)$$

$$\lambda_{ij} = \alpha_{ij} \min(\lambda_{ii}, \lambda_{jj}) \quad (0-14)$$

α_{ij} is a correction factor that has been expressed differently in the literature. In this study, different correlations have been analyzed and the following expression was chosen for the correction factor. Please note that α_{ij} was used in multi-component systems only. In binary systems, no correction factor was required, and model is purely predictive. In multi-component systems, correction factor is defined as:

$$\alpha_{ij} = 1 - a \cdot |\Delta H_i^{\text{sub}} - \Delta H_j^{\text{sub}}| \quad (0-15)$$

where "a" is an adjustment coefficient.

We compared experimental data of seven multi-component systems and adjusted "a" for all of them. For three oil systems where n-alkane weight fraction values were less than 0.15, "a" was calculated to be $3 * 10^{-6}$. However, for the case where only n-alkanes were present ($WF = 1$), very small "a" (close to zero) was needed. So, we suggest using "a" coefficients as follows:

$$\text{If } W_f \cong 1, \quad 0 \leq a < 8 \times 10^{-7} \quad (0-16)$$

$$\text{If } 0.15 < W_f < 1, \quad 8 \times 10^{-7} \leq a < 3 \times 10^{-6} \quad (0-17)$$

$$\text{If } W_f \leq 0.15, \quad a = 3 \times 10^{-6} \quad (0-18)$$

Please note that the mentioned recommendations are based on analyzing seven multi-component systems through various parameters including precipitation curve, solid phase composition and Critical Carbon Number (CCN). For each oil composition, all parameters were optimally predicted with one adjustment parameter at various conditions. This study is amongst the very few that verified Coutinho's model by analyzing different paraffin related parameters against the experimental data. (not just by precipitation data points).

The following derivation is used to calculate the solidified wax fraction in precipitation curve formation

$$S_f \text{ (Solidified wax weight fraction)} \left[\frac{\text{weight of solid phase}}{\text{weight of total fluid}} \right] = \quad (0-19)$$

$$\Sigma x_i^s Mw_i \left[\frac{\text{weight of solid phase}}{1 \text{ mole of solid phase}} \right] * n_s \left[\frac{\text{mole of solid phase}}{1 \text{ mole of total n - alkanes}} \right]$$

$$* \frac{1}{\Sigma z_i Mw_i} \left[\frac{1 \text{ mole of total n - alkanes}}{\text{wieght of nalkanes}} \right] * W_{NA} \left[\frac{\text{weight of nalkanes}}{\text{weight of total fluid}} \right]$$

In the calculation of activity coefficients of liquid and solid phases, thermo-physical properties, molar volumes and Van der Waals volumes are required. In the following section, we present the models and correlations which have been used in our thermodynamic software. The majority of the parameters are suggested by Coutinho et al.

One of the main findings of our study was to validate the aging process in wax deposition phenomenon using the thermodynamic model. For this purpose, we introduced a new parameter which represents the relative concentration of carbon number component in the n-alkane system ($C_{i,NA}$). In other word, if only the n-alkane system is considered within the oil sample, the relative concentration of each carbon number component will be considered as $C_{i,NA}$. Although, the relative concentration parameter does not represent the actual concentration, it is a very helpful parameter to determine CCN and verify the aging process. Please note that in SP-Depo, actual concentrations of different carbon numbers are calculated and presented in the next chapter of this dissertation.

$$C_{i,NA} = \frac{m_{i,NA}}{V_{NA}} \quad (0-20)$$

Where

$$V^{NA} = \sum_{i=1}^{i=N} (V_{i,NA}) \quad (0-21)$$

where $V_{i,NA}$ is calculated from DIPPR and GCVOL models

2.1.3 Thermo-physical properties

Heat and temperature of fusion are calculated from Coutinho et al. [19]. Among all the thermo-physical properties, melting temperature has the highest impact on the final results. The following correlation has been proposed by Coutinho for temperature of fusion.

$$T_i^f [K] = 421.6 - (421.6 + 1935991) \exp(-7.8945(CN - 1)^{0.07194}) \quad (0-22)$$

$$\Delta_{\text{fus}}H_i \left[\frac{\text{KJ}}{\text{mol}} \right] = 0.00355CN^3 - 0.2376CN^2 + 7.4CN - 34.814 \quad (0-23)$$

Heat and temperature of solid phase transition (Coutinho et al. [19]):

$$T^{tr} [K] = 420.42 - (420.42 + 134364) \exp(-4.344(CN + 6.592)^{0.14627})$$

$$\Delta^{tr}H = \Delta^{tr}H - \Delta^fH \quad (3-25)$$

$$\Delta^{tot}H_i \left[\frac{\text{KJ}}{\text{mol}} \right] = 3.7791CN - 12.654 \quad (3-26)$$

Heat of vaporization (Extension of Pitzer CSP models [32]):

$$\Delta^{vap}H \left[\frac{KJ}{mole} \right] = \Delta^{vap}H^* * RT_c \quad (3-27)$$

$$\Delta^{vap}H^* = \Delta^{vap}H^{*(0)} + \omega\Delta^{vap}H^{*(1)} + \omega^2\Delta^{vap}H^{*(2)} \quad (3-28)$$

$$\omega = 0.0520750 + 0.0448946n - 0.000185397n^2 \quad (3-29)$$

$$\begin{aligned} \Delta^{vap}H^{*(J)} &= b_1^{(J)}x^{0.3333} + b_2^{(J)}x^{0.8333} + b_3^{(J)}x^{1.2083} + b_4^{(J)}x + b_5^{(J)}x^2 \\ &\quad + b_6^{(J)}x^3 \end{aligned} \quad (0-30)$$

$$x = 1 - T_r \quad (3-31)$$

$$\ln(959.98 - T_c) = 6.81536 - 0.211145n_c^{\frac{2}{3}} \quad (3-32)$$

where the corresponding coefficients are:

Table 3-0-1: Coefficient table of Extension of Pitzer CSP models

	$\Delta H_v^{*(0)}$	$\Delta H_v^{*(1)}$	$\Delta H_v^{*(2)}$
b1	5.2804	0.80022	7.2543
b2	12.865	273.23	-346.45
b3	1.171	465.08	-610.48
b4	-13.116	-638.51	839.89
b5	0.4858	-145.12	160.05
b6	-1.088	74.049	-50.711

2.1.4 Molar volume

In our study, the molar volume term is very important because it is used not only by the thermodynamic model but also in the wax deposition modeling for diffusivity calculation of wax particles in the oil solution.

In SP-Wax, liquid phase activity coefficient formulas required the molar volume values of each carbon number component. We used DIPPR and GCVOL for molar volume calculation.

Molar volume for $7 \leq C_n \leq 20$ are calculated from DIPPR Correlations as:

$$V_{m,i} \left[\frac{m^3}{Kmol} \right] = \left(\frac{A}{B \left(1 + \left(1 - \frac{T}{C} \right)^D \right)} \right)^{-1} \quad (3-33)$$

where A, B, C and D are sets of coefficients which are unique for each carbon number component. The following table includes the coefficient values for carbon number starting from C7 to C20.

Table 0-2: Coefficients of DIPPR correlations for molar volume calculation

DIPPR	A	B	C	D
C7	0.6034	0.2602	540.26	0.2791
C8	0.50864	0.25476	568.83	0.2694
C9	0.46554	0.25556	595.65	0.2857
C10	0.4129	0.2524	618.45	0.2857
C11	0.37012	0.24999	638.76	0.2857
C12	0.346	0.2518	658.2	0.2896
C13	0.3228	0.2504	675.8	0.312
C14	0.30382	0.25588	692.4	0.273
C15	0.28834	0.25375	706.8	0.31579
C16	0.27356	0.25442	720.6	0.3238
C17	0.25217	0.25316	733.37	0.3052
C18	0.2413	0.25763	745.26	0.274
C19	0.22147	0.25012	755.93	0.3065
C20	0.20966	0.24934	767.04	0.3088

For other carbon numbers ($C_n < 7$ & $C_n > 20$), molar volume is calculated from GCVOL contribution method [26]:

$$\Delta v_i \left[\frac{cm^3}{mole} \right] = A_i + B_i^T + C_i T^2 \quad (3-34)$$

Table 0-3: GCVOL Coefficients

Comp	A [$\frac{cm^3}{mole}$]	B [$\frac{cm^3}{mole \cdot k}$]	C
CH3	18.96	$45.58 * 10^{-3}$	0
CH2	12.52	$12.94 * 10^{-3}$	0

2.1.5 Van der Waals volume

Another volume term which is needed in the calculation of liquid phase non-ideality is the Van der Waals volume. Bondi [25] used the group contribution method for V_w calculation.

$$V_{VNW,i} \left[\frac{m^3}{mole} \right] = \frac{\Sigma n_i \Delta v_i}{10^6} \quad (3-35)$$

Table 0-4: Van der Waals volume

Comp	Δv_i [$\frac{cm^3}{mole}$]
CH3	13.67
CH2	10.23

Now that all required parameters are available, the equations from 0-1 to 0-5 are solved iteratively till the desired accuracy is reached. The following chart illustrates SP-Wax thermodynamic structure.

2.2 SP-Depo wax deposition modeling software

In SP-Depo software, two general calculation options are included. The first option requires the user to provide equations for concentration and $\frac{\partial C}{\partial T}$ considering only one component which is referred as wax. In addition, the molecular diffusivity (D_{wo}) is considered by only one value. In this method, the thermodynamic model is not included

and it is referred to “conventional method” in this document. This method only provides predictions about the wax fraction and the thickness.

The second method, which is one of the main contributions of our study, employs a new thermodynamically-coupled model to predict wax deposition characteristics. This method uses SP-Wax thermodynamic tool for calculation of concentration, D_{wo} and $\frac{\partial C}{\partial T}$ during the wax deposition calculation. In our newly proposed modeling approach, we have used Panacharoensawad [10] governing equations where no precipitation wax mass flux scenario and $k_\alpha = 1$ are assumed. By using this calculation option, the deposit's solid phase composition will be predicted. Our new wax deposition model is referred to as “SP-Compo model” in this dissertation.

We developed our software for the lab scale flow loops because experimental data are only available from lab-scale experiments. The experimental data are crucial for model verification and have been extensively used to validation of our developed software.

In wax deposition experiments, usually counter-current coolant flow is present which results in the highest heat exchange. Therefore, in SP-Depo, the heat transfer calculations are performed for the case where counter-current coolant flow is present.

2.2.1 Definition of wax and MinC concept

In SP-Compo model, concentration, $\partial C / \partial T$ and diffusivity terms are calculated based on depositable carbon number components' thermodynamic properties. So, one of the challenges we encountered was to define a reliable method to determine the depositable carbon numbers. Fortunately, we introduced a new thermodynamic method to calculate the depositable carbon number range.

There is not a universal definition for the word “wax” in the literature. In the wax deposition research, wax usually refers to those n-alkane components that contribute to the deposition. For example, even though Heptane (C_7H_{16}) is present in the oil sample but, it is not considered as wax because it does not contribute to the deposition. This definition is also inconsistent because there are some carbon number components that participate at a

certain range of temperatures only. In other word, at different temperatures, the range of precipitable carbon number components also changes.

We previously mentioned that the main deriving mechanism for deposition is the radial concentration gradient (or $\partial C / \partial T$). Accordingly, in this study, we define the Depositable wax content as a group of carbon number components with positive $\partial C / \partial T$ at the deposit's interface temperature. In Figure 0-1, $\partial C / \partial T$ versus carbon number is plotted for different temperatures and only positive $\partial C / \partial T$ carbon numbers will diffuse toward the deposit. To be more elaborate, for example, if the deposit's interface temperature is at $T=10.5^{\circ}\text{C}$, only carbon number components larger than C21 will diffuse toward the deposit (X). Since the interface temperature increases with time, the minimum depositable (MinC) carbon number shifts toward larger n-alkanes too. In the second graph (Figure 0-2), MinC is plotted against temperature. Notably, for a certain temperature range, MinC stays the same and, as temperature increases, the range becomes smaller.

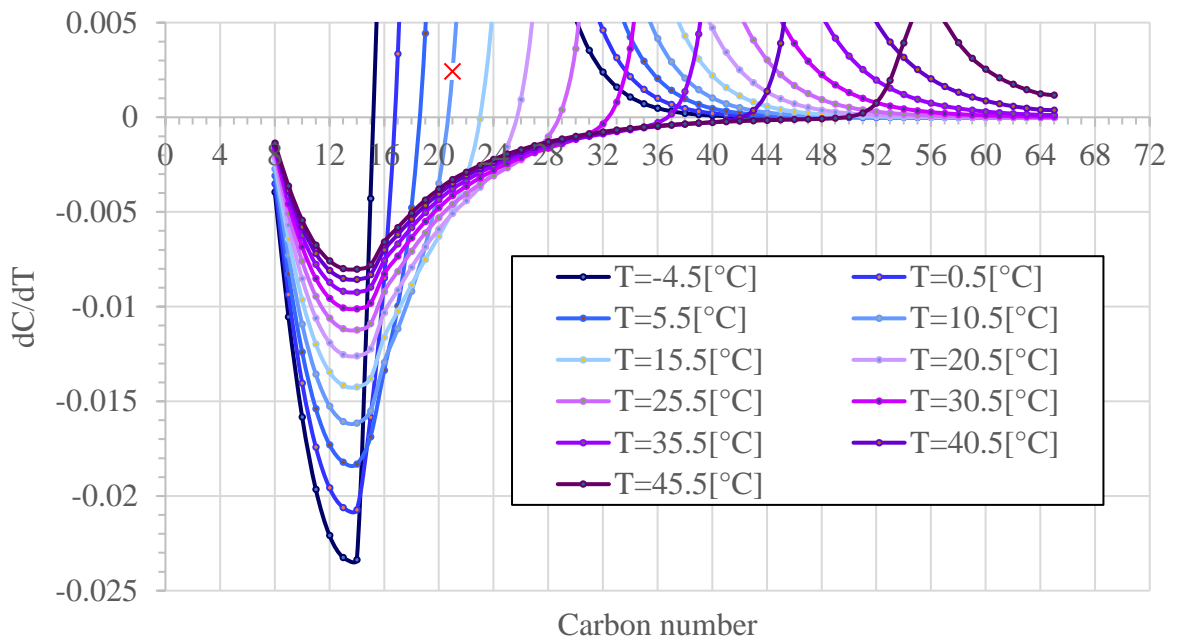


Figure 0-1: SP-Depo simulation: thermodynamically calculated $\frac{\partial C}{\partial T}$ versus carbon number for different temperatures. Smoothened input South Pelto composition have been used. X is the smallest depositable carbon number component at $T = 10.5^{\circ}\text{C}$

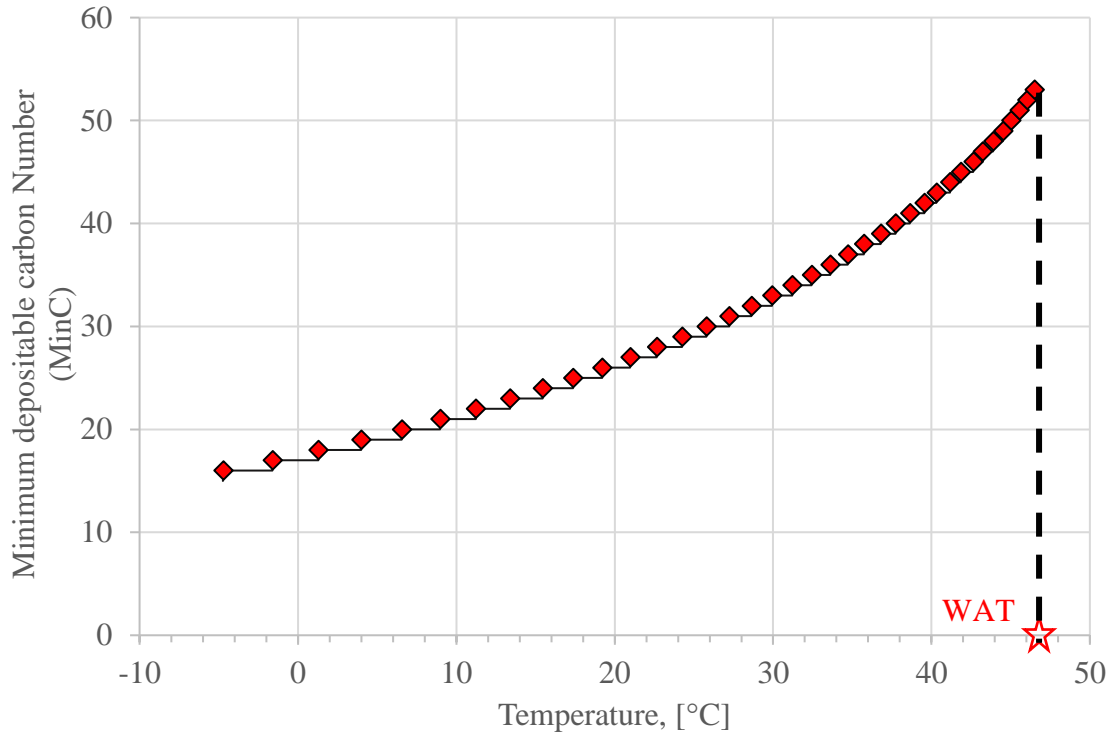


Figure 0-2: Minimum depositable carbon number versus temperature based on smoothed input South Pelto oil composition. The red points represent the lowest temperatures where MinC is shifted and the solid lines show the MinC within a temperature range.

2.2.2 Thermodynamically calculated parameters

As mentioned, the concentration gradient near the deposit is the primary deriving mechanism for wax deposition phenomenon. Therefore, it is very important to calculate the concentration very accurately. In our model, we use the thermodynamic model to calculate the concentration of each depositable carbon number component. However, the concentration parameter is not directly reported from the thermodynamic model. Therefore, we derived the following relations for concentration calculation.

In the following derivation, it is assumed that the temperature is below WAT and some part of the paraffinic components are in the solid phase. \tilde{m}_i is the dissolved amount of i^{th} carbon number n-alkane in the liquid-phase per one kilogram of oil and it is calculated as:

$$\tilde{m}_i = x_{w,i}^L \times W_f \times f_{NA}^L \quad (0-36)$$

where $f_{NA,L}$ is a w/w fraction of n-alkanes over the total amount of n-alkanes

$$f_{NA}^L = \frac{\sum z_{m,i} \times Mw_i - \sum n_s \times x_{m,i}^s \times Mw_i}{\sum z_{m,i} \times Mw_i} \quad (0-37)$$

and liquid w/w composition of n-alkanes in liquid-phase can be approximated as:

$$x_{w,i}^L = \frac{x_{m,i}^L \times Mw_i}{\sum_i x_{m,i}^L \times Mw_i} \quad (0-38)$$

The term “oil” means solid+ liquid which accounts for both n-alkanes and non n-alkanes. Now that the dissolved mass of each n-alkane component is known, we need to know the volume of the oil sample. So, our model requires an equation from the user to express the oil density for temperatures higher than WAT (no present solid phase). In Rittirong [38] and Panacharoensawad [10] studies, the experimentally measured densities of the total oil sample are reported for different temperatures above WAT and simple fitted equations are reported. These density data points quantify the expansion effect due to the temperature increase while no dissolution from the solid phase occurs. ϕ_L is defined as the volume of the oil sample over one unit mass of oil and is expressed as:

$$\Phi_L = \Phi_{exp} - \frac{f_{NA}^S}{\rho_{Wax}} \quad (0-39)$$

where $f_{NA,S}$ is the w/w fraction of the solidified wax particles over one unit mass of oil and is expressed as:

$$f_{NA}^S = W_f \times \frac{n_s \times \sum x_{m,i}^s \times Mw_i}{\sum z_{m,i} \times Mw_i} \quad (0-40)$$

Now that \tilde{m}_i and ϕ_L are known, one can calculate the actual concentration of i^{th} carbon number component in the system.

$$C_i \left[\frac{\text{kg NA}_{i,L}}{m_L^3} \right] = \frac{\tilde{m}_i}{\phi_L} \quad (0-41)$$

Please refer to the nomenclature section for each parameter’s definition and unit.

In our proposed model, we considered the depositable carbon number components as one grouped component and calculated the concentration as the summation of all depositable component’s concentrations:

$$C = C_{MinC} + C_{MinC+1} + \dots + C_N \quad (0-42)$$

And similarly, for $\frac{\partial C}{\partial T}$:

$$\frac{\partial C}{\partial T} = \frac{\partial}{\partial T} (C_{MinC} + C_{MinC+1} + \dots + C_N) \quad (0-43)$$

Or

$$\frac{\partial C}{\partial z} = \frac{\partial C_{MinC}}{\partial T} + \frac{\partial C_{MinC+1}}{\partial T} + \dots + \frac{\partial C_N}{\partial T} \quad (0-44)$$

We also calculated the diffusivity of n-alkanes in the oil using the thermodynamic model. Hayduk-Minhas diffusivity equation [66] (shown below) is used in SP-Depo.

$$D_{wo,i} = 13.3 \times 10^{-12} \times \frac{(T + 273.15)^{1.47} (\mu \times 1000)^\gamma}{V_{m,i}^{0.71}} \quad (0-45)$$

where,

$$\gamma = \frac{10.2}{V_{m,i}} - 0.791 \quad (0-46)$$

$V_{m,i}$ is the molar volume of i^{th} carbon number component which is calculated from DIPPR correlations [24] and the group contribution method (GCVOL) [26] as per Coutinho et al. suggestion[14]. Figure 0-3 contains the diffusivity of different carbon numbers at three different temperatures. As you can see, the diffusivity increases with temperature which is accounted in SP-Depo.

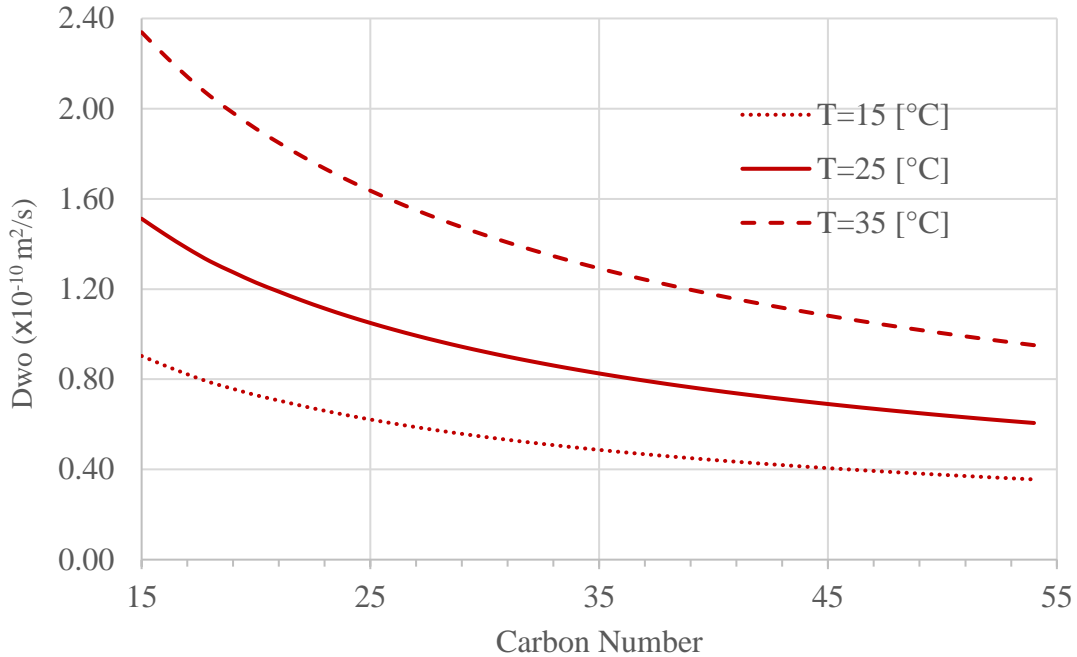


Figure 0-3: Diffusivity versus carbon number at three different temperatures
Now that the diffusivities of all carbon number components are known, the volume average will be used as the representative D_{wo} for our model.

$$\overline{D_{wo}} = \sum D_{wo,i} \xi_i \quad (0-47)$$

where

$$\sum \xi_i = 1.0 \quad (0-48)$$

2.2.3 Wax deposition theory

In this section, the wax deposition theory and supplementary transport equations are thoroughly elaborated. Initially, the When deposit is formed, the solid phase mass can be expressed as:

$$Mass_{sol} = \pi(R^2 - r_i^2)L_{pipe}\rho_{dep}\bar{F}_w \quad (0-49)$$

where, M , R , r_i , ΔL and \bar{F}_w are the precipitated mass, pipe's radius, effective pipe's radius in presence of wax deposit, pipe's length and average solid wax fraction, respectively. Then, change's rate of wax mass can be expressed as:

$$\frac{dMass_{sol}}{dt} = \frac{\partial Mass_{sol}}{\partial \bar{F}_w} \frac{d\bar{F}_w}{dt} + \frac{\partial Mass_{sol}}{\partial r_i} \frac{dr_i}{dt} \quad (0-50)$$

where,

$$\left(\frac{\partial Mass_{sol}}{\partial \bar{F}_w} \right)_{r_i} \frac{d\bar{F}_w}{dt} = \pi(R^2 - r_i^2)L_{pipe}\rho_{oil} \frac{d\bar{F}_w}{dt} \quad (0-51)$$

and,

$$\frac{\partial Mass_{sol}}{\partial r_i} \frac{dr_i}{dt} = -2\pi r_i L_{pipe} \rho_{dep} \bar{F}_w \frac{dr_i}{dt} \quad (0-52)$$

The first term represents the rate of wax mass increase because of the increase in solid wax fraction and the second term represents the contribution of thickness growth to the rate of wax mass increase.

2.2.4 Aging term

The first term (aging term) is only dependent on the wax mass flux going into the deposit and can be expressed as:

$$\frac{\partial Mass_{sol}}{\partial \bar{F}_w} \Big|_{r_i} \frac{d\bar{F}_w}{dt} = \left(-\overline{\mathcal{D}_e} \frac{\partial C}{\partial r} \Big|_{r_i^+} \right) 2\pi r_i L_{pipe} = \pi(R^2 - r_i^2) L_{pipe} \rho_{oil} \frac{d\bar{F}_w}{dt} \quad (0-53)$$

where $\overline{\mathcal{D}_e} \left[\frac{m^2}{s} \right]$ and $\frac{\partial C}{\partial r} \Big|_{r_i^+}$ are effective wax diffusivity in the deposit and concentration gradient in radial direction at deposit's interface location (in the deposit side), respectively. By simple mathematical manipulation, the above relation becomes:

$$\frac{d\bar{F}_w}{dt} = \frac{2r_i \left(-\overline{\mathcal{D}_e} \frac{\partial C}{\partial r} \Big|_{r_i^+} \right)}{(R^2 - r_i^2) \rho_{oil}} \quad (0-54)$$

Effective diffusivity term (\mathcal{D}_e) is calculated from the following formula [67]:

$$\overline{\mathcal{D}_e} = \frac{\overline{D}_{wo}}{1 + \alpha^2 \bar{F}_w^2 / (1 - \bar{F}_w)} \quad (0-55)$$

This equation was not originally developed for wax deposition however, Singh et al. [3] showed that it can be adopted to represent the effective diffusivity of wax components through a 3D network of wax crystals. Singh et al. [3] suggested that the wax crystal aspect ratio (α) increases linearly as wax fraction increases:

$$\alpha = 1 + k_\alpha \bar{F}_w \quad (0-56)$$

where k_α is an adjustment parameter for tuning the model. From another study, Lee [12] suggested another relation for α with the fitting parameter “A”.

$$\alpha = 1 + \sqrt{\frac{\bar{F}_w - \bar{F}_{wo}}{A}} \quad (0-57)$$

In SP-Depo, we included the option to use either of the two formulas for α as desired. However, in our exclusive proposed model, the value of k_α is set to be one and two other fitting parameters from Panacharoenawad wax deposition model (msr1 and msr2) [10] have been used instead.

2.2.5 Buildup term

Previously, the aging term in the change rate of wax mass is quantified. For the next step, the buildup term which is related to the increase in deposit’s thickness will be presented. From the following equation, it is believed that the difference between the total incoming wax mass flux and the wax mass flux associated with the aging process accounts for the buildup term.

$$-2\pi r_i L_{pipe} \bar{F}_w \rho_{oil} \frac{dr_i}{dt} = 2\pi r_i L_{pipe} \underbrace{[J_{M,Total} - J_{M,Aging}]}_{J_{buildup}} \quad (0-58)$$

where $J_{M,Total}$ is the convective wax mass flux in the oil side from the bulk to the deposit's interface $\left(-\overline{D}_e \frac{\partial C}{\partial r}\Big|_{r_i^+}\right)$ and $J_{M,Aging}$ is related to the diffusive mass flux of waxy components into the deposit side from the interface to the pipe's wall $\left(-\overline{D}_{wo} \frac{\partial C}{\partial r}\Big|_{r_i^-}\right)$. From the following schematic, $J_{M,Total}$ and $J_{M,Aging}$ are illustrated in wax deposition phenomenon.

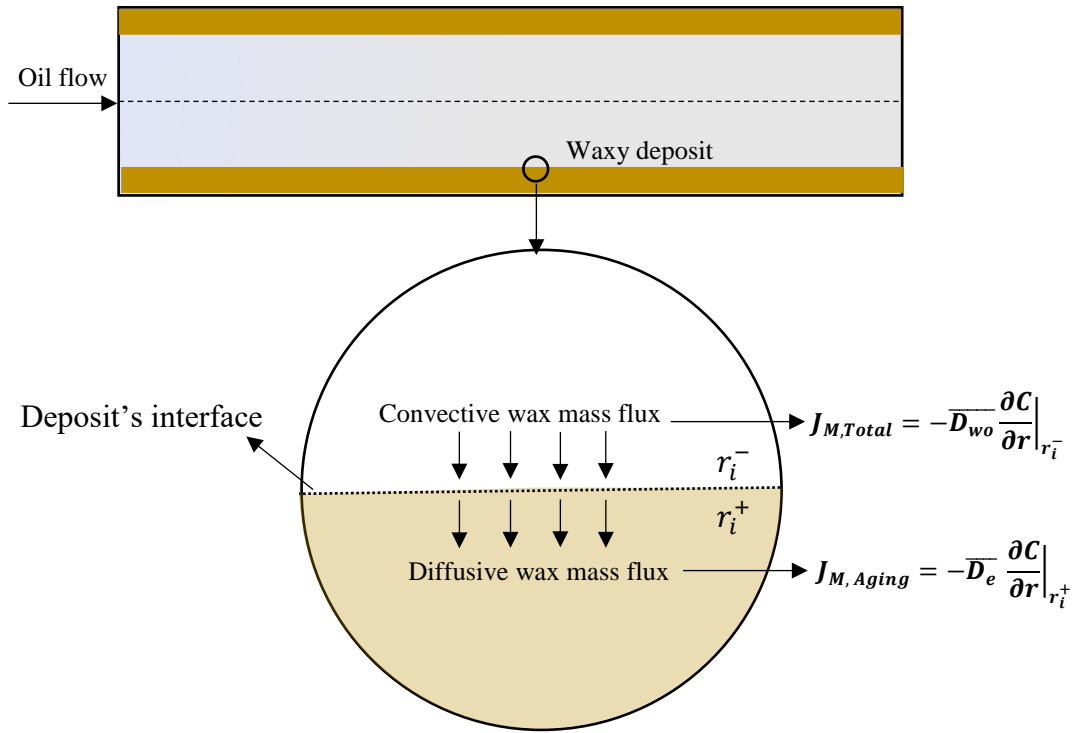


Figure 0-4: Incoming and diffusive wax mass flux at the waxy deposit's interface

The total incoming wax mass flux can be approximated by:

$$J_{M,IN} \equiv k_l(C_b - C_i) = -\overline{D}_{wo} \frac{\partial C}{\partial r}\Big|_{r_i^-} \quad (0-59)$$

As previously discussed, the concentration profile can be calculated using three wax mass flux scenarios. In the partial precipitation, the proposed approach from Lee [12] includes

the precipitation rate parameter (k_r) which could vary from 0 to infinity. When k_r approaches to infinity (solubility method), a minimum value for the wax mass flux is provided. However, studies have shown that the wax mass flux could be less than the solubility method [10]. This finding specifically reveals the importance of the shear effect which is ignored by Lee [12]. Moreover, the precipitation rate (k_r) range is very wide which could not be easily estimated using the optimization tools. Therefore, Panacharoensawad model [10] is chosen for our model. In Panacharoensawad model, the maximum tolerable shear stress parameter was introduced which increase linearly as \bar{F}_w increases. When shear stress reaches to the maximum tolerable value, the buildup term becomes zero and the depot's thickness does not increase. On the other side, it is assumed that the deposit can grow freely when there is no shear effect (oil velocity = 0). The following equations accounts for the above assumptions [10]. The maximum allowable shear stress is:

$$\tau_{max} = \tau_{ini} * MSR_1 * \bar{F}_w + \tau_{ini} \quad (0-60)$$

where it is related to the wax mass flux parameters as:

$$J_B = J_{BM} \frac{\tau_{max} - \tau}{\tau_{max}} = J_{BM} SR_1 \quad (0-61)$$

J_B and J_{BM} are actual and maximum buildup wax mass flux terms, respectively. In addition, SR_1 is referred as shear effect multiplier. The second fitting parameter from Panacharoensawad [10] is MSR_2 . This parameter is used to account for (k_α and k_r) which were used in the previous wax deposition models. SR_1 , and SR_2 are employed to adjust the growth and aging equations in wax deposition governing equations as follow [10]:

$$\frac{d\bar{F}_w}{dt} = \frac{2r_i \left(-\bar{D}_e \frac{\partial C}{\partial T} \frac{\partial T}{\partial r} \Big|_{r_i^+} \right)}{\rho_{dep}(R^2 - r_i^2)} SR_2 \quad (0-62)$$

and

$$\frac{dr_i}{dt} = \frac{-1}{F_w \rho} \left[\left(-\bar{\mathcal{D}}_{wo} \frac{\partial C}{\partial r} \Big|_{r_i^-} \right) - \left(-\bar{\mathcal{D}}_e \frac{\partial C}{\partial r} \Big|_{r_i^+} \right) SR_2 \right] SR_1 \quad (0-63)$$

where SR_2 is defined as:

$$SR_2 = MSR_2 \frac{\tau - \tau_0}{\tau_0}; 0 \leq SR_2 \leq 1 \quad (0-64)$$

Through SR_1 and SR_2 multipliers, the initial deposition formation and the deposit's growth rate are addressed [10]. All above parameters in above equations $\left(\frac{\partial T}{\partial r} \Big|_{r_i^+}, \frac{\partial C}{\partial T} \Big|_{r_i^+} \text{ and } \frac{\partial C}{\partial r} \Big|_{r_i^-} \right)$ are calculated by knowing the temperature and concentration profiles. In the next section (calculation and implementation), the detailed calculation procedures are explained.

Eq. 0-62 and 0-63 are solved using the Dormand-Prince (RKDP) ODE solving method [68] which uses adaptive time steps and shows good accuracy. RKDP has also been used for non-uniform discretization. In addition, Levenberg–Marquardt optimization tool [69] has been coded in SP-Depo for fitting parameter adjustment (e.g., MSR_1 and MSR_2)

2.2.6 Laminar Flow Formulation

The above formulation is specifically developed for the turbulent flow condition which is included in the SP-Depo software. However, we also investigated the wax deposition process under the laminar flow through a separate paper [70]. In that paper, we simulated a wax deposition predictor in C++ under the laminar flow. The results were confirmed by data of more than twenty-five flow-loop experiments [3]. More details are presented in later chapters of this document. Please note that the presented methodology is only included in our paper [70] (not in SP-Depo software)

Wax deposition equations under laminar flow are very similar to the equations related to the turbulent flow case (explained above). However, there are slight differences which are elaborated in this section.

For heat and mass transfer coefficient calculations, Chilton–Colburn analogy has been used where Hausen empirical Nusselt number correlation [71] is used for long pipes as shown:

$$Nu_p = 3.66 + 1.7813 \times 10^{-3} \frac{G_{z,p}^{5/3}}{(1 + 0.04G_{z,p}^{2/3})^2} \quad (0-65)$$

and for short lab-scale pipes, Seider and Tate correlation [72] is suggested as follows:

$$Nu_p = 1.24 G_{z,p}^{1/3} \quad (0-66)$$

where subscript "p" can be replaced by "mass" and "heat" for mass transfer and heat transfer coefficient calculations, respectively. Finally, Graetz number can be calculated as:

$$G_{z,heat} = \frac{Re \times Pr \times 2R}{x} \quad (0-67)$$

$$G_{z,heat} = \frac{Re \times Sc \times 2R}{x} \quad (0-68)$$

Then, heat and mass transfer coefficients are calculated as:

$$Nu_{heat} = \frac{hD}{k} = - \frac{D}{T_b - T_i} \frac{\partial T}{\partial r} \Big|_{r=r_i^-} \quad (0-69)$$

$$Nu_{mass} = \frac{k_l D}{D_{wo}} = - \frac{D}{C_b - C_i} \frac{\partial C}{\partial r} \Big|_{r=r_i^-} \quad (0-70)$$

So, the first term in Eq. 0-63 will be changed to:

$$-\mathcal{D}_{wo} \frac{\partial C}{\partial r} \Big|_{r_i^-} = k_l (C_b - C_i) \quad (0-71)$$

where C_b and C_i are solubility terms at the bulk and at the deposit's interface, respectively.

Eq. 0-71 considers instantaneous precipitation and it is another representation of the no precipitation wax mass flux scenario which is explained in Chapter 1. Furthermore, aspect ratio of the wax crystals in the deposit (α) is calculated using Eq. 0-56 where it is linearly correlated to the solidified wax fraction.

To correctly account for the mass balance, it is important to consider the axial depletion which is presented by the following relation:

$$\frac{dC}{dz} = -k_l(C_{b_0} - C_i) * 2\pi r_i * \frac{\rho_L}{w_h} \quad (0-72)$$

We solved the governing ODEs ($\frac{dr_i}{dt}$ and $\frac{d\bar{F}_W}{dt}$) using RK45 and solved Eq. 0-72 in each half/full time step of RK45. By applying this method, we made sure that the updated C_b is considered in our calculations. Eq. 0-72 was solved using RK4 method.

In order to tune the prediction to match the experimental data, the fitting parameter (k_α) was adjusted. Since one of the objectives of our paper was to understand the potential effects of different factors on k_α , Levenberg–Marquardt tool was used for fitting parameter adjustment.

CHAPTER 4

SOFTWARE DEVELOPMENT AND IMPLEMENTATION

In this section, the calculation procedure and software's structure of our two developed software will be thoroughly explained. SP-Wax is our first software which utilizes a very strong thermodynamic model for predicting different SLE characteristics of the waxy solutions. SP-Depo is our second software which is developed to model wax deposition phenomenon in pipe. In SP-Depo, a new wax deposition model is developed which incorporates SP-Wax thermodynamic model directly in the wax deposition calculation. For both software, the simulation results are verified with extensive experimental data.

2.3 SP-Wax software

The open-source software (SP-Wax) for the solid–liquid equilibrium (SLE) calculation of paraffin is presented. Paraffin modeling is important to many industries and engineering applications. SP-Wax provides reliable predictions for phase behavior of paraffinic solutions, which is crucial for petroleum industry. The Coutinho et al. thermodynamic model was primarily used and coded in SP-Wax. The developed simulation was validated by experimental data of binary and multicomponent systems. Solid phase compositions were successfully estimated, and aging process of wax deposition problem was analyzed. Within the software, core calculations were coded in C++ and OpenMP parallel programming technique was incorporated to improve the performance .A C# Windows Forms user interface was created to ensure the reusability of the software for both technical and non-technical users. The following flow chart represent the programming structure of SP-Wax.

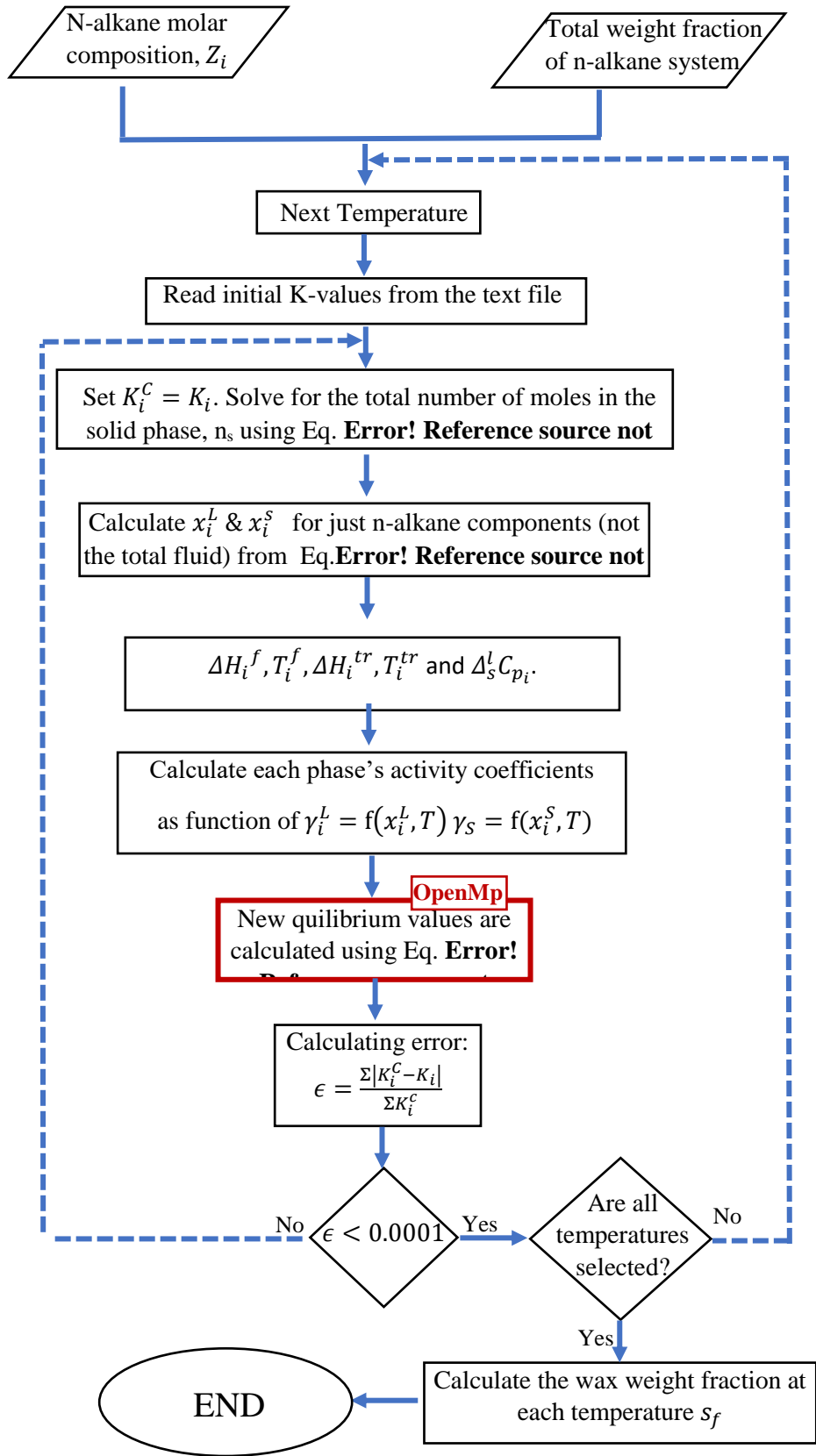


Figure 0-1:SP-Wax flowchart for calculation of the precipitation curve

We initially tried to code the SP-Wax in MATLAB however, the speed was extremely slow in the calculation of solid phase activity coefficients. So, if the speed of the thermodynamic model was not short enough, we might have encountered huge problems in the wax deposition software (SP-Depo). Therefore, we switched to C++ programming language and incorporated OpenMp parallel tool to optimize the performance even more. We were able to decrease the run-time from 50 seconds to less than 1 second for each temperature point. The simulation run-time was very important because the thermodynamic model was going to be called repeatedly within the wax deposition software (SP-Depo). Additionally, we further decreased the run-time by excluding those carbon number components with much lower melting temperatures from the calculations. The following graph shows the run-time of the simulation for South Pelto oil sample with 60 n-alkane components. Please note that SP-Wax incorporates 8 threads because it uses OpenMp parallel programming technique.

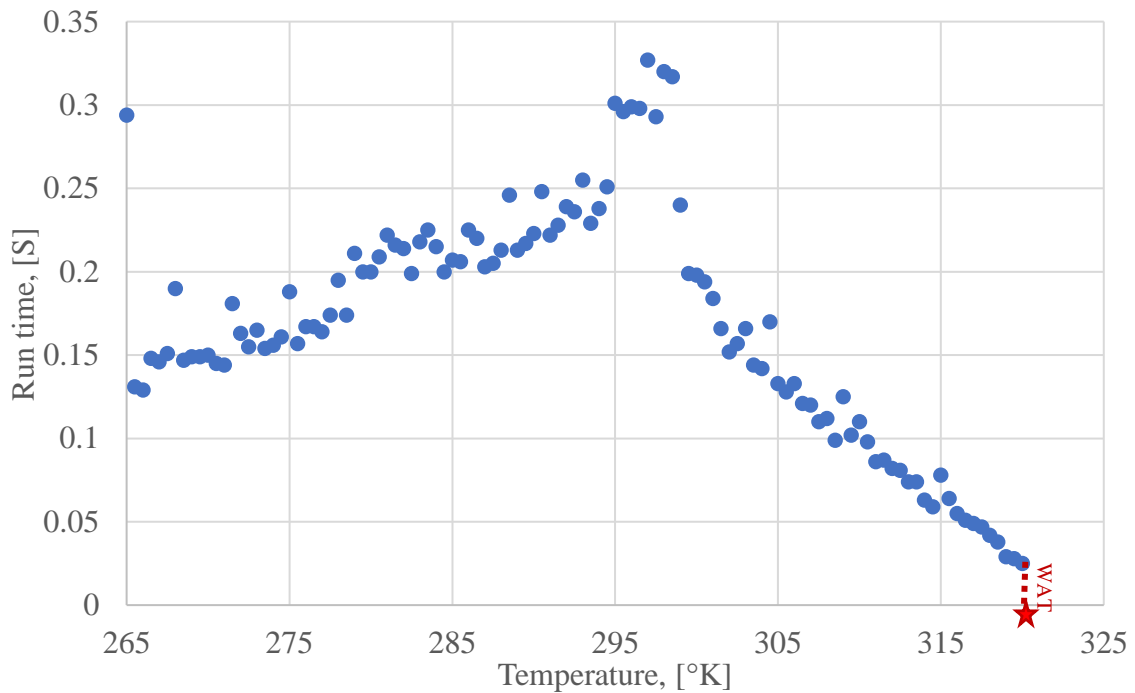


Figure 0-2:SP-Wax run-time at different temperatures

In SP-Wax, core computation (the thermodynamic model) is coded in C++ and a graphical user interface (GUI) has been developed in C# for maximum reusability. SP-Wax's functionality is divided into four categories including 1) Thermodynamics of binary

systems 2) Precipitation curve 3) Single-temperature SLE modeling 4) Critical Carbon Number (CCN) estimation. Last three categories are for multi-component systems. There are unique cpp and exe files for each of the mentioned functionalities. In the following picture, all source and executable files of SP-Wax are shown.

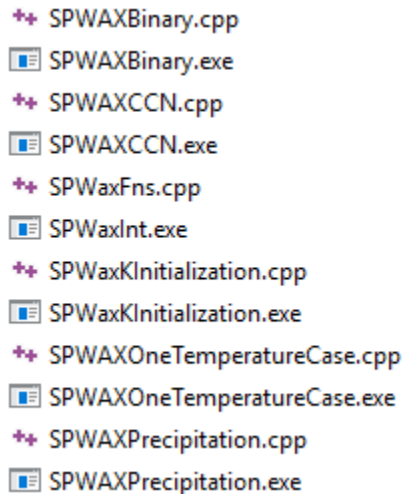


Figure 0-3: Source and executable files in SP-Wax (Computations of SLE model)

In the following section, all cpp and executable files are individually explained. Please note that each exe file will be executed from C# GUI when it is called.

2.3.1 SPWaxInt.exe

This exe file is for the GUI and should be clicked first by the user. Communication between C++ and C# is mainly done through the text files. The user provides the inputs in Windows Form interface and, C# generates set of text files that contain the inserted inputs. When “Run Simulation” button is clicked, corresponding C++ executable file will run. The C++ exe-file requires set of input files which have already been created by C#. So, the C++ exe-file will run successfully and will report the outputs in through text files. Then, the user can plot the data within the GUI. For data visualization, C# reads the newly created output text files (generated by C++ exe file) and plots the output data.

2.3.2 SPWaxFn (cpp & header)

These files include the functions which have been used in SP-Wax for the multi-component system SLE modes.

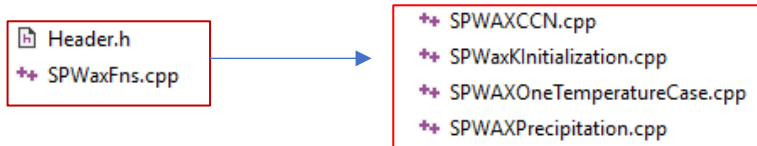


Figure 0-4: The header and cpp files in SP-Wax software

All multi-component system source files use the same functions which are defined and listed in “SPWaxFn.cpp” and “Header.h.” In SPWaxFn.cpp, more than seventy-five lines of comments are included in every step to elaborate all variables and functions. In the header file, the list of functions is:

```

double TempFusYang(int CN);
double HeatFusYang(int CN);
double HeatFus(int CN);
double HeatTrans(int CN);
double HeatVap(double T, int CN);
double TempFus(int CN);
double TempTrans(int CN);
double *ArrayRetA();
double *ArrayRetB();
double *ArrayRetC();
double *ArrayRetD();
double Vm(double T, int CN);
double Vw(int CN);
double LambdaCorr3(int CN1, int CN2, double T, double CF);
double LambdaCorr1(int CN1, int CN2, double T, double CF);
double LambdaCorr2(int CN1, int CN2, double T, double CF);
double GammaSolid(int CN1, double X_S[], int MinC, int MaxC, double T, double CF);
double GammaSolMes(int MinC, int CN1, int CompNum, int CarbonNum[], double X_S[], double T, double CF);
double GammaLiqMesFFV(int MinC, int NumOfCN1, int CN1, int CompNum, int CarbonNum[], double X_L[], double T);
double GammaLiqMesEFV(int MinC, int NumOfCN1, int CN1, int CompNum, int CarbonNum[], double X_L[], double T);
double objFunc(double nS, int CompNum, double Z[], double K[]);
double objFuncDer(double nS, int CompNum, double Z[], double K[]);
double Fsolve(double nS, int CompNum, double Z[], double K[]);
  
```

Figure 0-5: Function in SP-Wax software

Some of the functions are explained in the following section.

- `Vm(double T, int CN)`

Molar volumes are calculated by DIPPR correlations [24] and GCVOL method[26].
`*ArrayRetA()`, `*ArrayRetB()`, `*ArrayRetC()` and `*ArrayRetD()`

By these functions, coefficients of DIPPR molar volume correlations [24] are read from DIPP.txt which are used in SP-Wax. Following table contains coefficients for different n-alkane components for DIPPR correlations.

- `Vw(int CN)`

Van der Waal volume which is calculated from group contribution method proposed by Bondi[25].

- `LambdaCorr3(int CN1, int CN2, double T, double CF)`

Λ_{ij} is required in solid phase activity coefficient calculations. Energetic interaction parameter between two n-alkane are included in Λ_{ij} which is expressed differently in literature. We analyzed three models in the literature for Λ_{ij} (`LambdaCorr1`[18], `LambdaCorr2` [31] and `LambdaCorr3` [14]) and included all of them in our function source file. After comparing different cases, `LambdaCorr3` was used in SP-Wax with slight modification of the correction factor.

- `HeatFusYang(int CN)` and `double TempFusYang(int CN)`

These correlations are for heat and temperature of fusion for different carbon numbers. These two correlations are proposed by Yang et al. [31]. However, they are have not been used in SP-Wax. The functions are included for potential developers to use if desired.

- `HeatFus(int CN)` and `TempFus(int CN)`

Coutinho et al.[19] proposed two correlations for temperature and enthalpy of fusion for which are used in SP-Wax. Values form these two correlations are compared to experimental data which is presented in the last chapter of this manual.

- `HeatTrans(int CN)` and `TempTrans(int CN)`

Coutinho et al.[19] also provided correlations for temperature and enthalpy of solid phase transition. We used these two correlations in SP-Wax.

- `HeatVap(double T, int CN)`

Heat of vaporization is expressed through Extension of Pitzer CSP models[32]. There are uncertainties among experimental enthalpies of vaporization from different sources. Therefore, available correlations carry the mentioned uncertainties too. In this study, we compared the predictions from CSP model with two sets of experimental vaporization enthalpy data at $T = 25^{\circ}C$ and satisfactory results were observed.

- o **GammaSolMes** (solid phase activity coefficients)

For solid phase activity coefficient, two functions are created for Wilson model. **GammaSolMes** (shown below) is used in SP-Wax.

```
/*
Non-ideality of solid phase (activity coefficients, Gamma_Solid)
Wilson methodology
This function is primarily used for binary systems and has also been verified for multicomponent systems
*/
double GammaSolMes(int MinC, int CN1, int CompNum, int CarbonNum[], double Xs[], double T, double CF)
{
    double SumE = 0;
    double Sum1 = 0;
    double Sum2 = 0;
    for (int CN2 = MinC; CN2 < (CompNum + 1); CN2++)
    {
        SumE = SumE + LambdaCorr3(CN1, CarbonNum[CN2], T, CF)*Xs[CN2]; //checkt eh CN2-1
    }

    Sum1 = 0;
    for (int CN3 = MinC; CN3 < (CompNum + 1); CN3++)
    {
        double Sum2 = 0;
        for (int CN4 = MinC; CN4 < (CompNum + 1); CN4++)
        {
            Sum2 = Sum2 + LambdaCorr3(CarbonNum[CN3], CarbonNum[CN4], T, CF)*Xs[CN4];
        }
        Sum1 = Sum1 + LambdaCorr3(CarbonNum[CN3], CN1, T, CF)*Xs[CN3] / Sum2;
    }
    return(exp(-log(SumE) + 1 - Sum1));
}
```

MinC:	Minimum carbon number to be included in SLE calculation
CN1:	Desired carbon number that activity coefficient is calculated for
CompNum:	Total number of n-alkane components
CarbonNum[]:	Returns carbon number
Xs[]:	Solid phase composition
T:	Temperature
CF:	Correction factor

Figure 0-6:Solid phase activity coefficient function used in SP-Wax

- o **GammaLiqMesFFV** (liquid phase activity coefficients)

We analyzed several models for liquid phase activity coefficients and found that Flory-free volume [28] and Entropic free-volume [23] models are the best candidates to be included in SP-Wax. Both models are included in the function cpp file (`GammaLiqMesFFV`, `GammaLiqMesEFV`). Although, both models are good, `GammaLiqMesEFV` function has been used to express the liquid phase activity coefficients in SP-Wax. Function input variables are very similar to the solid phase activity coefficient function (`GammaSolMes`) which was thoroughly explained previously.

2.3.3 SPWaxBinary (.exe & .cpp)

SP-Wax is designed to work for binary and multi-component systems. `SPWaxBinary.cpp` and `SPWaxBinary.exe` are the only source and executable files for the binary system case. The user provides the required inputs and C# creates several text files which are needed for C++ executable files. The main output from binary n-alkane system is to obtain Wax Appearance Temperature (WAT) for different solute mole fraction values. For example, the created text files are shown in the following picture.

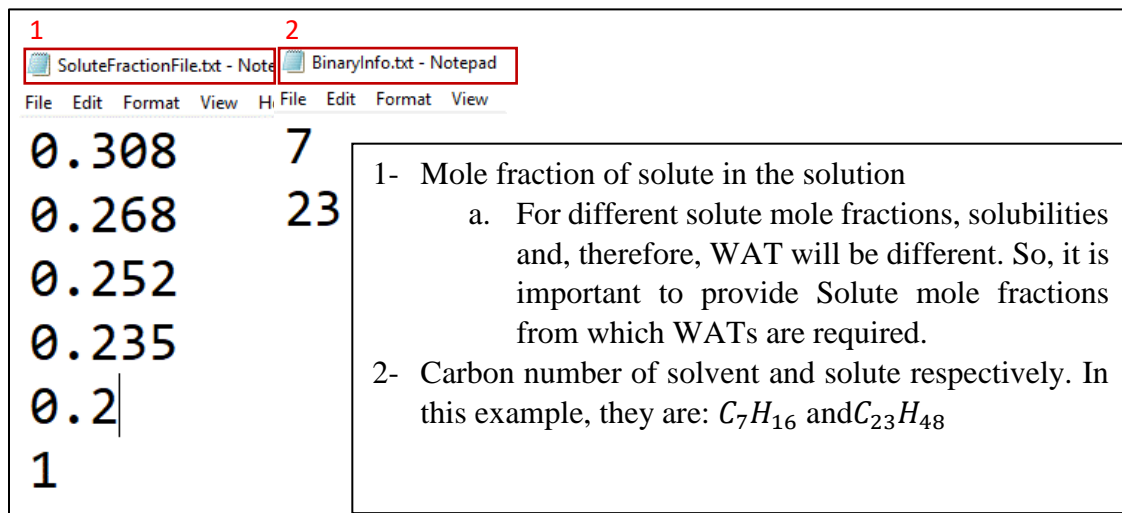


Figure 0-7: The created input files for the binary system option

SP-Wax reads one value of solute mole fraction and calculates n_s at different temperatures till it reaches to a high enough temperature where no more solidified particle is formed ($n_s = 0$). The corresponding temperature will be saved, and it will be reported as WAT for that specific solute mole fraction. Then, the next value of solute mole fraction is read, and the same procedure is followed. At the end, all saved WATs will be reported to a text file

which is called “OutPutBinary.txt”. Please remember that DIPR.txt has to be present in the same directory as SPWaxBinary.exe too.

This source code is designed to estimate the smallest temperature at which all solute components are dissolved in liquid phase. This temperature is referred Wax Appearance Temperature (WAT). Required functions and main calculation are included in SPWaxBinary.cpp. All functions are identical to those that are used in multi-component system functions that are listed in SP-WaxFn.cpp except two functions that are specifically defined for binary system case including “**BinarySys**” and “**BinarySysDer**”. “**BinarySys**” calculates solid mole fraction (n_s) based on given temperature and solute mole fraction. “**BinarySysDer**” calculates the derivative of “**BinarySys**” based on Temperature. Please refer to SPWaxBinary.cpp for more information about all other functions.

In the main section (“int main”), the general goal is to find the temperature that results in zero solid particles for function “**BinarySys**”. Newton Raphson was chosen to find the root which requires an initial value. There were two main difficulties that needed to be taken care of. The first one was the initial value for T . The second problem was encountered when too high initial temperature beyond WAT was selected in Newton Raphson, “nan” was resulted and crashed the program. We found that if a relatively close T is chosen for an initial guess, such convergence problems will be vanished. So, in the main body, we followed a step-by-step procedure to find a good initial value for temperature for Newton Raphson method to find WAT. The numerical method was validated by fifty experimentally measured WAT data points. In the following picture, first two while-loops are used to find proper initial value for temperature and the third while-loop is used to find WAT.

```

/*The temperature that does not result in nan value is detected here
in this while loop*/
while (isnan(BinarySys(FracParam[j], T)))
{
    T = T + step1;
    a = BinarySys(FracParam[j], T);
}

/*A new temperature step is used to move forward
to find WAT (by two following while loops)*/
step = 1;
a = BinarySys(FracParam[j], T);
while (abs(BinarySys(FracParam[j], T)) > 0.0001)
{
    T = T + step;
    a = BinarySys(FracParam[j], T);
    if (BinarySys(FracParam[j], T) < 0 || isnan(BinarySys(FracParam[j], T))) {
        T = T - step;
        break;
    }
}

a = BinarySys(FracParam[j], T);
while (abs(err) > pow(10, -9))
{
    T = T - BinarySys(FracParam[j], T) / BinarySysDer(FracParam[j], T);
    err = BinarySys(FracParam[j], T);
}

```

Figure 0-8: A snapshot of SPWaxbinary.cpp

2.3.4 SPWaxKInitialization (.exe & .cpp)

In the development process of the SP-Wax software, we found that convergence problem could be encountered in higher temperatures (close to WAT). The problem was because of the initial guesses of equilibrium constants. We solved this problem by generating sets of initial k-values at various temperatures which will be called with SP-Wax is executed. These initial k-values are generated by SPWaxKInitialization.cpp. In this C++ source file, set of K values are generated which will be used by other executable files in SP-Wax.

SPWaxKInitialization.cpp is a C++ source file that takes input information of the oil sample (from GeneralInput.txt) and calculates the equilibrium constant values at every half-temperature ($\Delta T = 0.5^{\circ}\text{K}$) ranging from 280.15°K to WAT. The calculated K values are reported in “KInitialVal.txt”. For this source file, initial values for equilibrium constants are also needed for $T = 280.15^{\circ}\text{K}$. There is a text file (“KInput.txt”) which

includes 62 K values for C_1 to C_{62} which are used in this source file as initial values of equilibrium constant at $T = 280.15^{\circ}K$. The initial equilibrium constants are not only temperature dependent. They are also dependent on oil composition. In other words, for each oil composition, new equilibrium constants need to be calculated which will be used throughout other SP-Wax functionalities.

In order to run SPWaxKInitialization.exe, following files (shown below) should be in the same directory.

-  [Data.txt](#) → Oil composition
-  [DIPP.txt](#) → DIPPR molar volume coefficients
-  [GeneralInputs.txt](#) → Inputs (provided in C# by the user)
-  [KInput.txt](#) → Initial K values at 280.15K
-  [SPWaxKInitialization.exe](#)

When SPWaxKInitialization.exe is ran, following two text files are generated:

-  [KInitialVal.txt](#)
-  [NumLine.txt](#)

where “KInitialVal.txt” is k-values for every half temperature starting from $280^{\circ}K$ to WAT and “NumLine.txt” is a text file that contains total number of temperature points.

2.3.5 SPWaxPrecipitation (.exe & .cpp)

This option is developed to predict the precipitation curve and Wax Appearance Temperature (WAT) of the provided oil composition for the desired temperature range. When input data are provided, C# produces text files that contain input data for C++ exe files. The following picture is an example of created text files as inputs to SPWaxPrecipitation.exe

GeneralInputs.txt - Notepad		PrecipitationCurveWAT.txt - Notepad	
File	Edit	Format	View
1 14.77	5 100		1- Wax content in total fluid
2 0.000003	6 280		2- Coefficient Adjustment
3 10	7 0.5		3- Minimum C_n to be included
4 62	8 0.0001		4- Total number of n-alkanes
	9 0.001		5- Number of points in curve

Starting temperature

Temperature interval

Acceptable error

Acceptable error

Figure 0-9: General required inputs for the multicomponent system option

Now that inputs are provided, the simulation can run to calculate the precipitation curve and WAT. However, these data are not enough to run the simulator. The following graph shows the required files which should be present in the same directory for SP-Wax to run:

- 📄 Data.txt → Coefficients of DIPPR for molar volumes
- 📄 DIPP.txt → N-alkane mole composition
- 📄 GeneralInputs.txt → Inputs (provided in C# by the user)
- 📄 KInitialVal.txt → Initial K values generated by SPWaxKInitialization.exe
- 📄 NumLine.txt → Number of temperature points in KInitialVal.txt
- 📄 PrecipitationCurveWAT.txt → More inputs for precipitation curve prediction (in C# by
- exe SPWAXPrecipitation.exe

The outputs are stored in following text files:

- WAT.txt (Wax Appearance Temperature is stored as second number)
- Wax weight fraction.txt (solid phase fraction values)
- SolidWComposition.txt (solid phase compositions of the temperature range)

For precipitation and WAT calculations, SP-WaxFn.cpp and Header.h are required to access the required functions in the main source file. In SPWaxPrecipitation.cpp, a major for-loop is used to iterate the desired temperatures. Inside the mentioned for-loop, SLE characteristics are calculated and saved to arrays. However, if temperature passes WAT, the program detects it and moves back to find WAT with the desired accuracy. Since, the program performs fast in higher temperatures, this method is a safe way to avoid any convergence problem.

2.3.6 SPWaxOneTemperatureCase (.exe & .cpp)

This option of the SP-Wax allows users to obtain different SLE characteristics of a multi-component solution at any desired temperature. The user provides the temperature and C# makes a text file with the given temperature which will be accessed by C++ executable file. The following data files are required to be in the same directory, so C++ exe file can run:

- 📄 Data.txt → N-alkane mole composition
- 📄 DIPP.txt → Coefficients of DIPPR for molar volumes
- 📄 GeneralInputs.txt → Inputs (provided in C# by the user)
- 📄 KInitialVal.txt → Initial K values generated by SPWaxKInitialization.exe
- 📄 NumLine.txt → Number of temperature points in KInitialVal.txt
- 📅 SPWaxOneTemperatureCase.exe
- 📄 TempCase.txt → Desired temperature °K

The output text files are as follow:

- Wax weight fraction.txt (Solid wax fraction in total fluid)
- Concentration.txt (Relative concentration of n-alkanes in the paraffin system)
- DissolvedMass.txt (mass of n-alkanes that are dissolved in the liquid phase)
- K_values.txt (equilibrium constant from the last iteration)
- LiquidMoleComposition.txt (normalized mole composition of n-alkanes in the liquid phase)
- LiquidWComposition.txt (normalized weight composition of n-alkanes in the liquid phase)
- SolidMoleComposition.txt (normalized mole composition of n-alkanes in the solid phase)
- SolidWCompositionOnetemp.txt (normalized weight composition of n-alkanes in the solid phase)

All above output text files are generated after running SPWaxOneTemperatureCase.exe. In SP-Wax, a combo-box has been designed that lets users choose the desired parameter to plot.

2.3.7 SPWaxCCN (.exe & .cpp)

Aging is one of the most important concepts in wax deposition phenomenon. In SP-Wax, a new parameter which represents the relative concentration of a specific n-alkane is defined which is used to predict CCN. Waxy deposits are in contact with the bulk fluid and pipe's wall with corresponding temperatures of T_{int} and T_{wall} . In SP-Wax, relative concentrations of all n-alkanes at T_{int} are subtracted from relative concentrations of all n-alkanes at T_{wall} . The smallest carbon number with positive relative concentration gradient value is considered to be Critical Carbon Number (CCN).

C# asks for two temperature values which are corresponded to T_{int} and T_{wall} in GUI. The two temperatures are then written to a text file which is called "TempCaseCCN.txt". The calculated relative concentration gradients are reported in a text file "ConcentrationGradient.txt". The following picture shows that the required files that need to be in the same directory to run "SPWaxCCN.exe"

-  Data.txt → N-alkane mole composition
-  DIPP.txt → Coefficients of DIPPR for molar volumes
-  GeneralInputs.txt → Inputs (provided in C# by the user)
-  KInitialVal.txt → Initial K values generated by SPWaxKInitialization.exe
-  NumLine.txt → Number of temperature points in KInitialVal.txt
-  SPWAXCCN.exe
-  TempCaseCCN.txt → T_{int} and T_{wall} for Relative concentration calculation

This source file calculates the relative concentration of the n-alkanes at two given temperatures (T_{wall} and T_{int}). Then, relative concentrations of n-alkanes at higher and lower temperatures will be subtracted. Resulted relative concentration gradient values will be exported to a text file "ConcentrationGradient.txt". The following picture is a snapshot of SP-Wax graphical user interface:

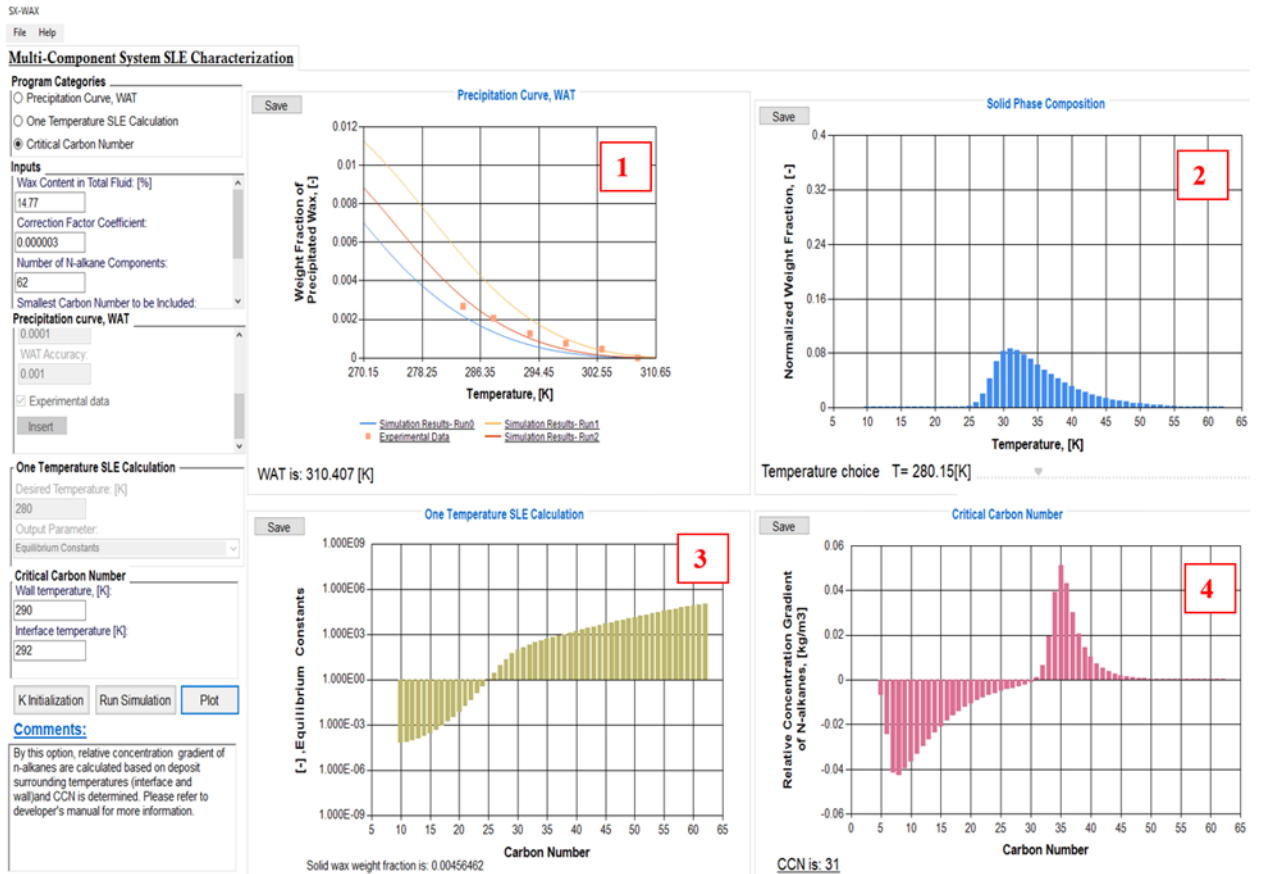


Figure 0-10: SP-Wax interface for multicomponent systems with various functionalities. The inputs are given through different textboxes on the left of the screen and the plots are created. In [1] the predicted and experimental precipitation curves can be plotted, in [2] the solid phase composition can be plotted for the given temperature range using a trackbar, in [3] different SLE characteristics can be plotted (as desired) for the provided temperature point and, in [4] the relative concentration gradient is plotted for CCN determination

2.4 SP-Depo software

Before going through the details about the computation procedure of SP-Depo, our software's structure will be discussed. In this section, a detailed description about different parts of SP-Depo's code is presented. In SP-Depo, the core calculation is coded in C++ through more than 12,500 lines of code in object-oriented programming style. C++ was chosen because it is one of the fastest programming languages available. To further optimize SP-Depo's performance, we have used OpenMp parallel programming technique

which employs maximum capacity of all processors. In Figure 0-11, it can be seen that almost 100% of all processors have been used periodically due to parallelism.

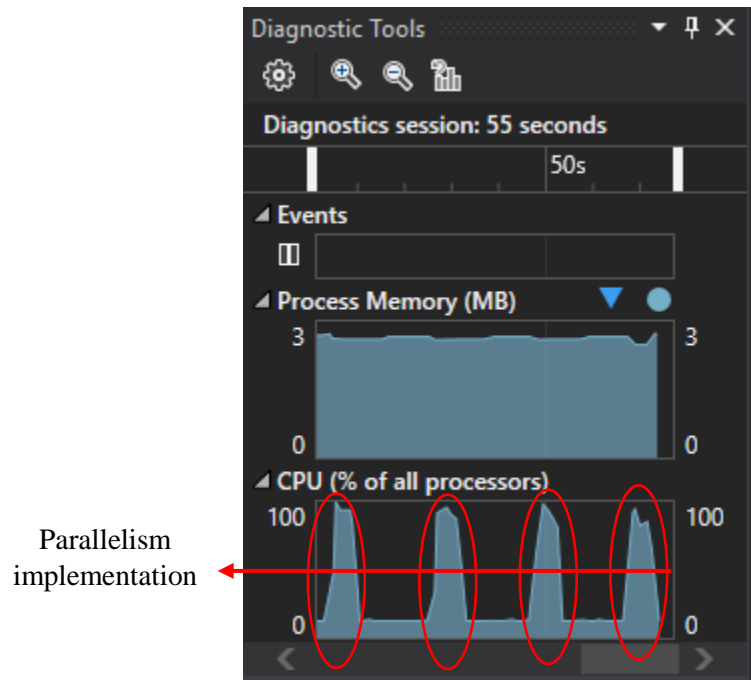


Figure 0-11: An example of SP-Depo's diagnostic session during LM run.

On the other side, a C# Windows Forms Graphical User Interface (GUI) has been developed for guaranteed practicality for technical and non-technical users. SP-Depo is the world's first compositional wax deposition software. In SP-Depo, several equations are solved analytically using various advanced numerical methods which have been coded through separate functions in the program. Some of the applied numerical techniques are: Newton-Raphson and bisection root-finding algorithms, PDE solving methods (e.g., Finite Difference Method, FDM), various matrix operations, ODE solving methods (e.g., Dorman Prince, RKDP), integration techniques, a modified regression method and Levenberg-Marquardt optimization algorithm. In the following section, only the program's structure in C++ will be discussed since It contains the scientific computation related to wax deposition modeling

The following graph shows a quick map of SP-Depo's header files in C++. Each header file (.h) is exclusively described later in this document.

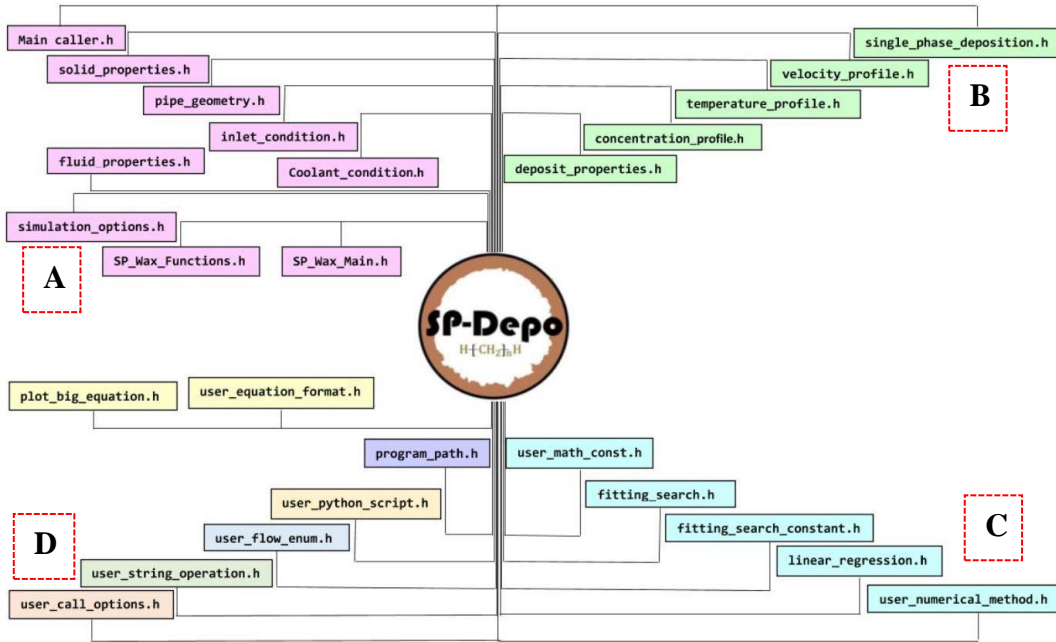


Figure 0-12: C++ header-files of SP-Depo

In the above graph, the header-files in “A” section represents those files that mostly contain the input information and are called repeatedly throughout the program. In section “B”, the wax deposition and transport equations are solved with constant communication with section “A” and “C”. In section “C”, all numerical methods are included which are responsible in calculation of different parameters in section “B”. In the last group (“D”), other files are included which are mainly responsible in data visualization, program’s directory, etc.

2.4.1 Primary programming path

In SP-Depo, the input files are read, many parameters are calculated using the transport equations and the two governing wax deposition ODEs (Eq.0-62 & 0-63) are solved numerically for full prediction of deposition profile. The primary path can be illustrated through five steps (shown below) within SP-Depo’s code. The order of the following steps is as if someone debugs the program from the outmost layer and proceeds into the most inner layer. The symbols show the most important executable methods which use functions from the inner layer classes.

- **Step 1**

SPDepo.cpp is where the entry point of the program exists (`int wmain(int argc, TCHAR **argv)`). Based on the argument input, the correct section of the code is executed. For this example, the “deposition single_phase” argument case is illustrated where the wax deposition prediction is performed with given fitting parameters. Through “**Deposition1PMain.Run(program_path)**”, the program runs the wax deposition model.

```

SPDepo.cpp
case spdepo::usr::kMainArgv2::deposition: {
    spdepo::usr::kMainArgv3 argv3;
    argv3 =
spdepo::usr::string_to_kmainarg3.at(argv[3]);
    switch (argv3) {

case(spdepo::usr::kMainArgv3::single_phase): {
    spdepo::Main1PhaseDeposition
    Deposition1PMain;

Deposition1PMain.Run(program_path); 
-----
    break;
}
}
    std::system("pause");
    return 0;
    break;
}

```

Figure 0-13: SP-Depo.cpp and Deposition1PMain.Run(program_path)

- **Step 2**

Within `void Main1PhaseDeposition::Run(ProgramPath p_path)`, all required object members of `deposition1` are initialized through different methods in `read_input` using the input files which are produced by C# GUI. With all provided input information, the calculation method will be called (`deposition1.Calculate()`) where the governing ODEs are solved numerically.

```

main_caller.cpp
void Main1PhaseDeposition::Run(ProgramPath p_path)
    ReadInput read_input;
    SPWax00::Thermo thermo_local;
    read_input.SetPath(p_path);
    Fluid oil = read_input.ReadLiquid1P();
    Solid pipe_material;
    PipeGeometry pipe;
    read_input.ReadPipe1P(&pipe, &pipe_material);
    InletCondition inlet = read_input.ReadInlet1P();
    CoolantCondition coolant_inlet;
    Fluid coolant_fluid;
    SimulationOptions sim_option;
    read_input.ReadCoolant1P(&coolant_inlet,
        &coolant_fluid, &pipe, &sim_option);
    read_input.ReadSimulationOption(&sim_option, coolant_inlet);
    Solid wax;
    wax.SetConstantProperties("wax", -950, -2000, 0.25);
    sim_option.SetWaxMaterialProperties(wax);
    SinglePhaseDeposition deposition1;
    deposition1.SetAll(sim_option,
        oil, coolant_fluid, inlet, coolant_inlet, pipe,
        pipe_material);
    thermo_local = read_input.ReadThermo1P(); //Added
    deposition1.SetThermo(thermo_local); //Added
    deposition1.SetProgramPath(p_path);

deposition1.Calculate(); 
    deposition1.SimplePostCalculation();

```

Figure 0-14: main_caller.cpp and deposition1.Calculate()

- **Step 3**

Within **deposition1.Calculate()**, the two governing ODEs (Eq.0-62 & 0-63) of the wax deposition theory are solved using the Dormand-Prince method. In the Dormand-Prince (DP) method, **WrapSolve1P** is the function that calculates the right-hand sides of the governing equations and returns them into a vector. The size of the returning vector is twice the number of axial sections. For example, if the pipe is discretized into 17 axial sections, the size of the returning vector will be 34. The first and second half of the returning vector will be associated with $\frac{dr}{dt}$ and $\frac{dF}{dt}$, respectively.

The Dormand-Prince ODE solving method is coded in `user_numerical_method.cpp`. In this `cpp` file, various numerical methods are independently coded as general functions which are utilized in different sections in SP-Depo. When the Dormand-Prince function (shown below) is executed, the pipe's effective radius, solid wax fraction and deposit's solid phase carbon number distribution of each axial section will be predicted for different time steps.



```

single_phase_deposition.cpp
void SinglePhaseDeposition::Calculate() {
    Initialize();
    std::vector<double> ri;
    std::vector<double> fw;
    std::vector<double> ri_fw;
    std::vector<double> eps_vec;
    std::vector<double> eps_fw_vec;
    long num_fn_call;
    CoreDepositionEquation DepEq;
    Storage_fit_eqs Storage_;
    ri = deposit_profile_.GetRiVec();
    fw = deposit_profile_.GetFwVec();
    DepEq.SetThermo(thermo_local, Is_Lm);
    DepEq.SetStorage(Storage_);
    DepEq.SetAll1Phase(*this);
    ptr_wrap = &DepEq;
    ptr_spdep = this; //compo_model
    ri_fw = ri;
    eps_vec.assign(ri.size(), 1.0e-4);
    eps_fw_vec.assign(fw.size(), 1.0e-3);
    ri_fw.insert(ri_fw.end(), fw.begin(), fw.end());
    eps_vec.insert(eps_vec.end(), eps_fw_vec.begin(),
    eps_fw_vec.end());
    //Time-loop is already in DormandPrinceMany
    ans_ri_fw_.clear();
    info_history.clear();
    if(DepEq.sim_dep_options_.GetPrecipitationCurveModel() ==
        usr::
            kPrecipitationCurveModel::user_defined){
        usr::DormandPrinceMany(WrapSolve1P, ri_fw.size(),
            &num_fn_call, &ans_t_, &ans_ri_fw_, ri_fw, 0.0,
            sim_dep_options_.GetDepositionDuration(),
            1, eps_vec, 100, 100, 3, 7000.0, 0.1, true, false, false);
    }
}

```



Figure 0-15: single_phase_deposition.h and Dorman-Prince method

- **Step 4**

As previously mentioned, `WrapSolve1P` returns a vector that contains the values of $\frac{dr}{dt}$ and $\frac{dF}{dt}$ for different sections of the pipe. Through the following structure, the `Solve1P(ri, fw)` was wrapped to be used as an input function in the `DormandPrinceMany` method.

```
single_phase_deposition.cpp

std::vector<double> WrapSolve1P(double t,
    const std::vector<double>& ri_fw_vec_vec)
{
    //ri_fw_vec_vec = {ri[0], ..., ri[N],
    fw[0], ..., fw[N]}
    int n_zsec = ptr_wrap->n_zsec_;
    std::vector<double>
    ri(ri_fw_vec_vec.begin(),
        ri_fw_vec_vec.begin() + n_zsec);
    std::vector<double>
    fw(ri_fw_vec_vec.begin() + n_zsec,
        ri_fw_vec_vec.end());
    return ptr_wrap->Solve1P(ri, fw); 
}
```

Figure 0-16: Main method to calculate the RHS of the governing ODEs

- **Step 5**

Solve1P(ri, fw) is the most important method in SP-Depo since it calculates temperature and concentration profile and reports the RHS of the two governing equations. There is one overloading function of **Solve1P** where each section's average temperature is also reported.



```

single_phase_deposition.cpp

std::vector<double> CoreDepositionEquation::Solve1P(
    const std::vector<double>& ri,
    const std::vector<double>& fw) {

&

    std::vector<double>
CoreDepositionEquation::Solve1P(
    const std::vector<double>& ri,
    const std::vector<double>& fw,
    std::vector<std::vector<double>>& TempInfo) {

```

Figure 0-17: two functions for calculation of ODEs

In the header-file map (shown previously), the header-files in “A” section will thoroughly be explained. Section “A” represents those files that mostly contain the input information and are called repeatedly throughout the program. For example, there are several class members in simulation_options.h which will be initialized by information from the input files. Later, those variables will be used in class methods of section “B”. In addition, we will discuss the theories associated with each calculation step within each header file. The following picture shows the header files associated with section “A”.

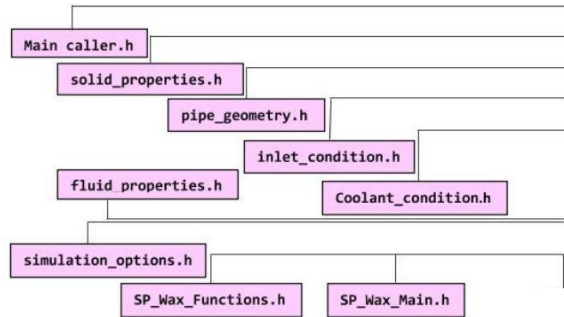


Figure 0-18: Input calling header-files (section “A”)

In the following sections, each header file associated with section “A” will thoroughly be explained.

2.4.2 **Main_caller.h** and **Main_caller.cpp**

Through Main_caller.h and Main_caller.cpp, the input files are read from the files which are produced by C# and then are assigned to the several class methods. The input files (produced by C#) are listed as shown in the picture.

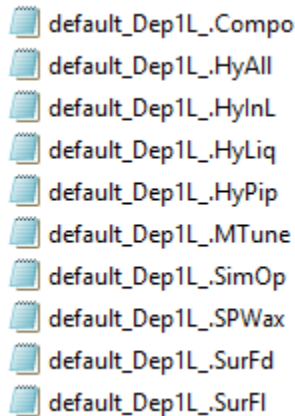


Figure 0-19: Created input files by C# which will be used by CPP files based on the provided input information by the user.

“default_Dep1L.Compo” represent the input n-alkane composition of the oil. “default_Dep1L.HyAll” includes all the input files for Load operation in C#. “default_Dep1L.HyInL” contains information about the inlet condition. “default_Dep1L.HyLiq” contains information about the rheological properties of the oil

including viscosity, density, specific heat capacity, thermal conductivity, etc. “default_Dep1L.HyPipe” has the pipe’s properties. “default_Dep1L.MTune” includes the required information for LM including the experimental data. “default_Dep1L.SimOp” contains the calculation options for wax deposition modeling including the time. Also, msr1 and msr2 should be specified in this file. “default_Dep1L.SPWax” contains the required input information for the thermodynamic model. “default_Dep1L.SurFl” includes the information about the surrounding including coolant temperature, flow direction, coolant flow rate, etc. All the above input files are reflected through several tabs in the interface of SP-Depo as shown in the following picture.

In some of the input tabs, the user is required to provide equations for certain parameters rather than just constant values. For example, fluid properties change with temperature and they need to be provided as equations. Later in this section, a complete manual will be presented about how to provide equations for some of the inputs. The associated header file is “User_equation_format.h”.

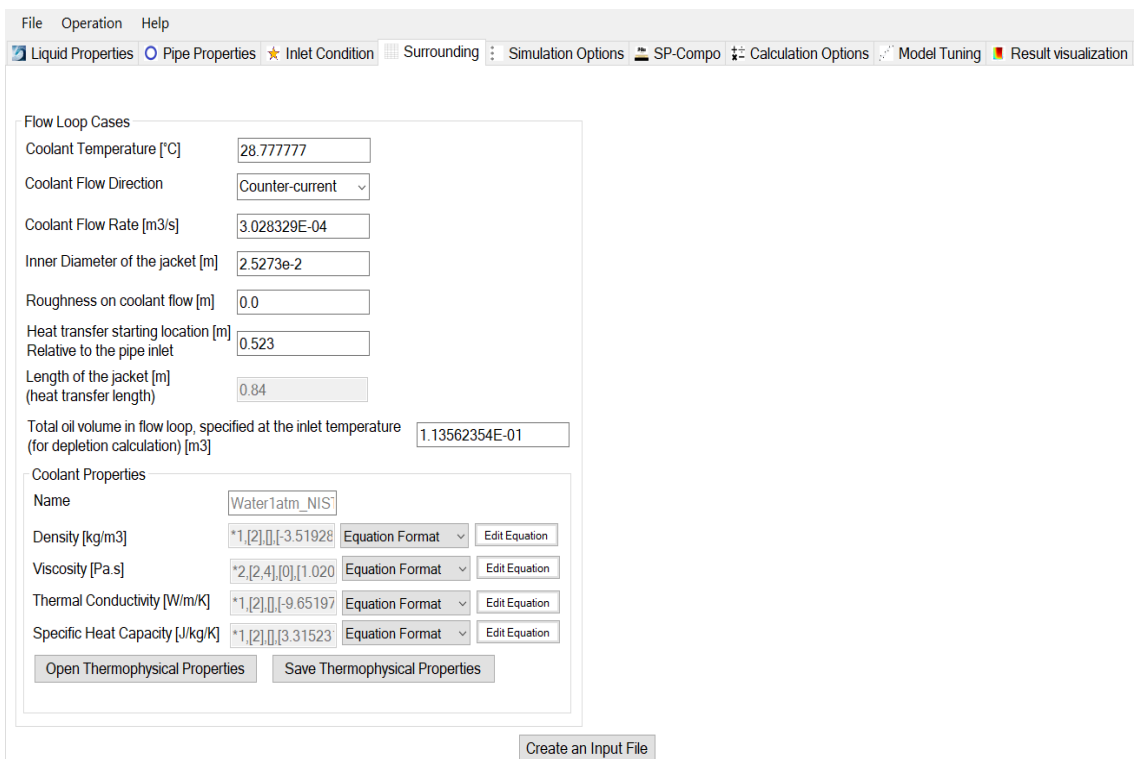


Figure 0-20: A screenshot of SP-Depo user-interface. Different tabs acquire different input information

Please note that each of the tabs are defined as separate classes in our code. In Main_caller.h & cpp, there are several functions that are responsible for reading the input information and assigning them into the objects with the same type as the mentioned classes.

```
Class: spdepo::Main1PhaseDeposition
Methods: void Run
Class: spdepo::Main1PhaseFittingSearch
Methods: void Run
Class: spdepo::ReadInput
Methods: Thermo ReadThermo1P, Fluid ReadLiquid1P,
          void ReadPipe1p, InletCondition ReadInlet1P, void
          ReadCoolant1P, void ReadSimulationOption, void SetPath
```

Figure 0-21: Class, and methods which are included in Main_caller.h

2.4.3 Solid_properties.h and Solid_properties.cpp

In these header and cpp files, the properties of the pipe are assigned to the “solid” object in Main_caller.h which will be passed to more inner layers of the program for the calculations in section “B” in Figure 0-12.

```
Class: spdepo::Solid
Methods: Solid (constructor), void SetFunctionalProperties,
          double GetProperty, void GetName
```

Figure 0-22: Class, and methods which are included in solid_properties.h

2.4.4 pipe_geometry.h and pipe_geometry.cpp

In this header and cpp files, the pipe and flow geometries are calculated and assigned to member variables. Some of these properties are: pipe cross-section area, annulus flow cross-section area, inner diameter, outer diameter, inner diameter of the jacketed pipe, hydraulic diameter of the jacketed pipe, pipe roughness, annulus/jacketed pipe roughness, annulus/jacketed pipe roughness, pipe total length. The following picture is a screenshot of the tab which takes the pipe’s input information.

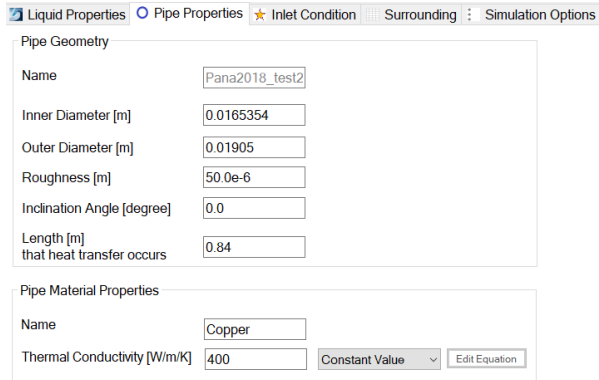


Figure 0-23: Pipe's input properties.

Class: spdepo::PipeGeometry
Methods: void SetProperties, void SetAngleInDegree, void SetAngleInRadian, double GetProperties, void SetProperties function overload, void GetName

Figure 0-24: Class, and methods which are included in pipe_geometry.h

2.4.5 inlet_condition.h and inlet_condition.cpp

In these files, the inlet conditions including the oil initial velocity and inlet temperature are assigned to the member variables.

Class: spdepo::InletCondition
Methods: void SetProperties, double GetProperties, void GetName

Figure 0-25: Class, and methods which are included in inlet_condition.h

2.4.6 coolant_condition.h and coolant_condition.cpp

In these files, the coolant properties are assigned to the class member variables. Some of the inputs are: coolant's inlet temperature, volumetric flow rate and jacket's flow type (only counter-current flow is included).

Class: spdepo::CoolantCondition
Methods: void SetAll, bool GetBool, double GetDouble

Figure 0-26: Class, and methods which are included in coolant_condition.h

2.4.7 fluid_properties.h and fluid_properties.cpp

The fluid properties usually change with temperature. So, in our simulation, the fluid properties need to be in the equation format as a function of temperature. In fluid_properties.cpp, the fluid equations are converted to readable functions by C++ which can be accessed by other objects. The following picture shows the user-interface section where fluid properties should be provided.

When “Edit Equation” button is clicked, the user is directed to another window where equations can be inserted for various liquid properties. Please refer to “user_equation_format.h & cpp” section for an instruction about inserting the equations.

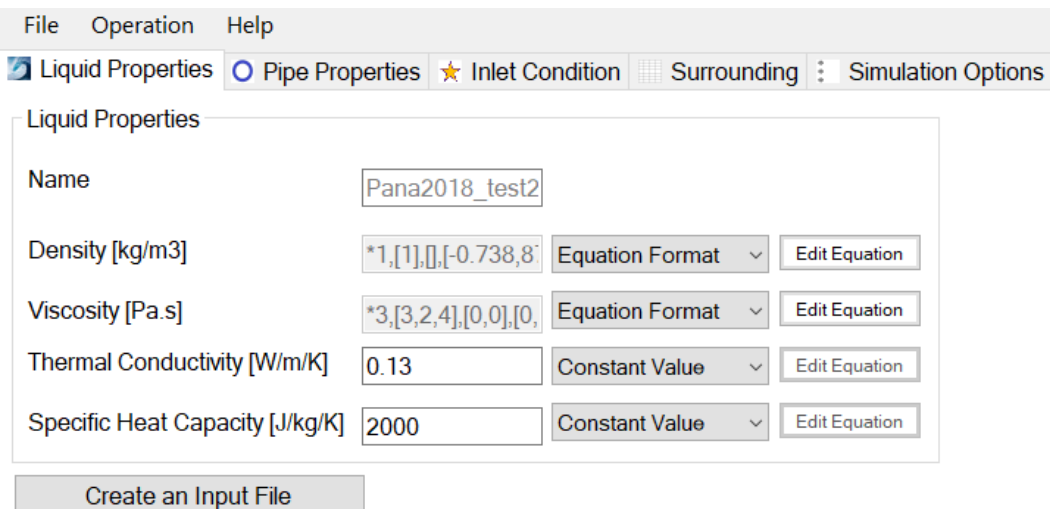


Figure 0-27: “Liquid properties” section of SP-Depo which takes the equations of rheological properties of the oil phase

```
Class: spdepo::Fluid
Methods: void SetConstantProperties,
          void SetConstantValueMember, void SetName, void
          SetFunctionalProperties, double GetProperty, void GetName,
          void GetName3
```

Figure 0-28: Class, and methods which are included in fluid_properties.h

2.4.8 simulation_options.h and simulation_options.cpp

Through this class, the member variables which are specified by the user will be accordingly assigned. As mentioned, in SP-Depo, we made it possible for users to choose

different wax deposition models. Some of the included wax mass flux models are: no precipitation method (Singh 2000), solubility method (Venkatesan 2004), and partial precipitation model (Lee 2008). In simulation_options header and cpp files, the chosen model options with their corresponding fitting parameters, which have been specified by the user, will be captured and assigned to the right member variables. The following picture shows the corresponding simulation-option tab in SP-Depo's GUI. The two precipitation curve models (conventional and SP-Compo) can be chosen in this tab.

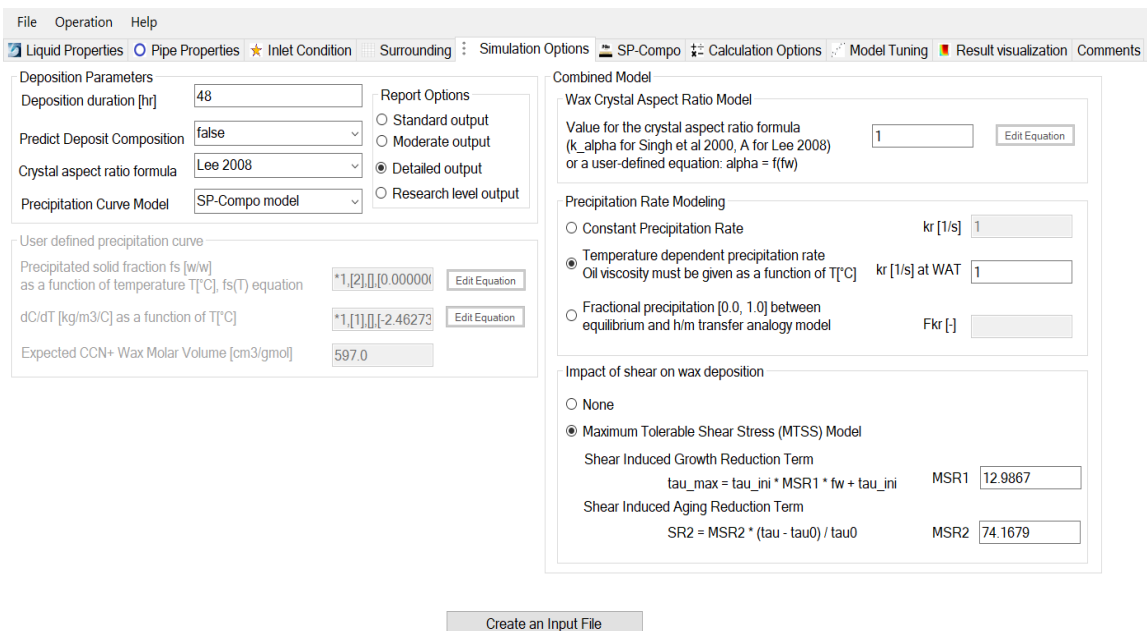


Figure 0-29: Simulation Option section in SP-Depo GUI

```

Class: spdepo::SimulationOptions
Methods: void SetAlphaOption, void SetAlphaEquation
           void SetAlphaEquation - Function overloading, void
           SetAlphaEquationLee2008Form, void SetAAlpha
           void SetPrecipitationRate ,void SetPrecipitationRateModel
           void SetKAlpha, void SetDepositionDuration, void
           SetSurroundingType, double GetDepositionDuration, double
           GetPrecipitationRate, usr::BigEquation GetAlphaEq
           usr::kDepositionOption GetAlphaOption, void
           SetKrAsAFunctionOfTemperature, bool
           GetKrAsAFunctionOfTemperatureOption, void SetWaxProperties,
           void SetWaxProperties - Function overloading, void
           SetUserDefinedPrecipitationEquation, usr::BigEquation
           GetUserDefinedPrecipitationEquation, void
           SetUserDefinedCdTEquation, usr::BigEquation
           GetUserDefinedCdTEquation, void
           SetUserTCReferenceForSolidFraction, double
           GetUserTCReferenceForSolidFraction, void
           SetUserWaxMolarVolume, double GetUserWaxMolarVolume, void
           SetInitialTotalOilVolume, double GetInitialTotalOilVolume,
           void SetWaxMaterialProperties, Solid
           GetWaxMaterialProperties, void SetPredictCompositionOption,
           bool GetPredictCompositionOption, void
           SetPrecipitationCurveModel, usr::kPrecipitationCurveModel
           GetPrecipitationCurveModel, void SetReportOption,
           usr::kReportOption GetReportOption, void SetTRefForKr,
           double GetTRefForKr, void SetDwoIniForKr, double
           GetDwoIniForKr, void SetShearDepositionModel,
           usr::kShearDepositionModel GetShearDepositionModel, void
           SetMSR1, double GetMSR1, void SetMSR2, double GetMSR2

```

Figure 0-30: class, and methods which are included in simulation_options.h

2.4.9 SP_Wax_Functions.h and SP_Wax_Functions.cpp

In our new proposed model, we included the thermodynamic model in the wax deposition modeling. SP-Wax thermodynamic software was added to SP-Depo model. This thermodynamic model is represented through two header files (`SP_Wax_Functions.h` and `SP_Wax_Main.h`). `SP_Wax_Functions.h` includes the functions which are used by `SP_Wax_Main.h`. The following picture is a screenshot of SP-Depo GUI's SP-Wax tab.

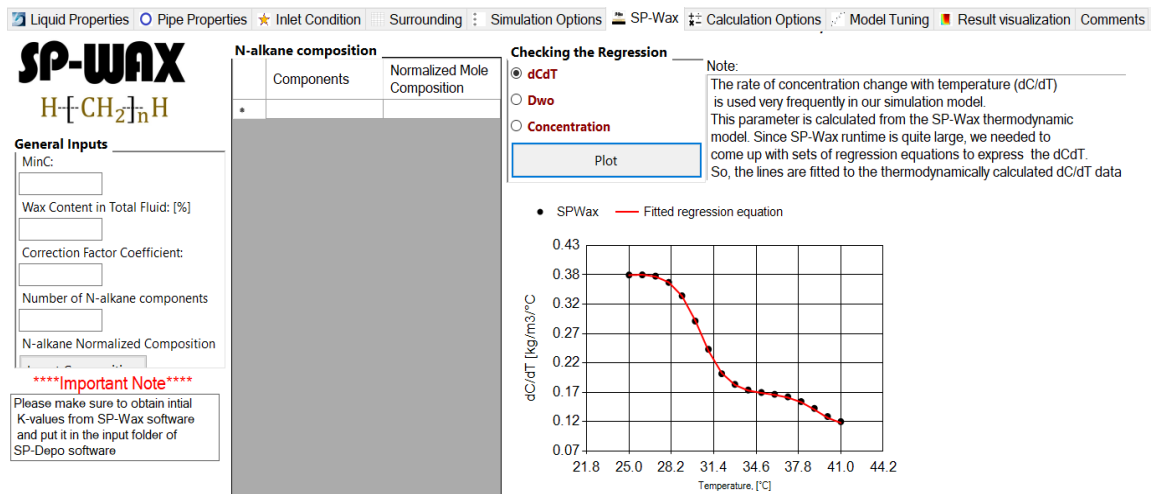


Figure 0-31: SP-Wax thermodynamic model tab in SP-Depo GUI

```

Class: spdepo::SPWaxOO::SPWaxInput
Methods: SPWaxInput - construction
Class: spdepo::SPWaxOO::SPWaxFuncs
Methods: SPWaxFuncs - construction, double HeatFus,
           double HeatTrans, double HeatVap, double TempFus, double
           TempTrans, double Vm, double Vw, double LambdaCorr3, double
           GammaSolMes, double GammaLiqMesEFV, double objFunc, double
           objFuncDer, double Fsolve, double KCal
  
```

Figure 0-32 : Class, and methods which are included in `SP_Wax_Functions.h`

2.4.10 SP_Wax_Main.h and SP_Wax_Main.cpp

In these files, some of the outputs include solid wax fraction, solid phase and liquid-phase compositions, equilibrium constants, each component's concentration, etc. In this

thermodynamic model, OpenMp parallel programming technique has been used which resulted in a huge decrease in our SP-Depo simulation run-time.

```
SP_Wax_Main.h

Class: spdepo::SPWaxOO::InputForThermo
Class: spdepo::SPWaxOO::Thermo
Methods: void setAll, void ThermoRange, double total_solubility,
           Void ThermoOneTemp, double Vm, void LR_InputFn, void
           division_function, std::vector<double> Z_w_from_Z_mole,
           usr::Polynomial LR_Total_Solubility_Fit_From_MinC,
           usr::Polynomial LR_Total_dCdT_Fit_From_MinC, usr::Polynomial
           LR_Solubility_Fit, usr::Polynomial LR_dCdT_Fit,
           usr::Polynomial LR_Precipitation_Fit, int MinCDetermination,
           double MolarVolume
```

Figure 0-33: Class, and methods which are included in SP_Wax_Main.h

In the header-file map, the section “B” includes the files that are responsible in solving wax deposition and transport equations. The main wax deposition governing equations are solved in `single_phase_deposition.cpp` where nearly all other inner-layer objects in section “A” and “C” and some parts of section “D” are called.

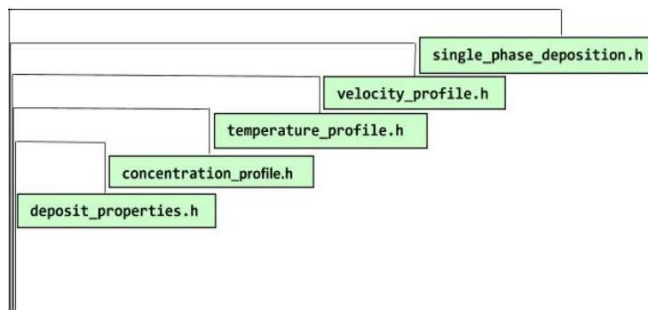


Figure 0-34: SP-Depo header-files about wax deposition and transport equations

In the following section, the header-files associated with the wax deposition and transport equations are explained.

2.4.11 `deposit_properties.h` and `deposit_properties.cpp`

In this section, deposit’s properties (thermal conductivity, total solid mass, etc.) are calculated through different class methods. Within the traditional modeling approach,

molecular diffusivity (D_{wo}), precipitation curve and $\frac{\partial C}{\partial T}$ are also considered here.

Accordingly, effective diffusivity is calculated based on the solid wax fraction and D_{wo} . Please note that the above parameters associated with SP-Comp model are calculated in different places (e.g., concentration_profile.cpp).

```
Class: spdepo::DepositProfile
Methods: void Initialize, void SetRiVec, void SetFwVecvoid
          void SetZMesh, void SetPipeRadius, double GetKDeposit,
          double CalculateKDep, double GetRhoDeposit,
          double GetPipeRadius, double GetTotalWaxMass,
          double GetTotalDepositVolume, int GetSecSize
Class: spdepo::WaxProperties
Methods: void SetAll, void SetPrecipitationCurve, double GetC,
          double GetDCDT, double GetSolidFrac, double
          CalculateDiffusivity,
          double CalculateEffectiveDiffusivityRatio
```

Figure 0-35: Class, and methods which are included in deposit_properties.h

2.4.12 temperature_profile.h and temperature_profile.cpp

As mentioned, in SP-Depo, the counter-current pipe-in-pipe heat exchange flow-loop is considered for heat transfer calculation in pipe. Basically, the deposit's interface temperature and the oil temperature near the waxy deposit are the two most important temperature values which should be known for wax deposition model. In SP-Depo, we used [Panacharoensawad approach \(2012\)](#) for temperature profile calculation in pipe. The boundary condition in radial temperature profile calculation was considered from the heat balance equation. Nusselt number in coolant is calculated from (Gnielinski, 2009):

$$Nu_c = \frac{(f/2) Re_c Pr_c 0.75 \beta^{-0.17} x_1 k_2}{k_1 + 12.7 \sqrt{\frac{f}{2}} (Pr_c^{\frac{2}{3}} - 1)} \quad (0-1)$$

$$k_1 = 1.07 + \frac{900}{Re_c} - \frac{0.63}{1 + 10 Pr_c} \quad (0-2)$$

$$k_2 = \left(\frac{Pr_c^{bulk}}{Pr_c^{wall}} \right)^{0.11} \quad (0-3)$$

$$x_1 = \left(1 + \frac{D_c}{L_c - z} \right)^{\frac{2}{3}} \quad (0-4)$$

where Reynold's number (Re_c), Prandtl number (Pr_c) and heat transfer coefficient (h_c) are calculated as:

$$Re_c = \frac{\rho_c V_c D_c^{hydraulic}}{\mu_c}$$

$$Pr_c = \frac{\mu_c C_{p,c}}{k_c} \quad (0-6)$$

$$h_c = \frac{Nu_c k_c}{D_c^{hydraulic}} \quad (0-7)$$

In the oil side and for turbulent flow, the velocity profile is calculated from (Tilton, 2008) as:

$$V^+ = \begin{cases} y^+ & y^+ \leq 5 \\ 5 \ln(y^+) - 3.05 & 5 \leq y^+ \leq 30 \\ 2.5 \ln(y^+) + 5.5 & 30 \leq y^+ \end{cases} \quad (0-8)$$

$$h_c = \frac{Nu_c k_c}{D_c^{hydraulic}} \quad (0-9)$$

$$y^+ = \frac{y}{\nu} \sqrt{\frac{\tau_w}{\rho_{oil}}} = \left(1 - \frac{r}{R} \right) \frac{Re}{2} \sqrt{\frac{f}{2}} \quad (0-10)$$

$$V^+ = \frac{V}{V^*} = \frac{V}{V_{av}} \sqrt{\frac{2}{f}} \quad (0-11)$$

$$\tau_w = \frac{1}{2} f \rho_{oil} V_{av}^2 \quad (0-12)$$

where average velocity is calculated as:

$$V_{av} = \frac{\dot{m}_{oil}}{\rho_{oil} \pi r_{i,ave}^2} \quad (0-13)$$

Then temperature profile will be determined using the following heat transfer equation as:

$$V_z \frac{\partial T}{\partial z} = \frac{1}{r} \frac{\partial}{\partial r} \left[r(\varepsilon_H + \alpha_H) \frac{\partial T}{\partial r} \right] \quad (0-14)$$

Please note that the heat of crystallization is not considered in the calculations. In the above equation, heat transfer eddy diffusivity (ε_H) can be calculated as:

$$\frac{\varepsilon_H}{\alpha_H} \equiv \frac{Pr}{Pr_T} \frac{\varepsilon}{\nu}; \quad Pr_T = 0.85 + \frac{0.015}{Pr} \quad (0-15)$$

And finally, $\frac{\varepsilon}{\nu}$ is calculated as:

$$\frac{\varepsilon}{\nu} = \begin{cases} (0.4y^+)^2 \left[1 - \exp\left(-\frac{y^+}{26}\right) \right]^2 \left| \frac{dV^+}{dy^+} \right| & y^+ \leq 80 \\ \frac{0.4y^+}{6} \left[1 + \frac{r}{R} \right] \left[1 + 2 \left(\frac{r}{R} \right)^2 \right] & y^+ > 80 \end{cases} \quad (0-16)$$

The equation 0-14 is solved using finite difference method [10]. He considered two boundary conditions as follows:

at $r = 0$, center of the pipe: (0-17)

$$\left. \frac{\partial T}{\partial r} \right|_{r=0} = 0$$

at the deposit interface in the oil side:

$$\left. \frac{\partial T}{\partial r} \right|_{r_i^-} = \frac{T_{i,N} - T_{i,N-1}}{r_N - r_{N-1}} = -\frac{(T_{i,N} - T_c)}{r_i k_{oil} \Omega_\Sigma} \quad (0-18)$$

where N represent the point at the deposit interface

In SP-Depo, by considering the boundary conditions, the PDE is solved as [10]:

$$\begin{bmatrix} 1 & -1 & 0 & \dots & 0 & 0 & 0 \\ C_2^T & A_2^T & B_2^T & \dots & 0 & 0 & 0 \\ 0 & C_3^T & A_3^T & \dots & 0 & 0 & 0 \\ \vdots & \vdots & \ddots & \vdots & \vdots & \vdots & \vdots \\ 0 & 0 & 0 & \dots & A_{N-2}^T & B_{N-2}^T & 0 \\ 0 & 0 & 0 & \dots & C_{N-1}^T & A_{N-1}^T & B_{N-1}^T \\ 0 & 0 & 0 & \dots & 0 & \frac{r_N k_{oil}}{\Delta r_N} & -\left(\frac{r_N k_{oil}}{\Delta r_N} + \frac{1}{\Omega_\Sigma} \right) \end{bmatrix} \begin{bmatrix} T_{i,1} \\ T_{i,2} \\ T_{i,3} \\ \vdots \\ T_{i,N-2} \\ T_{i,N-1} \\ T_{i,N} \end{bmatrix} = \begin{bmatrix} 0 \\ D_2^T \\ D_3^T \\ \vdots \\ D_{N-2}^T \\ D_{N-1}^T \\ \frac{-T_c}{\Omega_\Sigma} \end{bmatrix}$$

where

$$A_j^T = \frac{V_{z,ij}}{\Delta z_i} + \frac{1}{r_j(\Delta r_{j+1} + \Delta r_j)} \left[\frac{[r(\varepsilon_H + \alpha_H)]_{j+1} + [r(\varepsilon_H + \alpha_H)]_j}{\Delta r_{j+1}} \right. \\ \left. + \frac{[r(\varepsilon_H + \alpha_H)]_j + [r(\varepsilon_H + \alpha_H)]_{j-1}}{\Delta r_j} \right] \quad (0-19)$$

$$B_j^T = \frac{-1}{r_j(\Delta r_{j+1} + \Delta r_j)} \left[\frac{[r(\varepsilon_H + \alpha_H)]_{j+1} + [r(\varepsilon_H + \alpha_H)]_j}{\Delta r_{j+1}} \right] \quad (0-20)$$

$$C_j^T = \frac{-1}{r_j(\Delta r_{j+1} + \Delta r_j)} \left[\frac{[r(\varepsilon_H + \alpha_H)]_j + [r(\varepsilon_H + \alpha_H)]_{j-1}}{\Delta r_j} \right] \quad (0-21)$$

$$D_j^T = \frac{V_{z,ij} T_{i-1,j}}{\Delta z_i} \quad (0-22)$$

After calculating the radial temperature profile, the important term $\frac{\partial T}{\partial r} \Big|_{r_i^-}$ is determined which will

be directly used in the wax deposition model. Then, the other important term which is the temperature gradient at the interface but in the deposit side ($\frac{\partial T}{\partial r} \Big|_{r_i^+}$) is calculated as:

$$\frac{\partial T}{\partial r} \Big|_{r_i^+} = \frac{k_{oil}}{k_{dep}} \frac{\partial T}{\partial r} \Big|_{r_i^-} \quad (0-23)$$

Please note that the radial discretization is non-uniform and is calculated based on the one-seventh power-law velocity profile equation as follows:

$$\frac{v_{av}}{v_{max}} = f(r) = (1 - r_{ratio})^{1/7} \quad (0-24)$$

In SP-Depo, the derivative $\left(\frac{df}{dr_{ratio}} \right)$ will be calculated and, it will be provided to the Dormand-Prince ODE solving function. This adaptive method then provides a non-uniform discretization which be considered in out software. The derivative is as follows:

$$\frac{df}{dr_{ratio}} = -\frac{1}{7} (1 - r_{ratio})^{-\frac{6}{7}} \quad (0-25)$$

The following graph shows the temperature profile at early time.

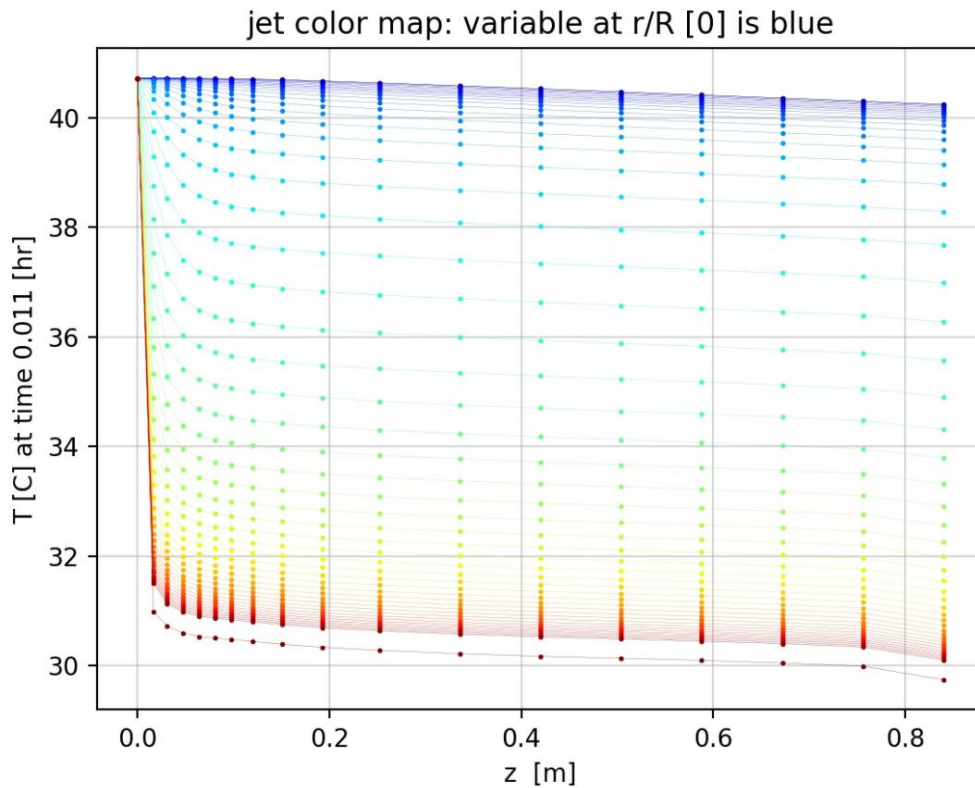


Figure 0-36: radial temperature profile in the pipe for different axial locations

In the wax deposition calculation, the deposit's interface temperature is the very important. Therefore, in the two following graphs, the deposit's interface temperature is plotted versus time and location.

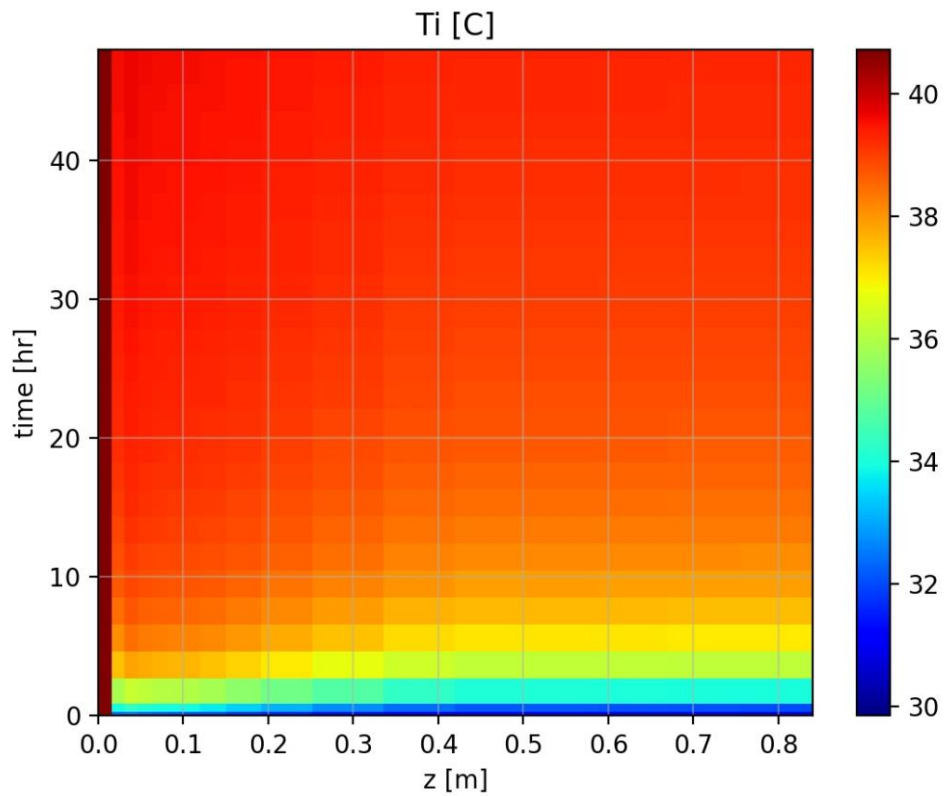


Figure 0-37: Deposit's interface temperature color map for different time and z locations

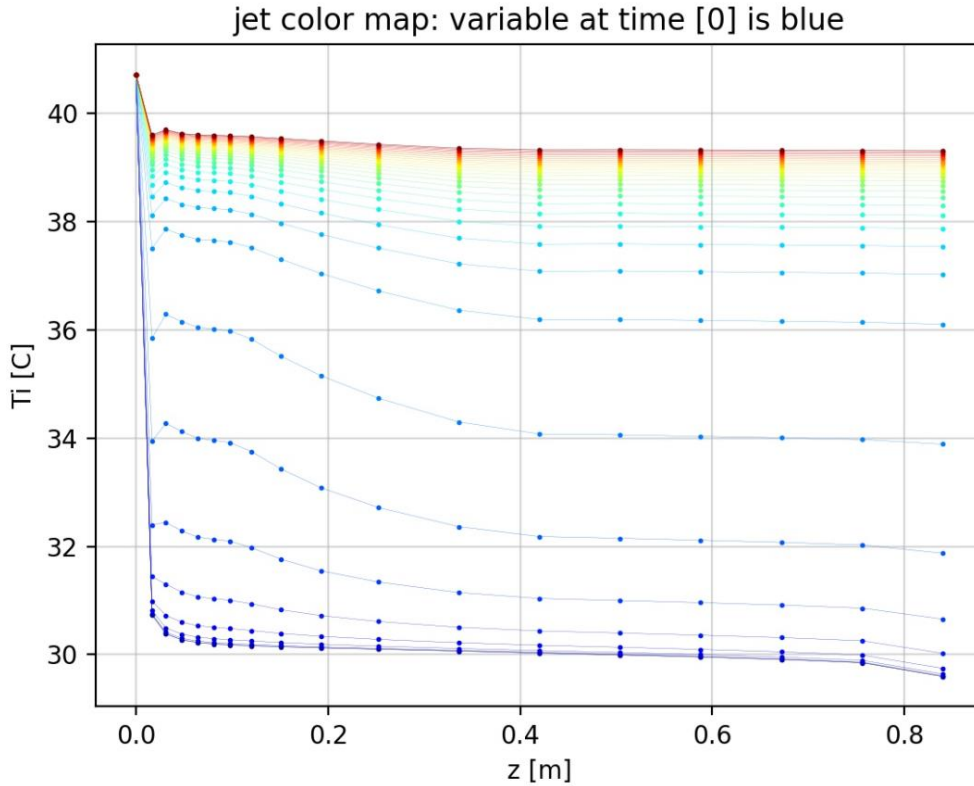


Figure 0-38: Deposit's interface temperature

```

Class: spdepo::heat_calculation::MacroZHeatBalance
Methods: void SetAll, void Solve, void GetProfile, void
MeshToSec,
    void ZDiscretization, void HeatBalanceVerification,
    void CalculateSectionT, int GetMeshSize, int GetSecSize,
    double NuTurbulentSlope, double ForwardTZProfile,
    double TZProfileLoop, double TurbulentPipeAverageNusselt,
    double TurbulentAnnulusAverageNusselt
Class: spdepo::heat_calculation::RadialTProfile
Methods: void SetAll, void Solve, void StandardOutput,
    void ZDepositGrouping, usr::TwoDVector<double>
    GroupTProfileCalculation, int SectionToGroupNumber, void
    PlotPColorGraph, void HeatBalanceVerification, double
    DVPlusByDYPlus, void CheckRadialHeat, void CheckAxialHeat
  
```

Figure 0-39: Class, and methods which are included in temperature_profile.h

Turbulent flow is known to be characterized by chaotic fluctuations in pressure and velocity. A set of equations are solved in SP-Depo to estimate the velocity profile of the

turbulent flow in pipe. These equations are expressed in Temperature_profile.h & cpp section. However, we will repeat them in this section too.

$$V^+ = \begin{cases} y^+ & y^+ \leq 5 \\ 5 \ln(y^+) - 3.05 & 5 \leq y^+ \leq 30 \\ 2.5 \ln(y^+) + 5.5 & 30 \leq y^+ \end{cases} \quad (0-26)$$

$$y^+ = \frac{y}{\nu} \sqrt{\frac{\tau_w}{\rho_{mix}}} = \left(1 - \frac{r}{R}\right) \frac{Re}{2} \sqrt{\frac{f}{2}} \quad (0-27)$$

$$V^+ = \frac{V}{V^*} = \frac{V}{V_{av}} \sqrt{\frac{2}{f}} \quad (0-28)$$

$$\tau_w = \frac{1}{2} f \rho_{oil} V_{oil}^2 \quad (0-29)$$

where average velocity is calculated as:

$$V_{av} = \frac{\dot{m}_{oil}}{\rho_{oil} \pi r_{i,ave}^2} \quad (0-30)$$

Velocity profile is crucial, because it is needed for radial temperature profile calculation.

```
Class: spdepo::SinglePhaseHydrodynamics
Methods: void SetAll, void SetFluidProperties, void SetInletFlow,
void SetPipeGeometry, void Solve, double
SolveOnlyShearStress,
void GetPipeGeometry, void GetInletCondition, void GetFluid,
std::vector<double> GetRMeshRatio, double GetProperties,
double HaalandEquation, void DiscretizeR, void
DiscretizeRRatioMesh_turbulent, void
DiscretizeRRatioMesh_laminar
double LaminarVelocitySlope_, double OneSeventhLaws_, double
OneSeventhLawsSlope, void SolveTurbulent, void SolveLaminar,
double VPlusTurbulent, double VLaminar
```

Figure 0-40: Class, and methods which are included in velocity_profile.h

2.4.14 concentration_profile.h and concentration_profile.cpp

As mentioned, SP-Depo has two primary calculation options for wax deposition calculation (traditional and SP-Compo). Concentration, $\frac{\partial C}{\partial T}$, and actual molecular diffusivities are

calculated and reported by `Get_dCdT_thermo`, `Get_C_thermo` and `Diff_thermo`. All these parameters are calculated from the SP-Wax thermodynamic model.

For concentration profile calculation, the following governing equation is solved numerically.

$$V_z \frac{\partial C}{\partial z} = \frac{1}{r} \frac{\partial}{\partial r} \left[r(\varepsilon_M + D_{wo}) \frac{\partial C}{\partial r} \right] - k_r(C - C(T)) \quad (0-31)$$

$$\frac{\varepsilon_M}{D_{wo}} \equiv \frac{Sc}{Sc_T} \frac{\varepsilon}{\nu}; \quad Sc_T = 0.85 + \frac{0.015}{Sc} \quad (0-32)$$

This equation has been reported by Lee-2008 and k_r is the precipitation rate which is treated as a fitting parameter. As previously mentioned, the suggested model by Panacharoensawad 2012 puts $k_r = 0$ for no precipitation wax mass flux case.

Similar to temperature profile calculation, the governing PDE is solved numerically using the backward finite difference method. The boundary conditions are:

$$\text{At } r = 0, \frac{\partial C}{\partial r} = 0 \quad (0-33)$$

$$\text{At } r = r_i, C = C(T_i) \quad (0-34)$$

By knowing the concentration profile, the total wax mass flux can be calculated as:

$$J_{total} = -D_{wo} \frac{C_N - C_{N-1}}{r_N - r_{N-1}} \quad (0-35)$$

Then, in SP-Compo model, the concentration profile for the grouped component will be estimated. A partial differential equation for concentration profile has been solved using the finite element method (FEM).

As previously stated, the above parameters are calculated for all individual carbon numbers and they are used to calculate the concentration, $\frac{\partial C}{\partial T}$ and molecular diffusivity for the grouped component in SP-Compo wax deposition model. `Get_dCdT_fit_eqns` and `DwoFit` are the methods to create the fitted regression equations for the thermodynamic parameters. Within these two methods, the SP-Wax thermodynamic model is called for a specific range of temperature and the produced data are saved into vectors. Then, the regression equations are fitted to the previously generated data (by SP-Wax). So, in `Get_C_thermo`, `Get_dCdT_thermo` and `Diff_thermo`, the thermodynamic properties are calculated using the fitted equations (NOT the thermodynamic model). In this way, the run-time was improved considerably.

```

Class: spdepo::mass_calculation::RadialCProfile
Methods: void SetAllContinue, void SetAll, void ThermoSetAll,
           void Solve, void StandardOutput, void ZDepositGrouping,
           void GroupTCPProfileCalculation, int SectionToGroupNumber,
           void PlotDefaultCProfile, void PlotDefaultTProfile,
           void PlotPColorGraph, void HeatBalanceVerification
           void InitializeCompositionalModel, void
           UpdateInletComposition,
           void Get_dCdT_fit_eqns, double Get_C_thermo,
           double Get_dCdT_thermo, double Diff_thermo, int MinC_cal,
           void DwoFit, double DVPlusByDYPlus, void CheckRadialHeat,
           void CheckAxialHeat

```

Figure 0-41: Class, and methods which are included in concentration_profile.h

2.4.15 single_phase_deposition.h and single_phase_deposition.cpp

Inarguably, single_pase_deposition.h & cpp contain the most important components of the SP-Depo software. The governing equations of wax deposition modeling ($\frac{dF_w}{dt} = f, \frac{dr_i}{dt} = g$) are solved using numerus objects from nearly all classes. For further model improvement, future developers are advised to give extra attention to these files.

```

Class: spdepo::Storage_fit_eqs
Methods: Storage_fit_eqs()
Class: spdepo::SinglePhaseDeposition
Methods: void SetThermo, void SetAll, void SetProgramPath,
           void Calculate, void SimplePostCalculation,
           void DetailedPostCalculation, void PrintStandardOutput,
           void PrintDetailedOutput, void PrintParameters, void
           PrintPicture, void PrintXY, usr::TwoDVector<double>
           GetRiFwAns, void pass_flag, std::vector<double>
           ACN_determination, std::vector<double> ACN_determination -
           function overloading,, void PlotEveryCTProfileOneByOne, void
           PlotEveryCTProfile4Tasks, void Initialize
Class: spdepo::CoreDepositionEquation
Methods: void SetStorage, void SetAll1Phase,
           std::vector<double> WrapSolve1P_1, std::vector<double>
           WrapSolve1P, std::vector<double> Solve1P,
           std::vector<double> Solve1P - function overloading

```

Figure 0-42: Class, and methods which are included in single_phase_deposition.h

In this method “`void SinglePhaseDeposition::Calculate()`”, the wax deposition ODE governing equations are solved.

In the wax deposition calculation, there are many numerical methods which should be employed repeatedly. Therefore, we separately defined these numerical techniques and included them in separate header and cpp files. In this section, the classes and methods of each header-file are listed. Please note that the coded numerical methods are double-checked by known-solution scenarios in EXCEL.

2.4.16 fitting_search.h and fitting_search.cpp

In these files, parameters related to LM optimization algorithm are defined which are called when fitting parameters are being estimated.

```
Class: spdepo::FittingDepositionCall
Methods: std::vector<double> WrapDepositionCall, void SetData,
           std::vector<std::vector<double>> GetData, void
           SetNDeltaData, void SetNFWData, void SetDeposition, void
           SetGraphPlottingDeltaData, std::vector<std::vector<double>>
           GetGraphPlottingDeltaData, void SetGraphPlottingFWData, void
           SetGraphPlottingACNData, std::vector<std::vector<double>>
           GetGraphPlottingFWData, std::vector<std::vector<double>>
           GetGraphPlottingACNData, void SetUseFWDataForSearching, bool
           GetUseFWDataForSearching, void SetUseDeltaDataForSearching,
           bool GetUseDeltaDataForSearching, void SetDoSearching, bool
           GetDoSearching, SinglePhaseDeposition GetDeposition, void
           SetSimulationOption, void SetFittingBool, void
           SetUseLogSpace, void Initialization, void
           SetRelativeEpsForDerivative, double
           GetRelativeEpsForDerivative, void SetRelativeEpsForStopping,
           double GetRelativeEpsForStopping, void SetInitialMuLM,
           double GetInitialMuLM, void SetMaxLMIteration, int
           GetMaxLMIteration, std::vector<double> GetScalingVector,
           std::vector<double> GetInitialGuess, std::vector<int>
           GetFittingBoolIndex, std::vector<std::string>
           GetFittingBoolName
Class: spdepo::SearchFunctionWrap
Methods: void SetFunctionToBeSearched,
           void SetErrorVectorCalculation
```

Figure 0-43: Class, and methods which are included in fitting_search.h

2.4.17 linear_regression.h and linear_regression.cpp

The thermodynamic model takes about 0.5-1 seconds to run and to calculate various thermodynamic properties of the system at one temperature. In the wax deposition model, concentration, $\frac{\partial C}{\partial T}$ and diffusivity (which are calculated from the thermodynamic model) should be accessed many times and it is not feasible to call the thermodynamic model every time the mentioned parameters are required in SP-Depo. Therefore, we developed a unique regression model to represent the thermodynamic data. Since we adopted a modified regression model, it will be illustrated by an example and different graphs.

In this section, a regression model is coded to estimate solubilities and $\left(\frac{\partial C}{\partial T}\right)_i$ points. After analyzing the shape of the data points, we found that the data can be fitted by polynomial equations through three zones. In the following graph, three polynomial equations are fitted to a sample set of $\frac{\partial C}{\partial T}$ data points for $C_{46}H_{94}$. The data points are divided into three sections. First, the maximum point is found, and a three-degree polynomial is fitted to the data from the beginning to the point right before the maximum. For the second zone, a two-degree polynomial is fitted to three data points including the maximum and neighboring data points. Finally, for the last zone, a three-degree polynomial is fitted starting from one data point after the maximum till the last data point. For the following case, the average R^2 for all three zones for this specific example is $R^2 = 0.998$. In the next graph, $\frac{dC}{dT}$ curves for different carbon number are then shown.

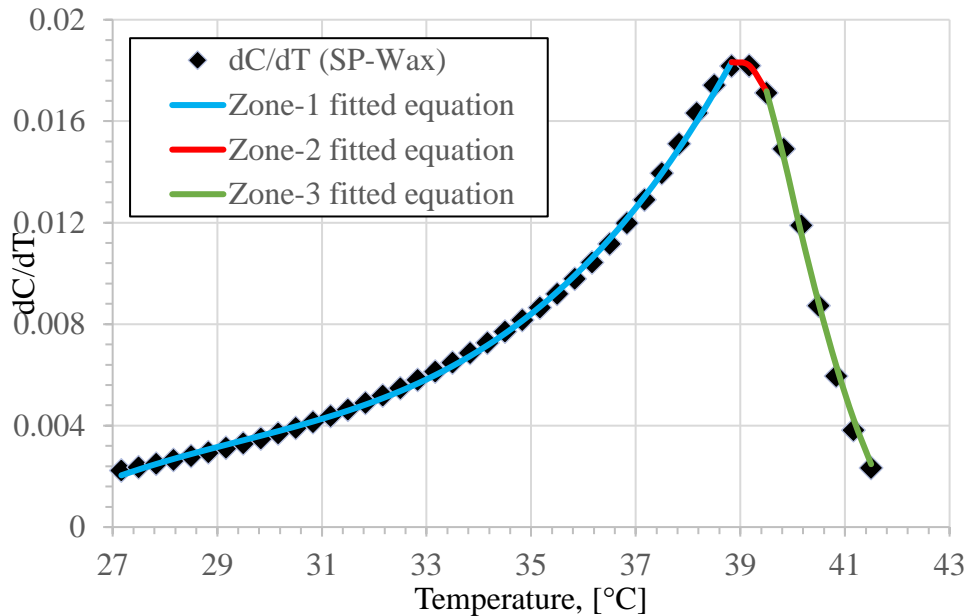


Figure 0-44: $\frac{dC}{dT}$ versus temperature for $C_{46}H_{94}$. The data points are generated by the SP-Wax thermodynamic model and the solid lines are generated by the fitted three-zone regression equations.

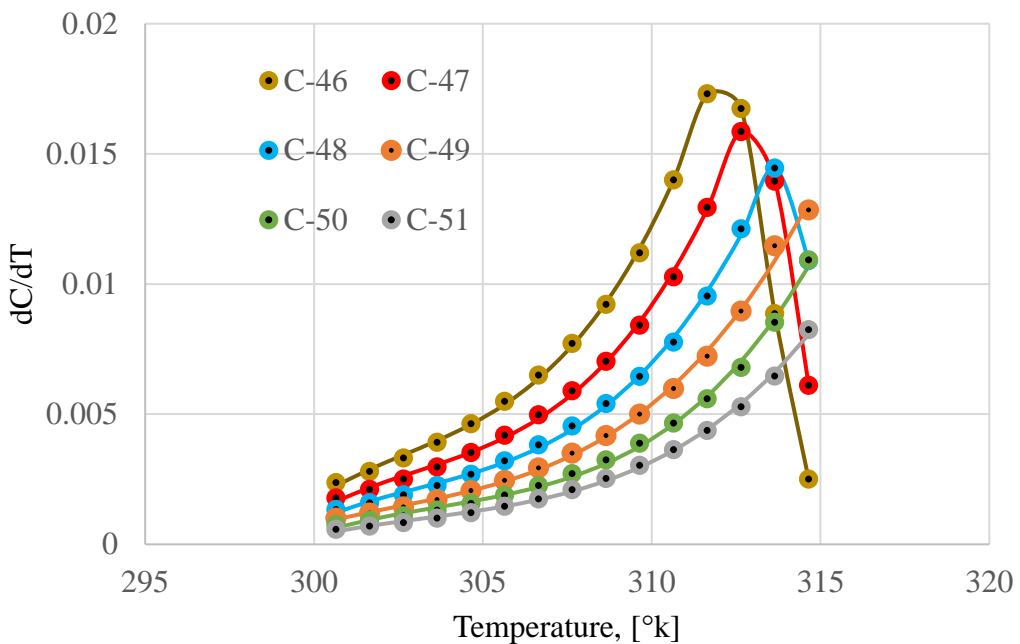


Figure 0-45: SP-Depo simulation: dC/dT curves for carbon numbers C 46-51

In addition, since the performance of our software is massively dependent on the accuracy of the fitted regression equations, we made it possible for the user to check the

fitted equations in the GUI. The following three graphs show the total concentration, $\frac{dC}{dT}$ and D_{wo} with the fitted equations.

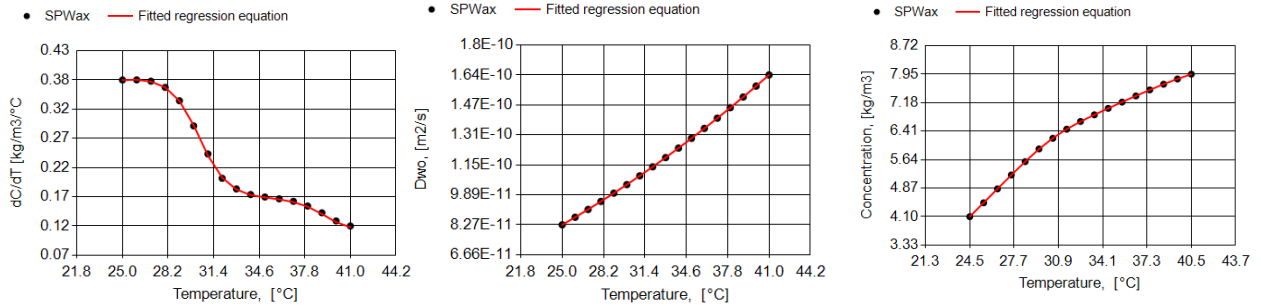


Figure 0-46: concentration, $\frac{dC}{dT}$ and D_{wo} versus temperature. The data points are generated by the SP-Wax thermodynamic model and the lines are from the fitted regression equations.

```
Class: spdepo::usr::Polynomial
Methods: double operator(), double operator_combined
Class: spdepo::usr::LinearRegressionEqFit
Methods: void SetAll, void calculate, Polynomial GetPoly()
          std::vector<std::vector<double>> MatMult,
          std::vector<std::vector<double>> MatTrans,
          std::vector<double> GaussianEliminationWithBackSubstitution,
```

Figure 0-47: Class, and methods which are included in linear_regression.h

2.4.18 user_numerical_method.h and user_numerical_method.cpp

user_numerical_method.cpp consists of more than 1800 lines of code with many numerical methods including: Bisection method, Newton-Raphson method, combined root finding method (Bisection and Newton-Raphson), trigonal Thomas matrix, matrix multiplication, Dorman-Pronce 1D and more than 1D, Simpson 1/3 integration method, Gaussian Elimination with Back-Substitution, Levenberg-Marquardt optimization algorithm, matrix transpose, interpolation. Please note that the above numerical methods are coded in a way that takes the function as their inputs. In this way, these methods will be reusable and can be used whenever needed.

```
spdepo::usr::
Methods: void EmptyCallBack, double BisectionMethod,
```

```

        double Newto Method, void InitialGuessScan, double
Simpson13,
        double Trapezoidal, double TryNewtonThenBisection, void
ThomasTridiagonal, void TridiagonalToDense, void
MatrixMultiply2D,
        void MatrixMultiply2D,TwoDVector<double>
TransposeNbyMMatrix,
        void DormandPrince1D, void DormandPrinceMany, void
DormandPrinceMany - function overloading, void
DormandPrinceMany - function
overloading,usr::TwoDVector<double> MeshToSec,
std::vector<double> LevenbergMarquardt, std::vector<double>
LevenbergMarquardt - function overloading,
std::vector<double> GaussianEliminationWithBackSubstitution,
double SumSquare, std::vector<double> Interpolation, int
FindFirstLeftIndex, double MaxSecondColumn, double
AverageSecondColumn,
Class: spdepo::usr::LMObject
Methods: std::vector<double> ErrorCalculation,
std::vector<double> RunLM, void SetFunction, void
SetCallBack, void SetDataForFitting, usr::TwoDVector<double>
GetDataForFitting, void SetScalingVector, void
SetDefaultEchoCallBack, void SetEmptyCallBack, void
SetEpsilonForDerivative, double GetEpsilonForDerivative,
void SetEpsilonForStop, double GetEpsilonForStop, void
SetMuLMInitial, void SetMaxIteration, int GetMaxIteration,
void SetMaxMuLoopIteration, int GetMaxMuLoopIteration, void
PrintStandardOutput, void SetOutputPath, std::wstring
GetOutputPath

```

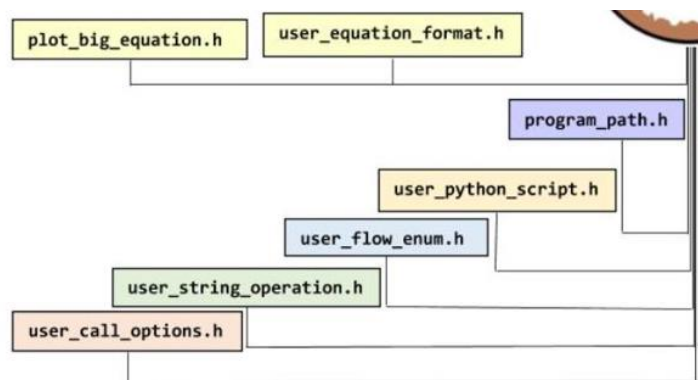


Figure 0-49: Header files in section "D"

The above header files are primarily related to enum classes and the software's structure of the SP-Depo code. Please note that python is used for data visualization with high quality graphs.

2.4.19 `user_equation_format.h` and `user_equation_format.cpp`

As previously shown, some of the input parameters are needed with equation format. For example, oil density is greatly dependent on the temperature and should be expressed through an equation. We made it possible for the user to insert equations for these parameters. The following graph shows the main window of SP-Depo which requires the user to provide the input information. In the “Liquid Properties” tab, equations are required for the fluid properties.

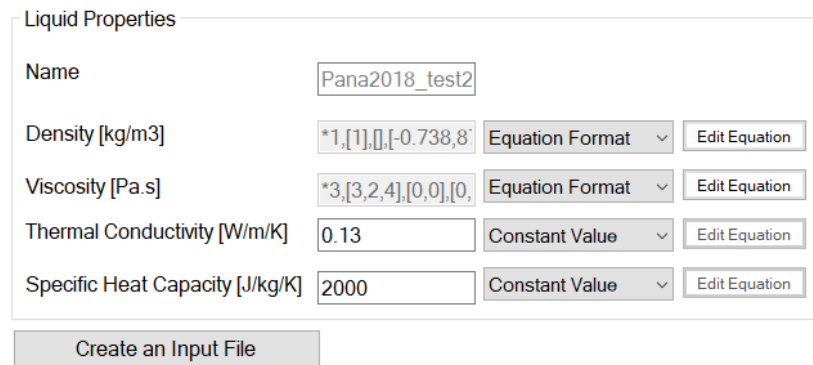


Figure 0-50: Liquid Properties input tab in SP-Depo

If user clicks “Edit Equation” button, the following window will be opened. Through the newly opened window, the user can choose the correct equation type and coefficients. One can click “Help” for the complete manual guidance where “Equation Description” and “Big Equation Creation Guidelines” will be accessed (Figure 0-52 and Figure 0-53)

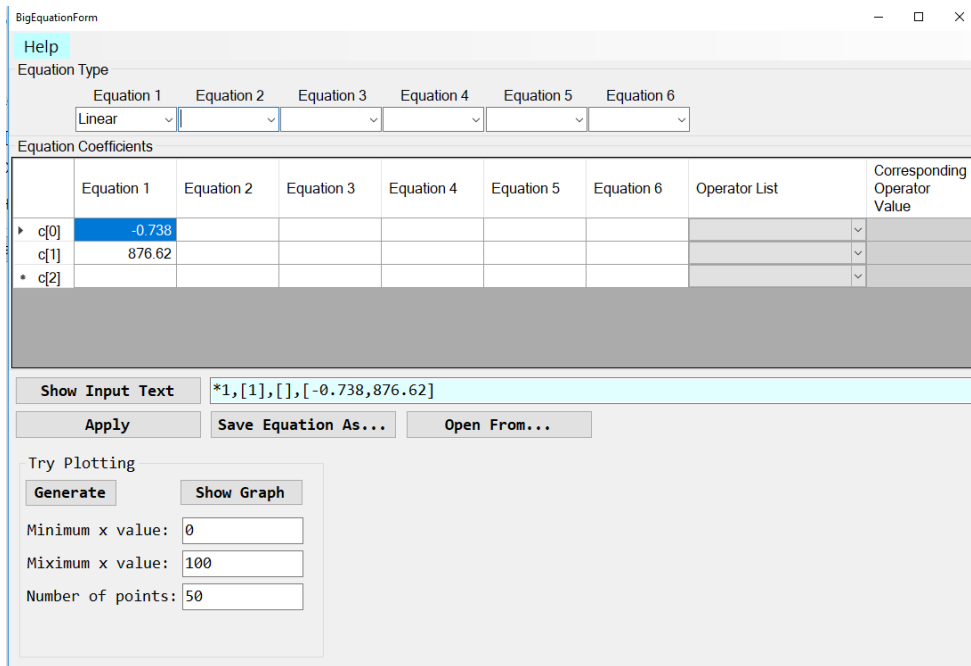


Figure 0-51: Equation insertion tab where user can provide the equation for non-constant variables including the fluid properties

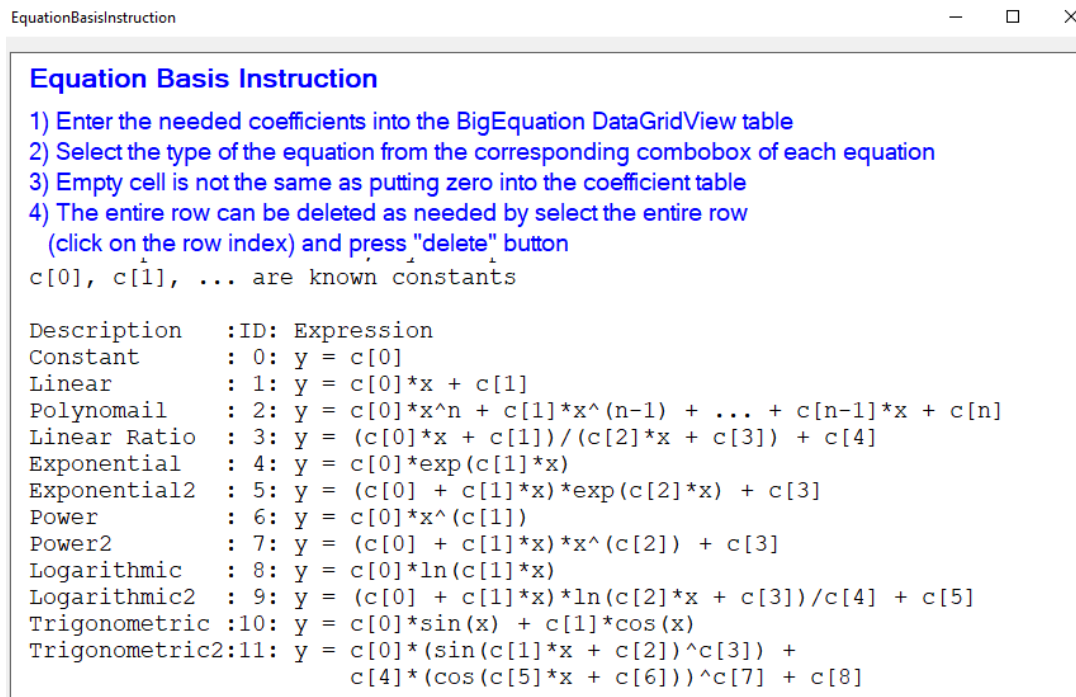


Figure 0-52: Equation Description manual

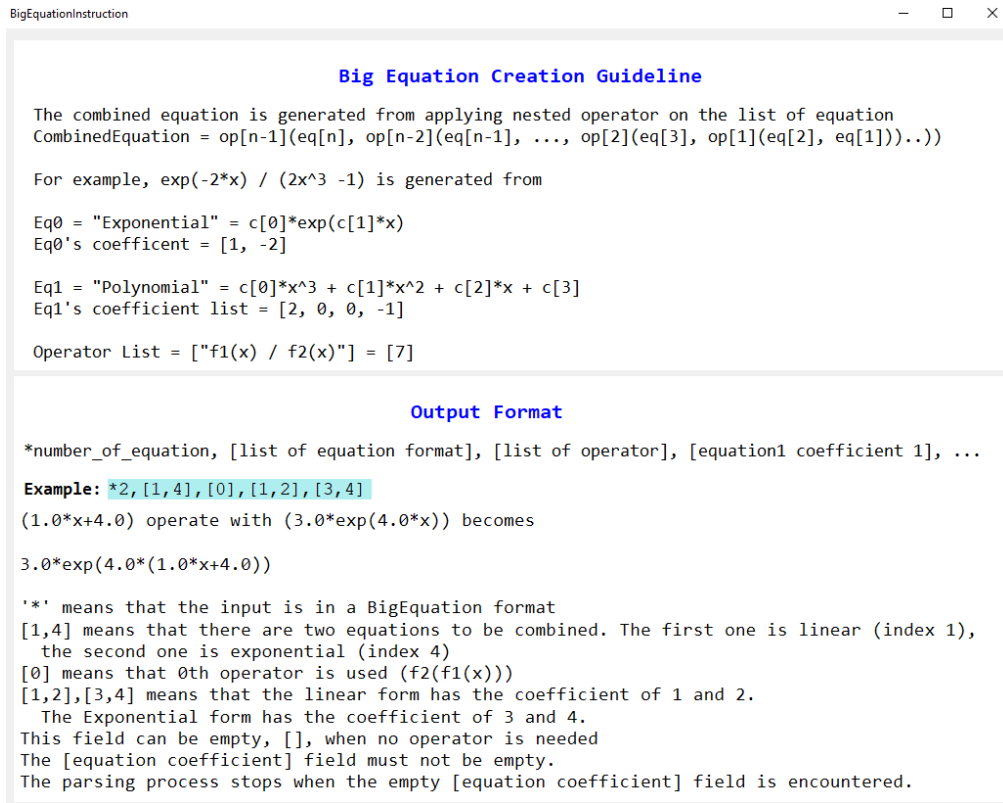


Figure 0-53: Big Equation Creation Guidelines

In Figure 0-53, the number corresponding to the operator list can be set in “Operator List” (Figure 0-51). In the following figure, the available operators are shown.

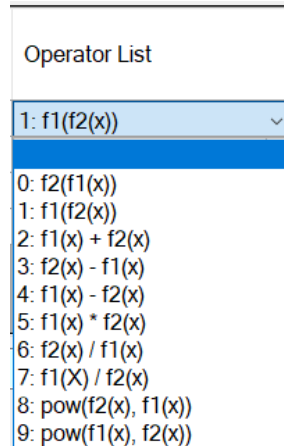


Figure 0-54: Operator List assignment

Our proposed equation insertion method covers nearly every typical equation format. The following picture shows the available equation types which can be used by the user.

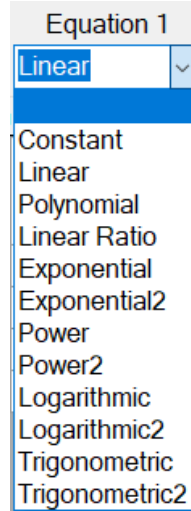


Figure 0-55: Available equation types

CHAPTER 5

RESULTS AND DISCUSSION

To verify our two developed software, we used experimental data from different resources and compared them to our simulation results. For SP-Wax, our software's performance and accuracy have been validated by experimental data of five binary and seven multicomponent systems. For SP-Depo, we used the data from twelve flow-loop experiments for our model and software verification.

2.5 SP-Wax thermodynamic model and software

In SP-Wax thermodynamic model, empirical correlations are used for some of the thermophysical properties. We initially compare these correlations to available experimental data. Then, we present some of the experimental data which have been used

in our model verification and, finally, SP-Wax simulation results will be compared to extensive experimental data.

2.5.1 Validation of empirical correlations

Several empirical correlations are used to express many parameters including thermo-physical properties, molar volume, etc. In our study, we double-checked the accuracy of those correlations by comparing them to the experimental data and other correlations. For the first parameter, we checked the DIPPR and GCVOL methods for molar volume calculation. Validity of both methods have been verified using experimental data. The two following graph shows comparison between two molar volume models and experimental data [34] for two temperature points. From the following plots, it is shown that both models successfully tracked the experimental data.

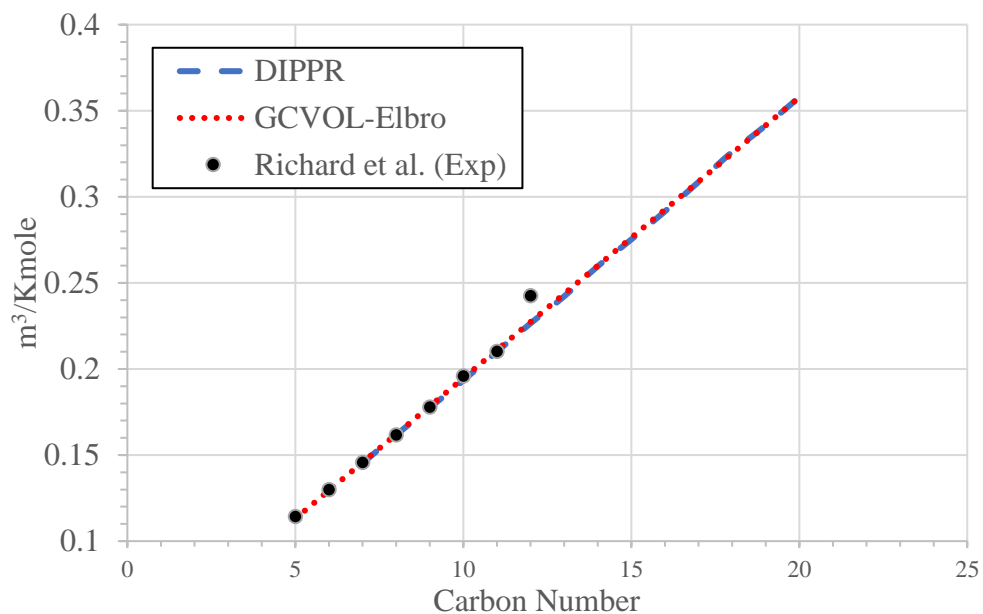


Figure 0-1: Molar volume comparison between experimental data [34] and correlations from DIPPR and GCVOL models at $T=288.15^{\circ}\text{K}$

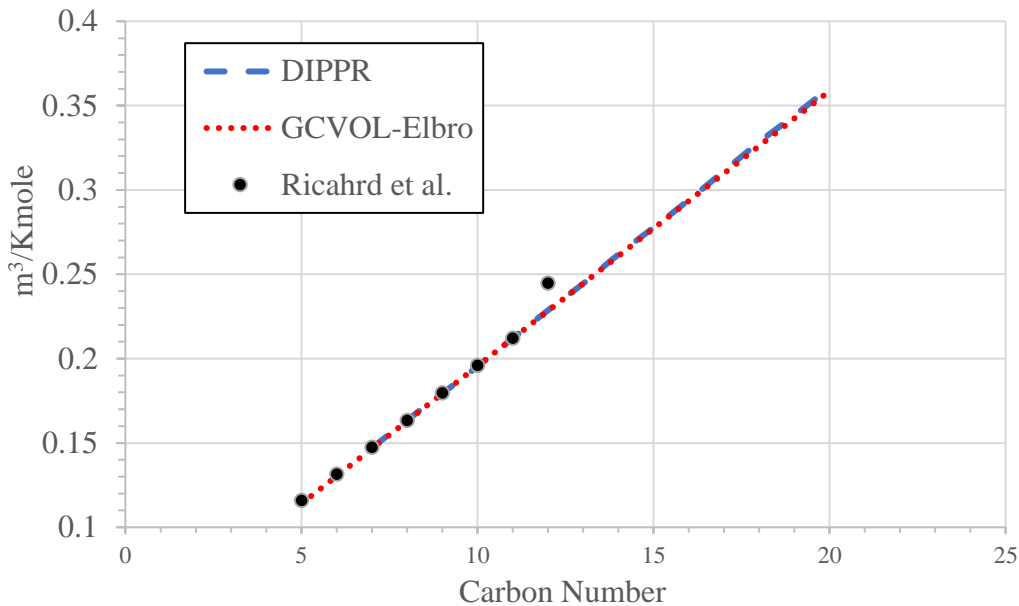


Figure 0-2: Molar volume comparison between experimental data [34] and correlations from DIPPR and GCVOL models at T=298.15°K

For the next step, the correlations for thermo-physical properties are evaluated. In SP-Wax, enthalpy and temperature of fusion are correlated using Coutinho's formulas. In the two following graphs, results from the correlations are compared to the experimental data reported by Broadhurst [35]. Fusion temperature is accurate with only 1% uncertainty while Coutinho model does not represent very good accuracy in estimation of fusion enthalpy for even carbon numbers ranging from 9 to 20.

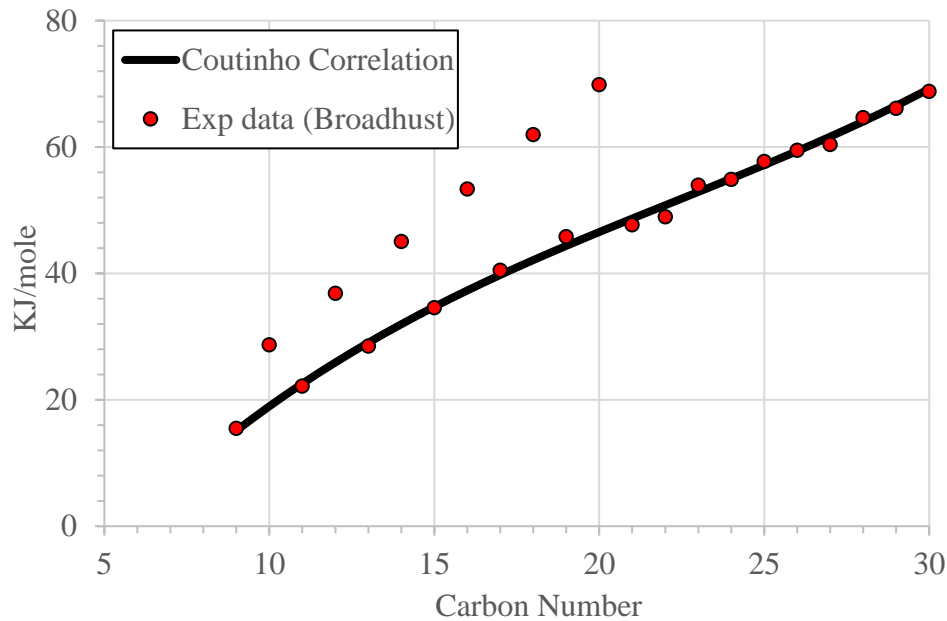


Figure 0-3: SP-Wax Enthalpy of fusion prediction using Coutinho et al. model correlation versus experimental data of Broadhurst

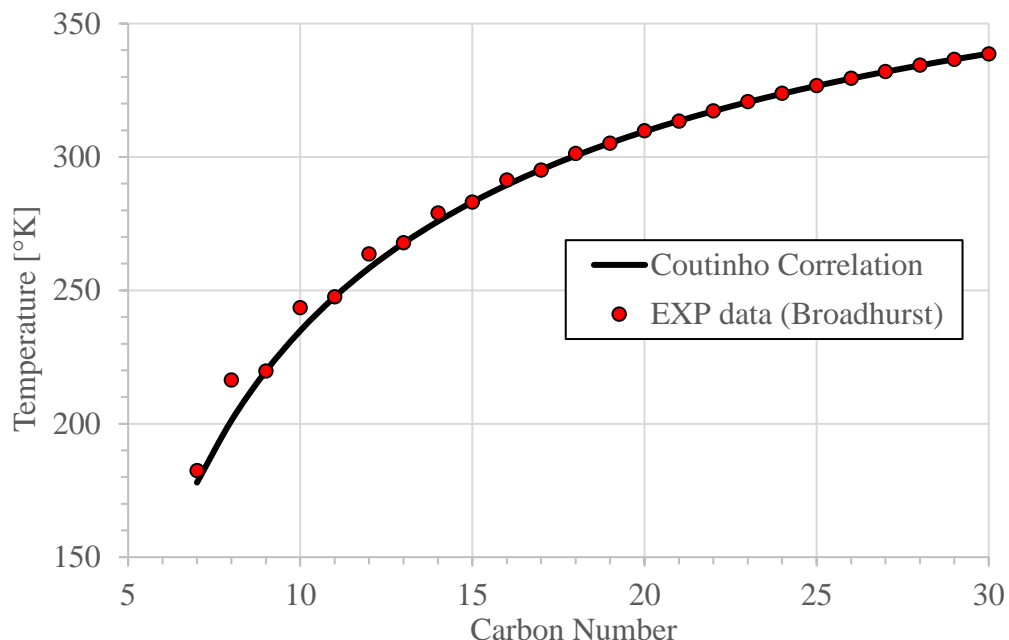


Figure 0-4: SP-Wax Temperature of fusion prediction using Coutinho et al. model correlation versus experimental data of Broadhurst

Similarly the enthalpy and temperature of solid phase transition correlations which are used in SP-Wax were compared to the experimental data reported by Broadhurst [35].

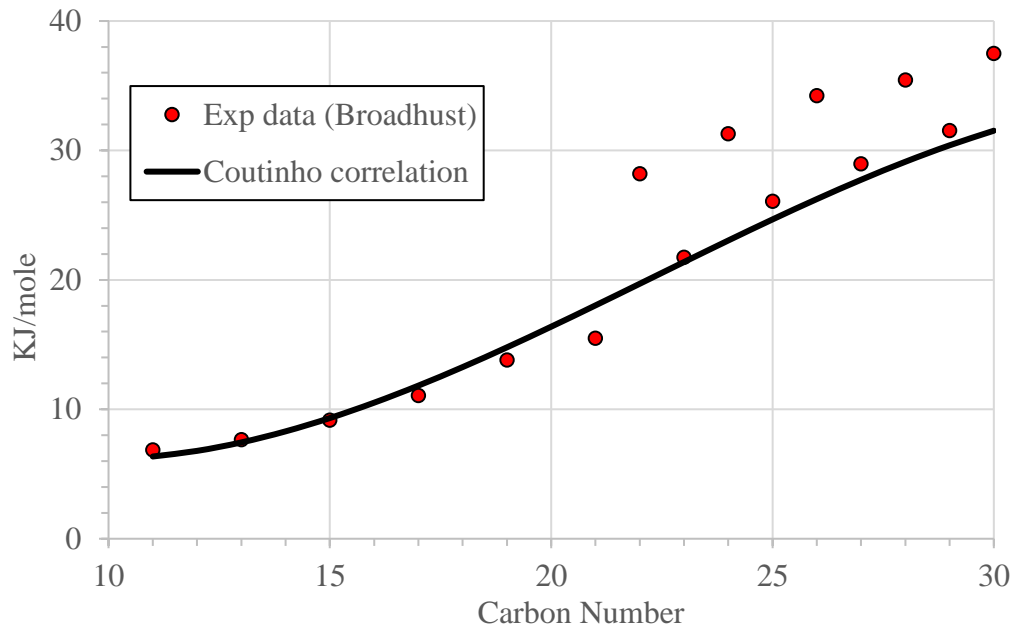


Figure 0-5: SP-Wax Enthalpy of solid phase transition prediction using Coutinho et al. model correlation versus experimental data of Broadhurst

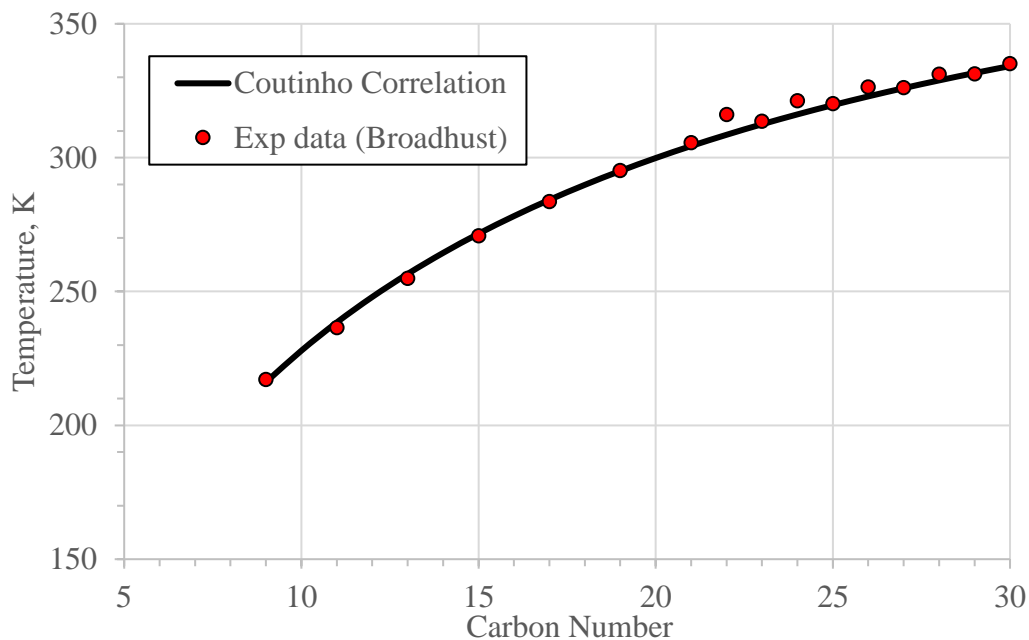


Figure 0-6: SP-Wax Temperature of solid phase transition prediction using Coutinho et al. model correlation versus experimental data of Broadhurst

The next investigated parameter is the heat of vaporization. Heat of vaporization is needed to calculated heat of sublimation in solid phase activity coefficient modeling. Extension of

Pitzer CSP models [32] have been used and compared to experimental data. In the following graph, Pitzer CSP predictions are plotted against experimental data at $25^{\circ} C$.[73], [74]. Our proposed correlation successfully predicts the experimental data.

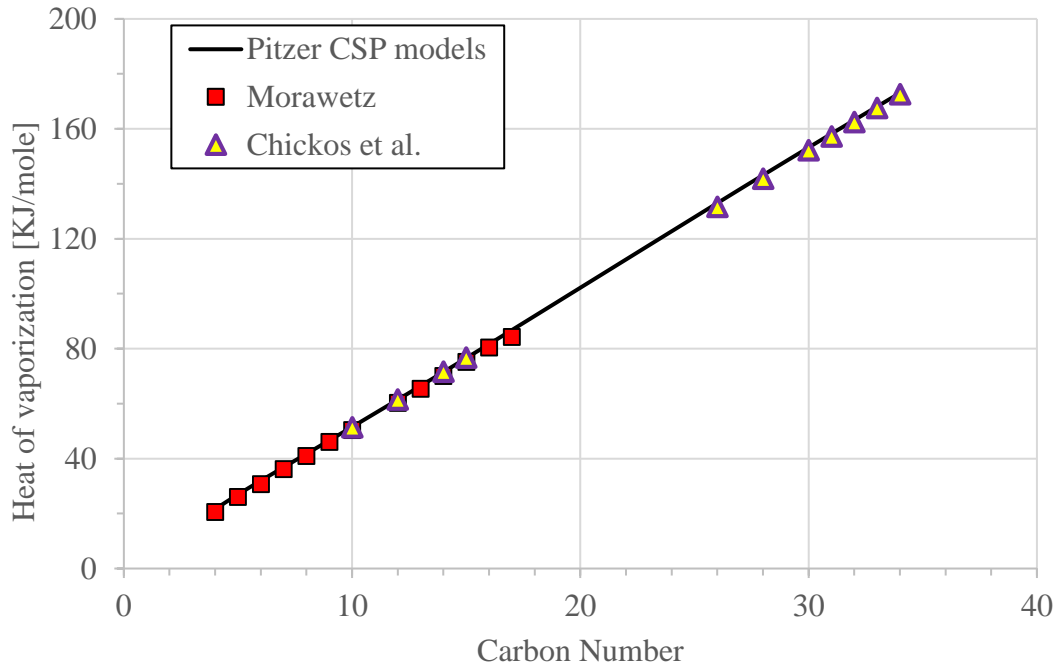


Figure 0-7: CSP model prediction of vaporization enthalpy for different carbon numbers at $T=25^{\circ}C$ versus experimental data (Morawetz and Chickos et al. [73], [74]).

2.5.2 Experimental dataset

For the next step, we needed to find reliable source of experimental data to verify our developed model. In this section, we provide a brief overview of the experimental data which have been used for our model verification. we compared the results obtained from SP-Wax to experimental data of five binary and seven multicomponent systems. various experimentally measured properties from different sources are tabulated. We have referred to these experiments multiple times and it is beneficial to present them exclusively in one section. In binary systems, SP-Wax performance was verified by forty-nine experimentally measured WAT data points from five different systems. In multi-component systems, various aspects of SP-Wax were verified through experimental data of seven different oil compositions including nineteen precipitation points, one-hundred and forty-seven solid phase composition data and five CCN values. South Pelto [10] and Garden Banks [38] are

two oil samples which have been used in our study for verification purposes. For both oil samples, input composition and other input data are available. In addition, different types of experimentally measured data have been reported including, precipitation data, solid phase CND, CCN and WAT. The two mentioned oil samples are evaluated through series of flowing experiments by Panacharoenawad and Rittirong. Please note that, HTGC method has been used to measure the composition of the deposit which contains solid wax particles and the trapped oil. This is why the measured composition needed to be subtracted by the liquid phase composition to obtain solid phase CND. The following table contains the experimental WAT data of the binary system.

Table 0-1:Binary system experimental data [30][75]

System	Temperature, [°C]	solute mole fraction in liquid phase	System	Temperature, [°C]	solute mole fraction in liquid phase
n-C28 in n-C7	22.9	1.56E-02	n-C32 in n-C7	16.1	1.37E-03
	23.75	1.74E-02		17.9	1.83E-03
	24.3	2.04E-02		19.6	2.30E-03
	24.55	2.06E-02		20.7	2.76E-03
	26.2	2.57E-02		22.1	3.43E-03
	29.15	3.76E-02		22.7	3.69E-03
	35.2	7.74E-02		24.3	4.79E-03
	38.8	1.14E-01		25.2	5.54E-03
n-C25 in n-C7	44.15	4.69E-01		26.55	6.82E-03
	42.65	3.91E-01		27.9	8.05E-03
	42.25	3.76E-01		28.4	8.61E-03
	41.05	3.56E-01	n-C36 in n-C7	18.1	3.29E-04
	37.75	2.57E-01		19	3.56E-04
	37.25	2.23E-01		19.25	3.75E-04
	28.25	1.04E-01		20.3	4.31E-04
	27.55	9.80E-02		22.1	5.98E-04
n-C23 in n-C7	32.05	2.68E-01		22.9	6.70E-04
	31.35	2.52E-01		23.25	7.54E-04
	31.15	2.35E-01		24.4	9.18E-04
	28.15	2.00E-01		25.8	1.16E-03
	27.75	1.71E-01		27.1	1.42E-03
	25.65	1.42E-01		29.25	2.11E-03
	24.05	1.17E-01		31.4	2.64E-03

	21.05	9.30E-02		32.65	3.25E-03
	19.45	7.20E-02		34.1	4.04E-03
	13.35	5.20E-02			

Since our thermodynamic simulation is only a function of temperature, we needed to have accurate temperature information. In Rittirong and Panacharoensawad studies, different temperatures have been calculated using the experimental thickness and wax fraction data. Bulk, wall and interface temperatures are presented in the following table from both studies.

Table 0-2: Supplementary data from Garden Banks and South Pelto oil case experiments [10] [38]

Oil Type	South Pelto	South Pelto	South Pelto	Garden Banks	Garden Banks
Test #	27	28	29	AR-21	AR-7
T _b [C]	40.55	40.48	40.33	25.08	26.02
T _w [C]	29.54	29.30	29.53	16.80	16.47
T _i [C]	37.51	35.99	34.00	18.01	19.73

Precipitation data of three oil samples are available and will be used for verification purposes of our thermodynamic model.

Table 0-3: Experimental precipitation data for Garden Banks [38], Fleming et al. [29], and Zheng et al. [6]

System	T[°C]	Precipitated weight fraction
Garden Banks	10.75	2.69E-03
	15.00	2.06E-03
	20.04	1.27E-03
	25.03	7.64E-04
	30.01	4.65E-04
	35.00	0
	-10.01	3.08E-01
	-0.01	2.46E-01
	9.99	1.64E-01
	14.85	1.22E-01
Fleming et al.	19.85	8.14E-02
	24.92	4.64E-02
	29.93	1.84E-02
	34.35	0
	5.00	1.70E+00
	10.00	1.35E+00
	15.00	1.03E+00
	20.00	7.48E-01
	25.00	5.10E-01
	30.00	3.26E-01
Zheng et al.	35.00	1.47E-01

Please refer to Rittirong for details about testing conditions. In addition, compositional input data of n-alkanes for South Pelto and Garden Banks are plotted in the next graph. For smoother CND plots, exponentially fitted lines (with $R^2 > 0.98$) have been used for composition. The effect was on precipitation curve was checked and it is small when fitted data were used for composition instead of actual input composition data. From the following graph, the composition data of heavier components are extrapolated. Please note that such extrapolation is somewhat subjective.

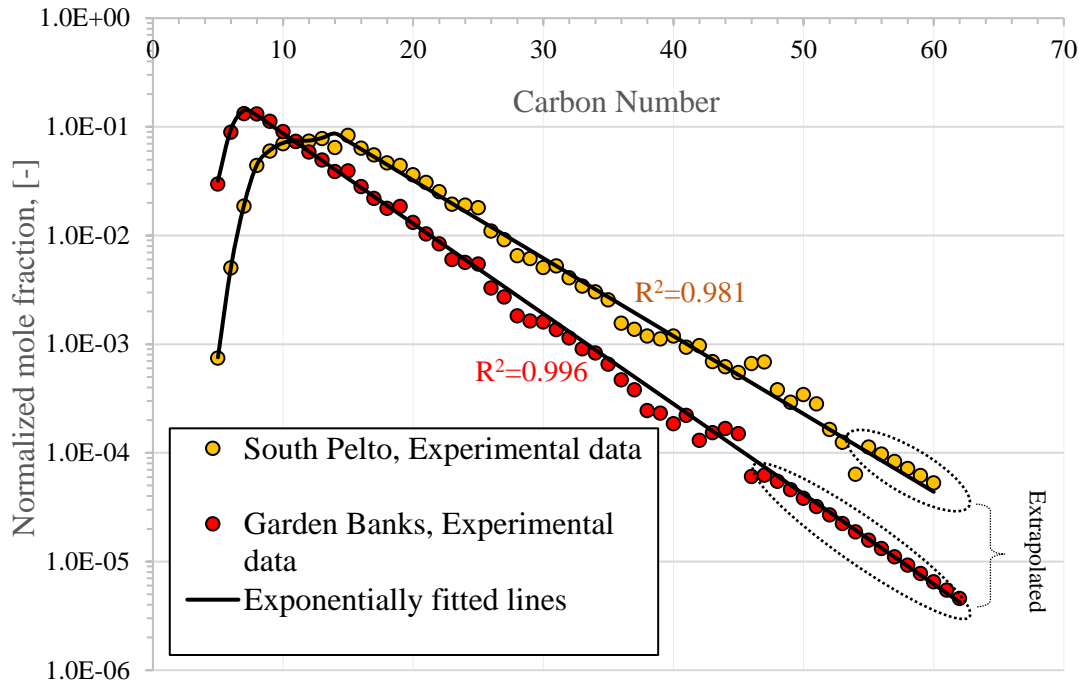


Figure 0-8: Compositional input data of n-alkanes for oil cases of Garden Banks and South Peltro and exponentially fitted lines

2.5.3 Binary System Model Validation

SP-Wax predictions have been validated by experimental data of five binary systems. The dissolved solute mole fractions at various WAT values from SP-Wax were compared to the literature data [30][75] and satisfactory agreement was obtained as shown in. The dissolved solute mole fraction decreases as either the temperature decreases (or $1000/T$ increases) or the n-alkane chain length becomes longer, as expected.

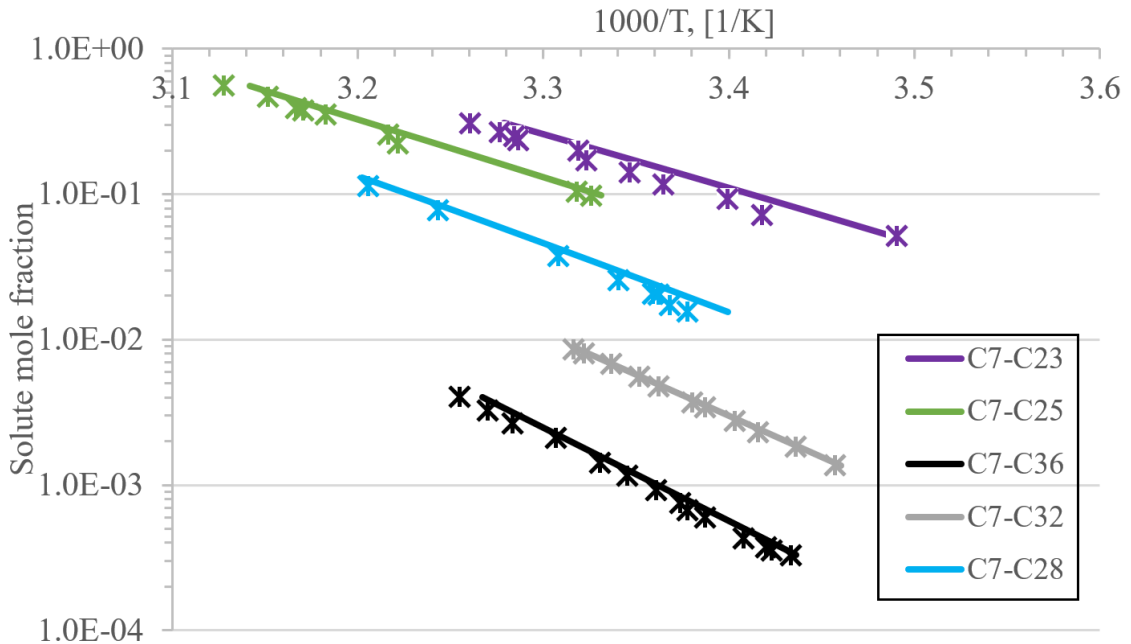


Figure 0-9: SP-Wax predictions and experimental data [30], [75] (\times symbol) of solid solubilities for five binary system at 1 bar (Table 0-1)

2.5.4 Multicomponent System Model Validation

One important aspect of a reliable thermodynamic model is its accuracy to predict the mass of precipitated paraffin in different temperatures (precipitation curve). Experimental precipitation data [6], [29], [38] were used to validate SP-Wax software. Fleming et al. [29] reported the experimental and predicted precipitation data points. Their prediction was based on Coutinho et al.'s model [20] using UNIQUAC approach for solid phase non-ideality. For another case, Rittirong [38] reported experimental precipitation data along with simulation results from TUWAX and PVTsim thermodynamic software. Notably, SP-Wax is far more accurate than all other simulation results. Zheng et al.'s [6] precipitation data are from the direct centrifugal technique. The direct technique is subject to less uncertainty because it does not need to calculate the precipitated amount based on the estimated enthalpy of crystallization of wax [76]. Zheng et al.'s [6] input composition for n-alkanes were reported graphically from C15 to C36. In our study, we extrapolated the composition for the wider range of carbon numbers, however, the extrapolation is somewhat subjective, and it is not unique. SP-Wax predictions of precipitation curve are in very good agreement with all three experimental data sets. SP-Wax prediction is almost identical to Fleming et al.'s prediction. Both studies use Coutinho thermodynamic model.

However, Fleming used UNIQUAC to express solid phase's activity coefficients and SP-Wax used the Wilson method. As per Coutinho's comparison, both methods should result in similar predictions which is true in our analyzed case. This is another indication of the validity of our developed thermodynamic software.

For Fleming et al. [29], the precipitation curves with three different values of adjustment parameter " a " ($0, 3 \times 10^{-7}$ and 8×10^{-7}) were calculated and shown in Figure 4(a). In their case, only n-alkane components were present ($W_f = 1$) and very small adjustment was needed. Among the three curves, the best fit resulted from $a = 3 \times 10^{-7}$ with $R^2 = 0.997$. For oil cases of Zheng et al. [6] and Rittirong [38], the optimum adjustment coefficient was chosen to be $a = 3 \times 10^{-6}$ with R^2 of 0.95 and 0.96, respectively.

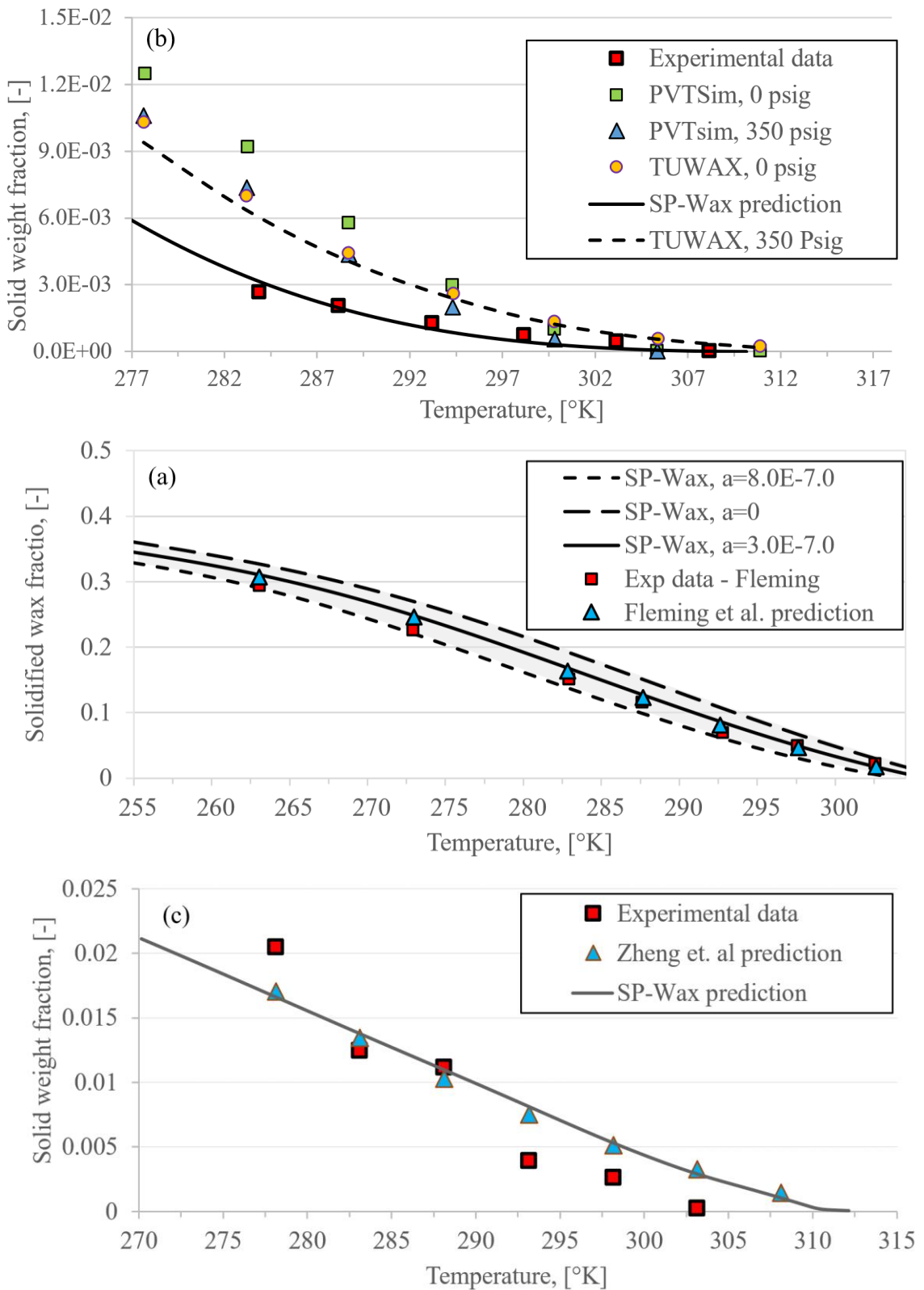


Figure 0-10: SP-Wax precipitation curve validation against Fleming et al.(a) [29], Rittirong(b) [38], and Zheng et al.(c) [6].

In addition to Figure 0-10, we compared SP-Wax predictions to experimental precipitation data of three more multicomponent systems from Dauphin et al. [77]. Notably, SP-Wax successfully predicts the experimental precipitation data.

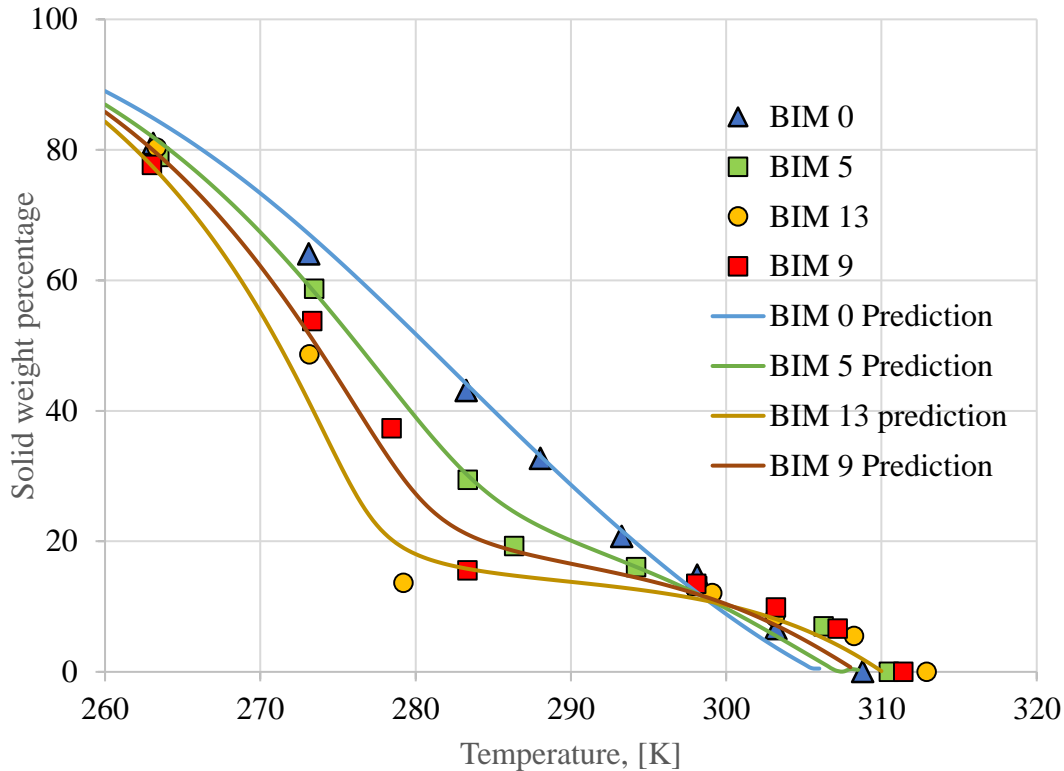


Figure 0-11: SP-Wax predictions versus precipitation data of Dauphin et al. [77]

Corresponding correction factor coefficient for each oil case is presented in the following table.

Table 0-4: Correction factor coefficients of different oil systems from Dauphin et al. [77]

Case	a
Bim 5	4.0E-07
Bim 0	4.0E-07
Bim 9	3.0E-07
Bim 13	2.0E-07

In addition to the precipitation curve prediction which is used in the pseudo-single-wax-phase modeling approach [3], [11], [12], [78], the solid phase composition information is

also important for a compositional-based model [6] and for analyzing the CCN of wax deposit for both single-phase [78] and multiphase cases [43], [65]. SP-Wax's ability to predict solid phase composition was validated through five sets of experimental CND data from Rittirong [38] and Panacharoensawad's [10] single phase wax deposition test results. The following graph shows the SP-Wax predictions against experimental solid phase CND data. SP-Wax predictions are in good agreement with experimental data for all cases. The slight overestimation is expected because, SP-Wax takes only the final-time temperature which is always higher than the average temperature over the time of the experiment.

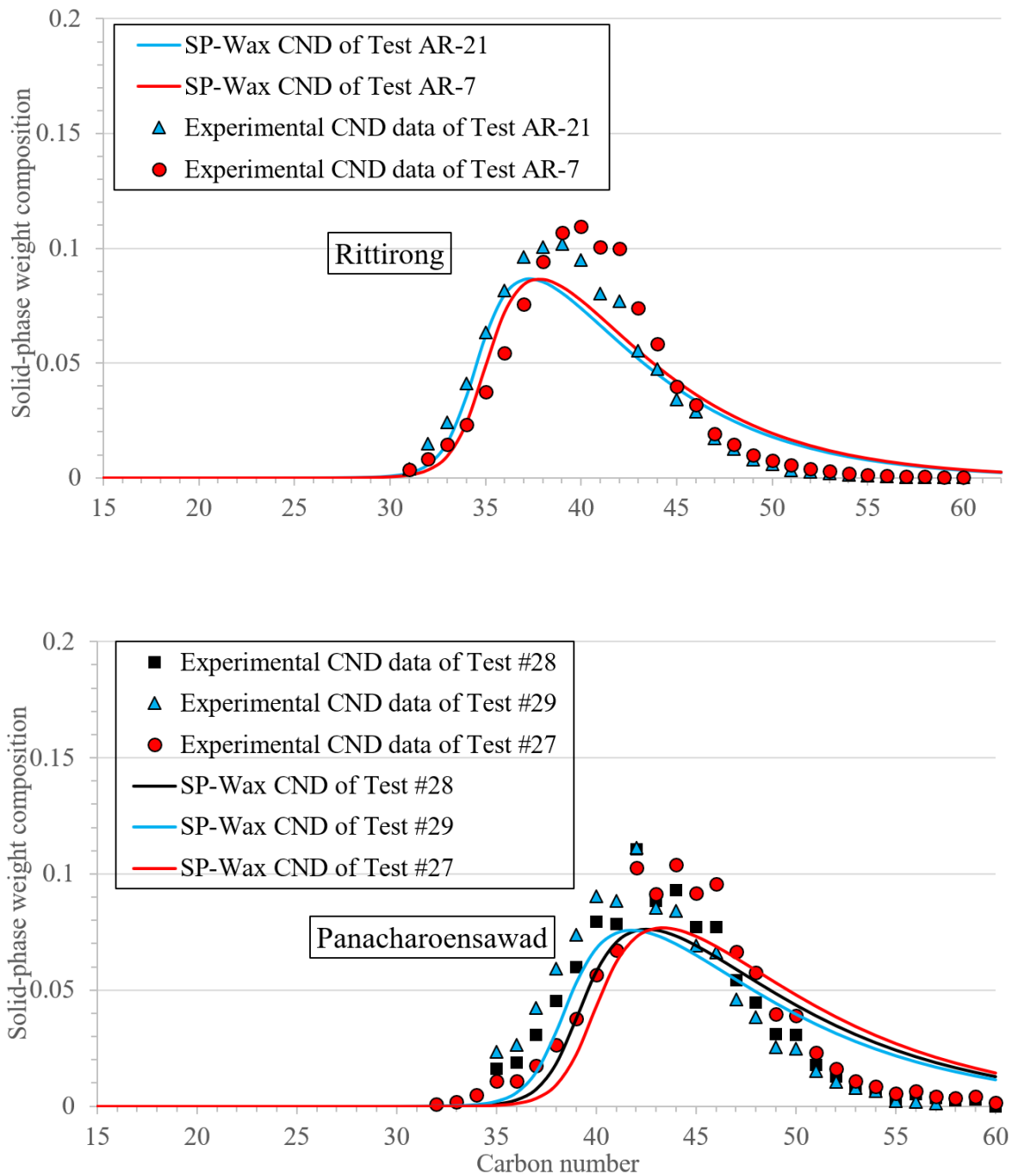


Figure 0-12: Solid phase CND data of paraffin deposit. SP-Wax predictions versus CND experimental data of Ritirong [38] and Panacharoensawad [10] at average deposit temperature $T_{avg} = 0.5(T_{int} + T_{wall})$ at the end of each test

2.5.5 Thermodynamic Verification of CCN and Aging Process

Lastly, the relative concentration gradient from SP-Wax is used to estimate the CCN in five different tests. In our analysis, the pre-calculated deposit's temperatures, which were reported in the literature [10], [38], were used to calculate the relative concentration gradient for CCN estimation. The relative concentration gradient is defined as the ratio of the dissolved mass of i^{th} carbon number over the volume of all n-alkanes in liquid phase (in m^3). In SP-Wax, CCN is estimated by determining the smallest carbon number with positive relative concentration gradient. We note that the CCN estimation typically requires significant overhead calculations as part of wax deposition modeling. However, this thermodynamic property (CCN) can be estimated as a function of deposit's temperature. Since the deposit's temperature can be determined using experimental measurements at the final time (the time at which the composition was determined by HTGC), CCN can be predicted by SP-Wax. CCN is closely related to the aging concept where lighter n-alkanes diffuse out of the deposit and heavier n-alkanes ($>\text{CCN}$) diffuse toward the well through a counter-diffusion process due to concentration gradient. In our study, we verified this phenomenon thermodynamically. In Figure 0-13, within the red highlight carbon number range, it can be seen that the relative concentration of lighter n-alkanes ($<\text{CCN}$) are higher at wall temperature in compare to the deposit's temperature. This implies that the existing concentration gradient derives the light n-alkanes diffuse out of the deposit. On contrary, the heavier n-alkanes ($\text{CCN}<$) will diffuse toward the wall due to concentration gradient from paraffin deposit to the pipe's wall.

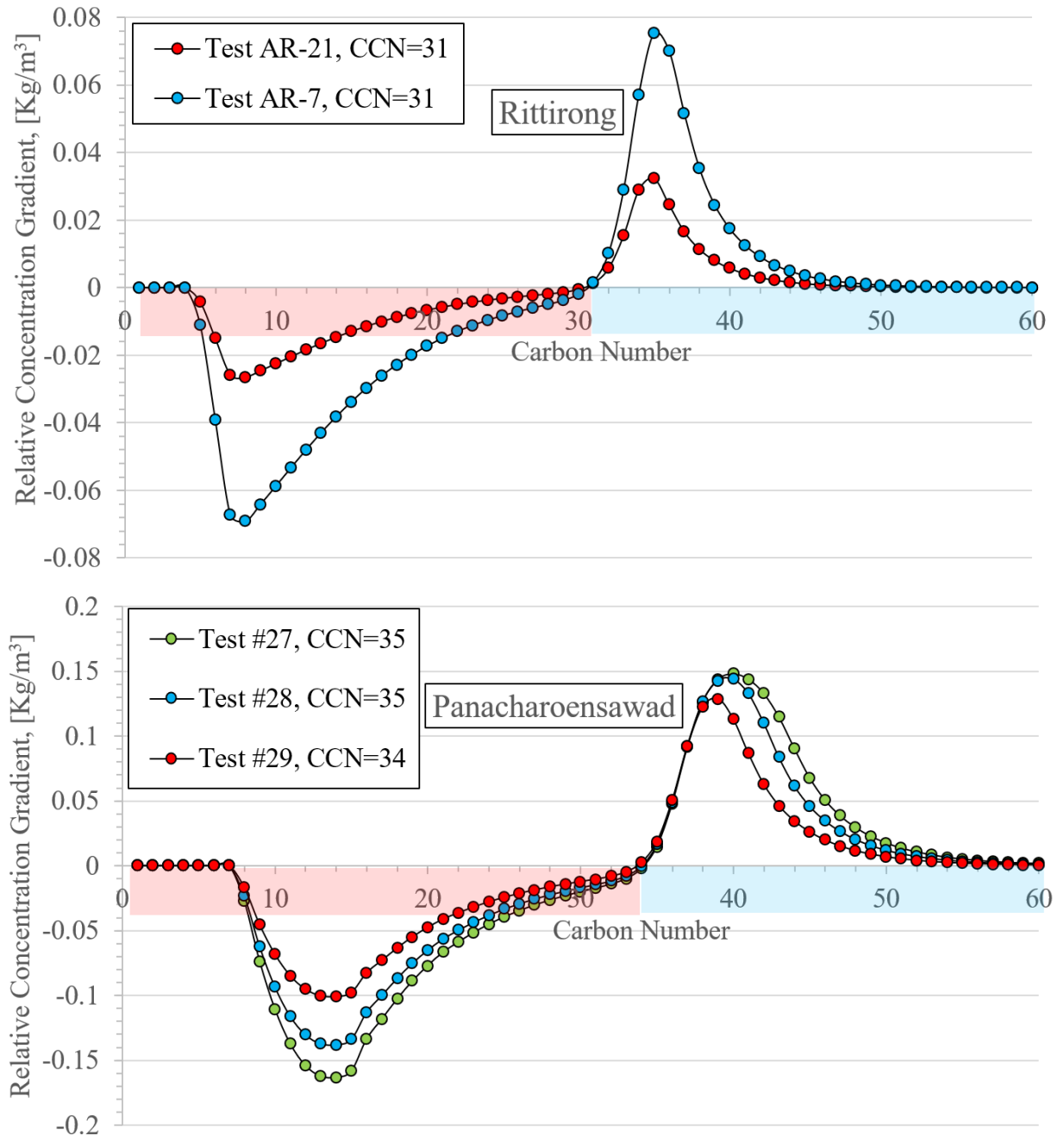


Figure 0-13: SP-Wax relative concentration gradient predictions for five tests of Ritirong [38] and Panacharoensawad [10]. Associated CCN values are annotated in the graph for each test. Blue and red highlighted sections are referred to carbon number components that diffuse in and out of the deposit, respectively.

The numerical values of solid phase Average Carbon Number (ACN), mode and CCN predictions with test temperature values used in SP-Wax simulation are shown in the following table. In addition to the comparison in the above graphical form, the numerical

value shown below confirm the match of SP-Wax to the literature data.

Table 0-5: Temperatures data at the end of experiments for five tests plus experimental data [10], [38] and predictions of Average Carbon Number (ACN), Mode, and Critical Carbon Number (CCN). South Pelto and Garden Banks are the names of oil samples that have been used by Panacharoensawad [10] and Ritirong [38], respectively.

Oil Type	South Pelto	South Pelto	South Pelto	Garden Banks	Garden Banks	Mean Absolute Relative percentage error %*
Test #	27	28	29	AR-21	AR-7	
T_b [C]	40.6	40.5	40.3	25.1	26.0	
T_w [C]	29.5	29.3	29.5	16.8	16.5	
T_i [C]	37.5	36.0	34.0	18.0	19.7	
ACN (Exp)	44.8	43.6	42.8	40.5	39.6	
ACN (Pred)	47.3	46.6	45.9	41.9	41.4	5.49
Mode (Exp)	44	42	42	40	39	
Mode (Pred)	43	43	42	38	37	2.96
CCN (Exp)	35	35	35	30	30	
CCN (Pred)	35	35	34	31	31	1.90
Correction Factor Coefficient	3.0E-06					

* Mean relative percentage error % is defined as $\frac{1}{NN} \sum_{ii=1}^{NN} \left| \frac{y_{Sim,ii} - y_{Exp,ii}}{y_{Exp,ii}} \right| 100$.

Table 0-5 contains the relative error of the model for solid solubilities of binary systems and precipitation curves of multicomponent systems. The relative error formula which is used in Table 0-5 is as follows:

$$\text{Estimated relative error} = \frac{\frac{1}{NN} \sum_{ii=1}^{NN} \left| y_{Sim,ii} - y_{Exp,ii} \right|}{\frac{1}{NN} \sum_{ii=1}^{NN} \left| y_{Exp,ii} \right|} 100 \quad (0-1)$$

where, NN, y_{sim} and y_{Exp} are the total number of cases, simulated and experimental sample parameters, respectively

Table 0-5 shows that the model has the average estimated relative error of about 22% and 3.7% for the case of multicomponent precipitation curve and the binary system WAT, respectively. SP-Wax requires accurate input n-alkane compositions. In multicomponent systems, the accumulative error of input compositions is higher than in binary systems, simply because more components are present. In some multicomponent cases, such as in

Zheng et al. [6], the n-alkane input composition data are incomplete and the extrapolation of the n-alkane composition is needed. This contributes to the model prediction's uncertainty.

Table 0-6: Estimated relative error of the SP-Wax prediction for precipitation curves (Figure 4) of multicomponent systems.

Case	System	Estimated Relative error [%]
Rittirong	Multicomponent	20.0
Zheng et al.	Multicomponent	28.7
Fleming et al.	Multicomponent	17.1

Furthermore, the average absolute errors of WAT prediction for the binary systems are calculated and shown in Table 3. The results show that SP-Wax can successfully predict the solid solubility of binary systems.

Table 0-7: Temperature differences between predicted and experimental WAT parameter of five binary systems.

System	Average temperature difference [°C]
C7-C23	1.83
C7-C25	1.10
C7-36	0.74
C7-C32	0.22
C7-C28	1.28

2.6 Wax Deposition in Laminar Flow

We developed a C++ simulation to predict different characteristics of wax deposition phenomenon under laminar flow [70]. We, then, compared our simulated results to the experimental data reported by Singh et al. [3]. Table 0-8 represents the operating conditions of the investigated experimental data [3].

Table 0-8: Operating conditions of Singh et al. wax deposition tests [3]

Data Source	Case#	ID_{pipe}	μ_{oil}	ρ_{oil}	T_{bulk}	t_{test}	$T_{ambient}$	Q
		[cm]	[pa.s]	$\left[\frac{kg}{m^3}\right]$	[°C]	[day]	[°C]	$\left[\frac{gal}{s}\right]$
Singh et al. (Laminar flow)	1	1.44	0.0087	838.5	22.2	5.0	8.3	1.0
	2						8.3	2.5
	3						8.9	4.0
	4						7.2	1.0
	5						4.4	1.0

Through our developed simulation, we predicted the deposit's thickness and solid wax fraction for all five cases. In Figure 0-14, the simulated results are plotted against the experiment data for deposit's thickness versus solid wax fraction. The predictions show great accuracy as they successfully track the experimental data for all five flow conditions.

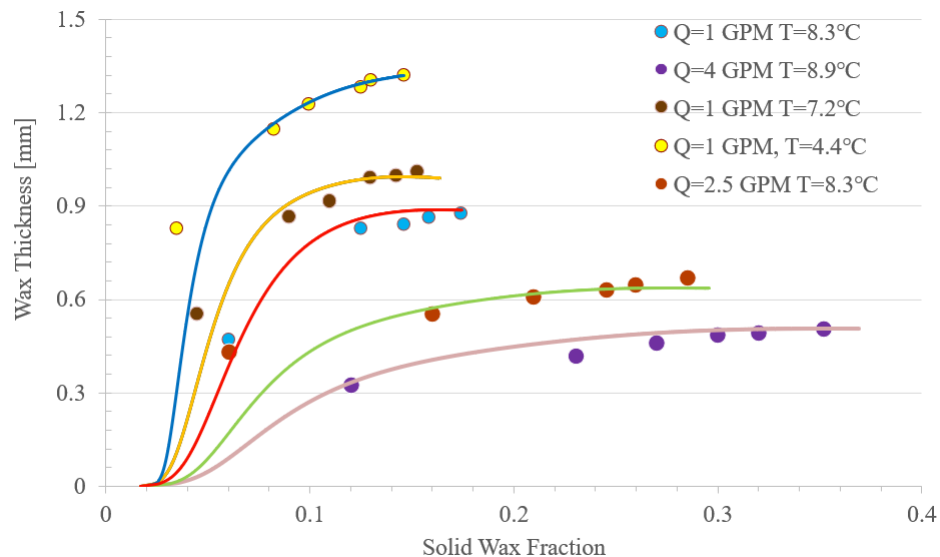


Figure 0-14: Deposit's thickness versus solid wax fraction. Points represent the experimental data and the solid lines are created by our developed simulation

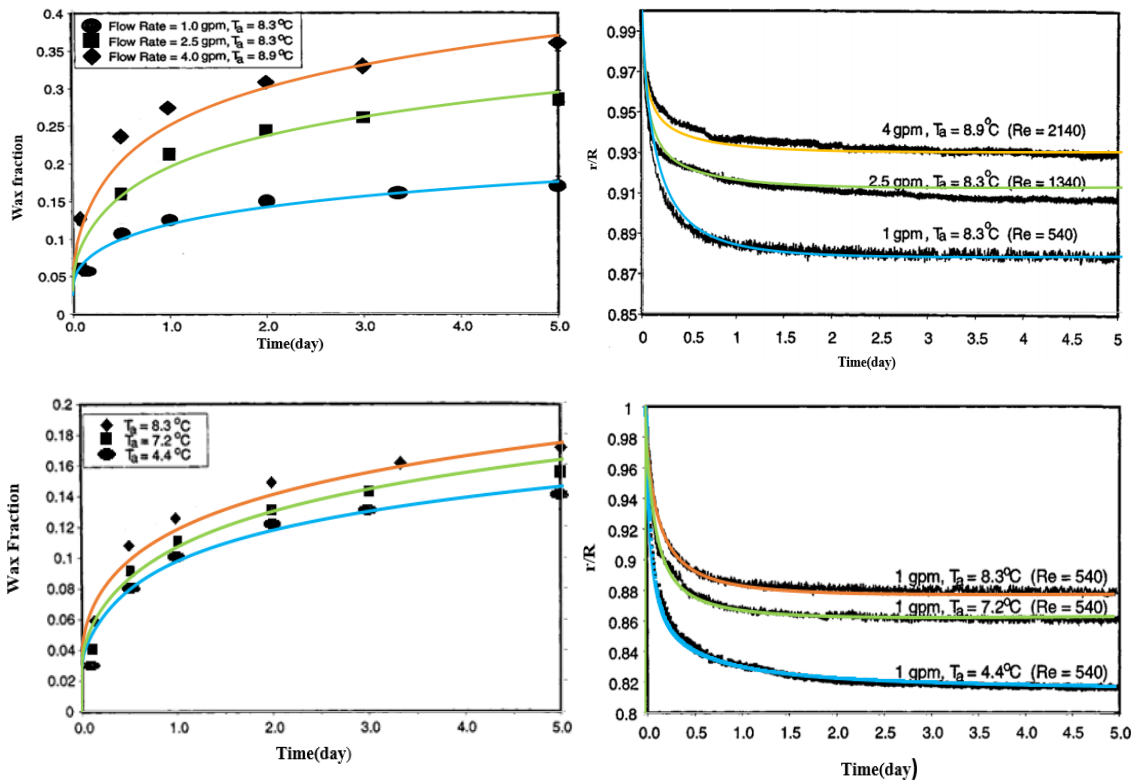


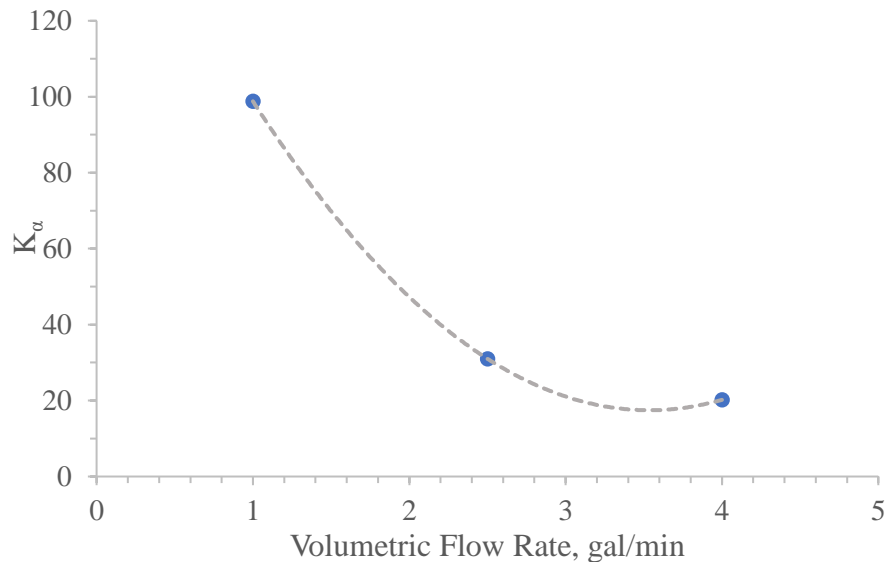
Figure 0-15: Simulation results versus experimental data for solid wax fraction and effective pipe's radius parameters. Colored lines are generated by our simulation and the rest are experimental data [3].

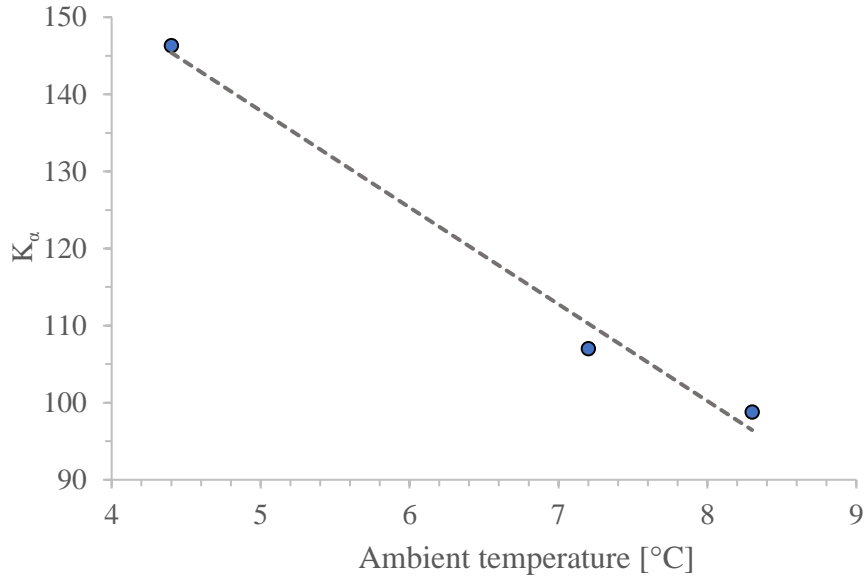
In our modeling approach, we updated the bulk concentration axially using Eq. 0-72 and included it in the RK45 steps. This approach resulted in a slightly more accurate predictions in compare to Singh et al. predictions [3]. We also analyzed the crystal aspect ratio parameter (Eq. 0-56) based on the fitted k_α values. The following table contains the adjusted k_α values which are reported by the Levenberg-Marquardt optimization tool.

Table 0-9: k_α values for different testing flow conditions

$T_{ambient}$ °C	Q gal/min	K_α
8.3	1.0	98.8
8.3	2.5	31
8.9	4.0	20.2
7.2	1.0	107
4.4	1.0	146.3

From Table 0-9, it can be noticed that “ α ” decreases as flow rate increases. Assuming the same ambient temperature, the isolated effect of flow rate has been illustrated in Figure 0-16. Additionally, by assuming constant flow rate, k_α increases as temperature decreases (Figure 0-17).

Figure 0-16: LM adjusted k_α versus volumetric flow rate

Figure 0-17: k_α versus ambient temperature for $Q_{\text{oil}} = 1 \text{ gal/min}$

Finally, we derived the wax crystal aspect ratio values from the \bar{F}_w predictions and plotted them versus solid wax fraction. Notably, the slopes are very similar to those reported in Table 0-9.

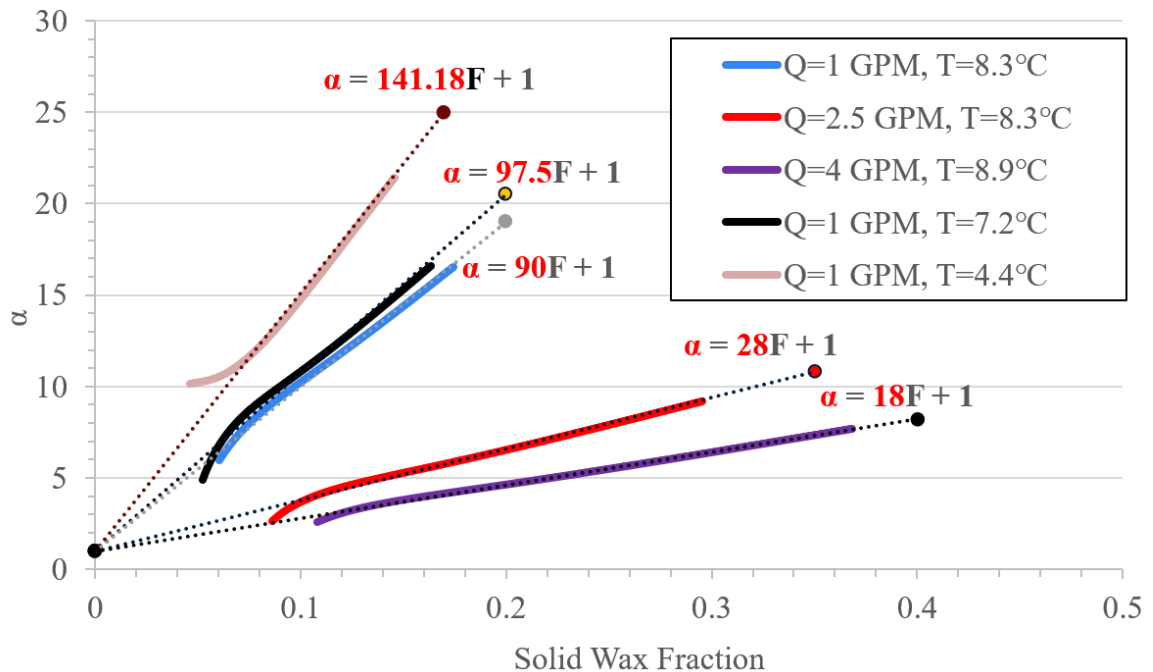


Figure 0-18: Derived crystal aspect ratio versus solid wax fraction for five operating conditions

2.7 SP-Depo Wax Deposition Model and Software

In this section, SP-Depo's accuracy will be verified by data from flow-loop experiments reported by Pancharoensawad [10]. Therefore, when we refer to a test number or a test condition, it is from Pancharoensawad dissertation [10] where all digitized data are available. The data types associated with each flow-loop experiment include deposit's thickness, solid wax fraction and deposit's solid phase carbon number distribution. In the following table, test conditions is presented [10].

Table 0-10: Test conditions of the used experiments [10]

Test #	Oil Velocity [m/s]	time [hr]	T _{h,inlet} [°F]	Q _c [gpm]	T _{C,inlet} [°F]
36	2.25	48	107.1	4.4	83.8
24	2.24	48	105.3	4.8	82.9
25	2.24	32	105.8	4.8	82.9
26	2.25	16.4	106.3	4.8	82.8
27	2.24	4	105.5	4.8	82.8
32	1.83	48	105.5	4.4	83.1
18	1.83	48	104.9	4.7	83.2
31	1.83	32	104.5	4.4	83.3
20	1.83	32	105.4	4.7	83.1
19	1.83	16	105.5	4.7	83.1
30	1.83	16	104.9	4.4	83.1
28	1.83	4	105.4	4.4	83
21	1.19	48	105.2	4.8	84.3
23	1.19	32	104.8	4.7	84.1
22	1.19	16	105.1	4.7	84.2
29	1.19	4	105	4.4	84

For n-alkanes composition, there are three reported compositions in Panacharoenawad [10] from different sources as shown below. We use the composition from Bruno (2006) in our study.

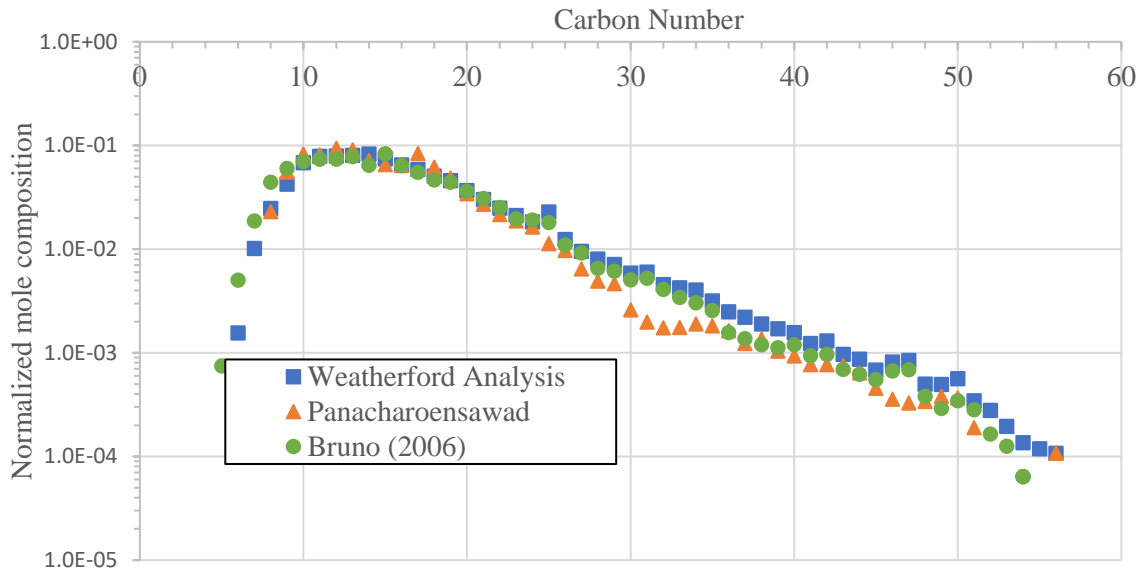


Figure 0-19: Normalized mole composition of South Pelto oil (used in Panacharoensawad [10])

In Table 0-11, the experimental thickness, solid wax fraction and solid phase average carbon number data are presented.

Table 0-11: Experimental data of deposit's thickness, F_w and ACN

Test #	Thickness [mm]	\bar{F}_w [%]	ACN
24	0.79	24.8	46.2
36	0.8	28.6	46.3
25	0.74	23.2	46.3
26	0.66	19.8	46.1
27	0.39	10.8	44.6
18	1.03	23	45.3
32	1.15	22	45.7
20	1.16	18.3	45.6
31	1.14	18.1	45.4
19	0.92	12.6	44.8
30	1	14.1	45.2
28	0.28	8.1	43.6
21	1.19	12	44.3
23	0.96	12.1	44
22	0.61	9.1	43.4
29	0.22	6.1	42.8

2.7.1 Minimum depositable carbon number (MinC)

As we discussed in chapter three, concentration, $\frac{\partial C}{\partial T}$ and D_{wo} are calculated from SP-Wax thermodynamic model. Therefore, all required inputs (Figure 0-9) for SP-Wax are also needed for SP-Depo. In our SP-Wax thermodynamic model, the user should provide a value for the correction factor coefficient for Eq. 0-15 based on the experimental precipitation data for each n-alkane composition. Although, the precipitation data are not available for the South Pelto oil case, we used the deposit's solid phase CND to determine the correction factor coefficient for Weatherford and Bruno n-alkane compositions as follow:

$$a = \begin{cases} 3 \times 10^{-6} & \text{Weatherford n - alkane composition} \\ 2 \times 10^{-6} & \text{Bruno n - alkane composition} \end{cases} \quad (0-2)$$

Another important input parameter of SP-Wax thermodynamic model is the minimum carbon number or MinC. MinC is defined to be the smallest carbon number which contributes to the deposition which is very similar to CCN. For MinC determination, the user should refer to Figure 0-2 and choose the minimum depositable carbon number based on the lowest operating temperature which usually is the coolant temperature. In our dataset [10], the coolant temperature is constant for more than sixteen single-phase flow-loop experiments and based on raw HTGC data of the deposit's composition, CCN is approximated to be 33 which is very similar to our simulation prediction of CN = 33.

Expectedly, deposit mostly contains oil with smaller fraction of the solidified phase. Therefore, raw HTGC data should show two carbon number distributions for both liquid and solid phases (Figure 0-20). It is almost impossible to know what the exact composition of each phase is using the HTGC data. However, it is possible to approximate each phase's composition. One method is to assume that carbon numbers before CN = 33 are only in liquid-phase and heavier n-alkanes are both in both phases. This assumption seems reasonable because our thermodynamic model also shows that it is nearly impossible for carbon numbers smaller than CN = 33 precipitate at coolant temperature (Figure 0-21).

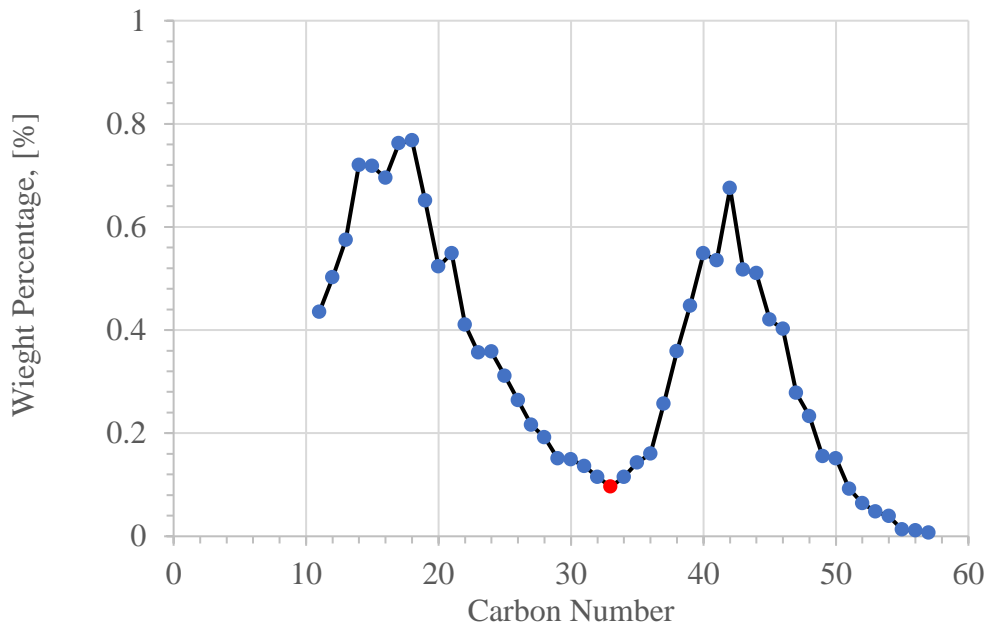


Figure 0-20: Deposit's raw HTGC data for Test #29 where CCN=33 is determined by red

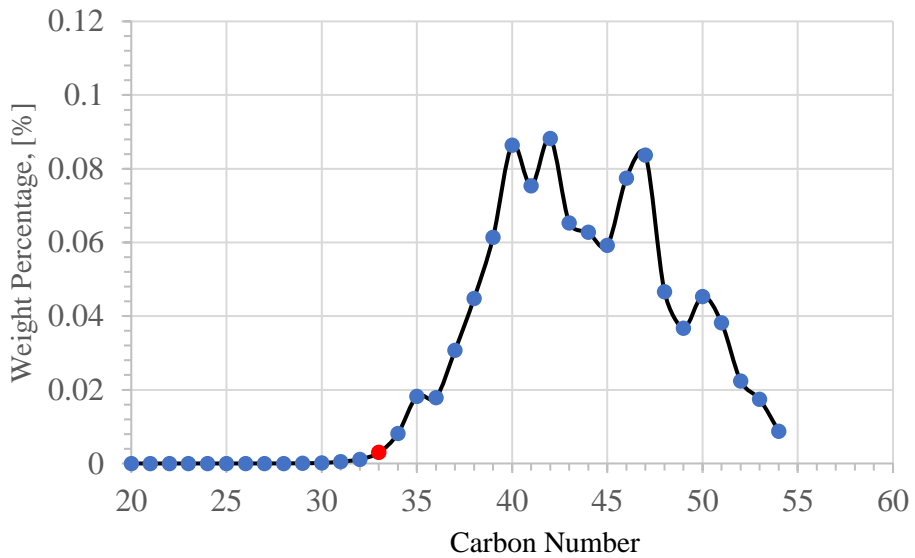


Figure 0-21: SP-Wax simulation: deposit's solid phase CND at coolant temperature ($T=28.77^{\circ}\text{C}$)

So, by accepting the above assumption, if we subtract the oil composition from the deposit's composition, the solid phase composition can be approximated. In Figure 0-22, the data for $\text{CN} > 33$ were extrapolated using the equation which was resulted from fitted regression to data from $\text{CN} = 27$ to 33.

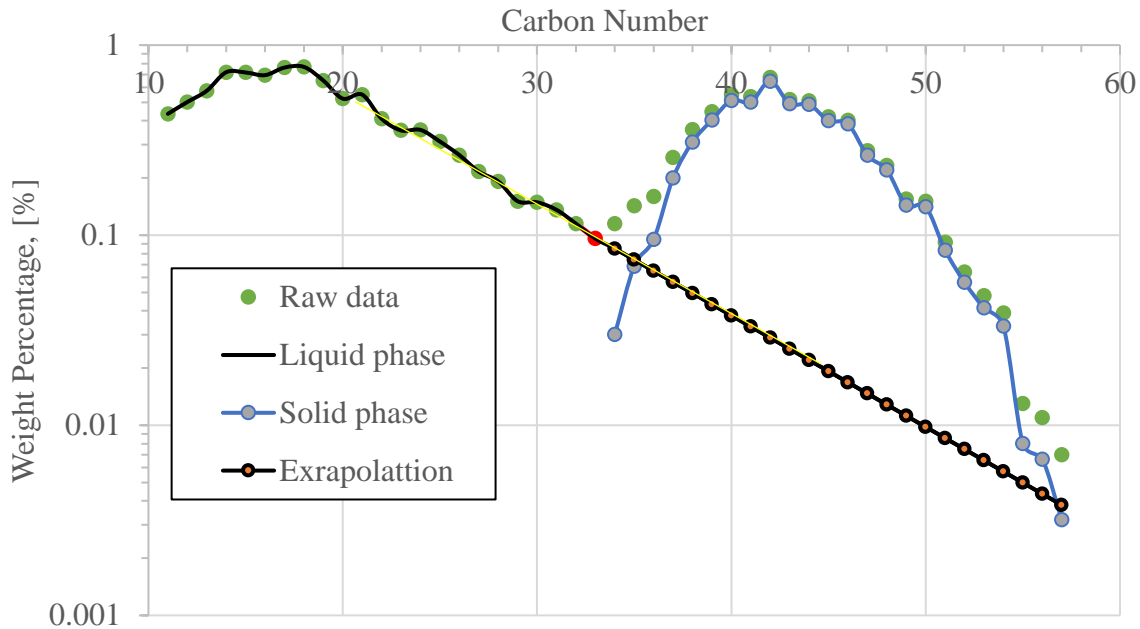


Figure 0-22: HTGC data with separated liquid and solid compositions.

Therefore, our developed method for determination of minimum depositable carbon number (MinC) is consistent with the experimental data.

2.7.2 Thickness and solid wax fraction predictions

After knowing the MinC, all required inputs are enough to run the wax deposition model. However, it is crucial to recheck the fitted regression equations to the thermodynamic data. In SP-Depo, we made it possible for the user to check fitted lines to concentration, $\frac{\partial c}{\partial T}$ and D_{wo} . The following graphs, shows that all thermodynamic parameters are well represented by the fitted curves.

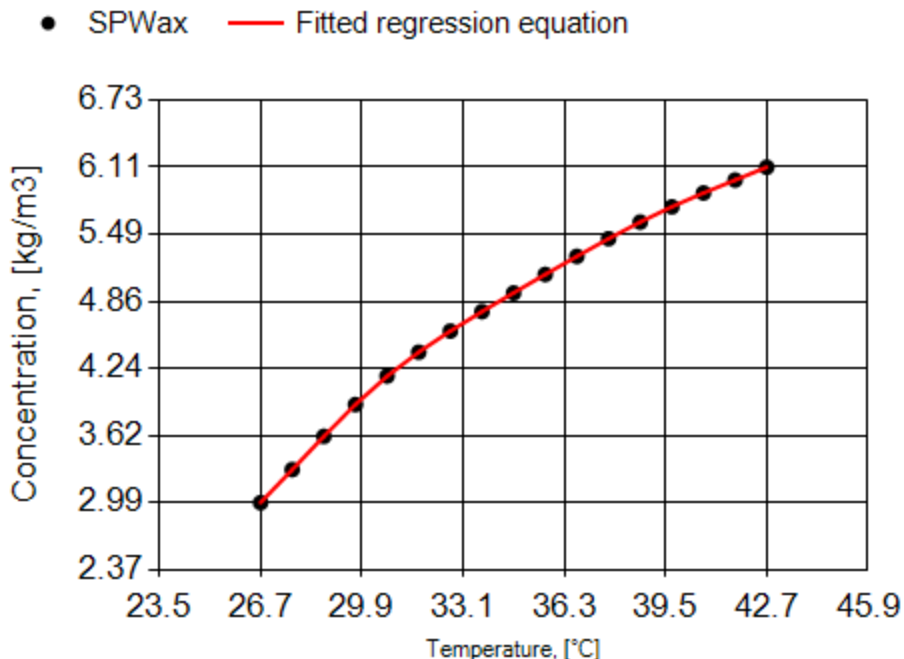


Figure 0-23: Concentration calculated from the SP-Wax thermodynamic model with fitted regression curve for South Pelto oil case

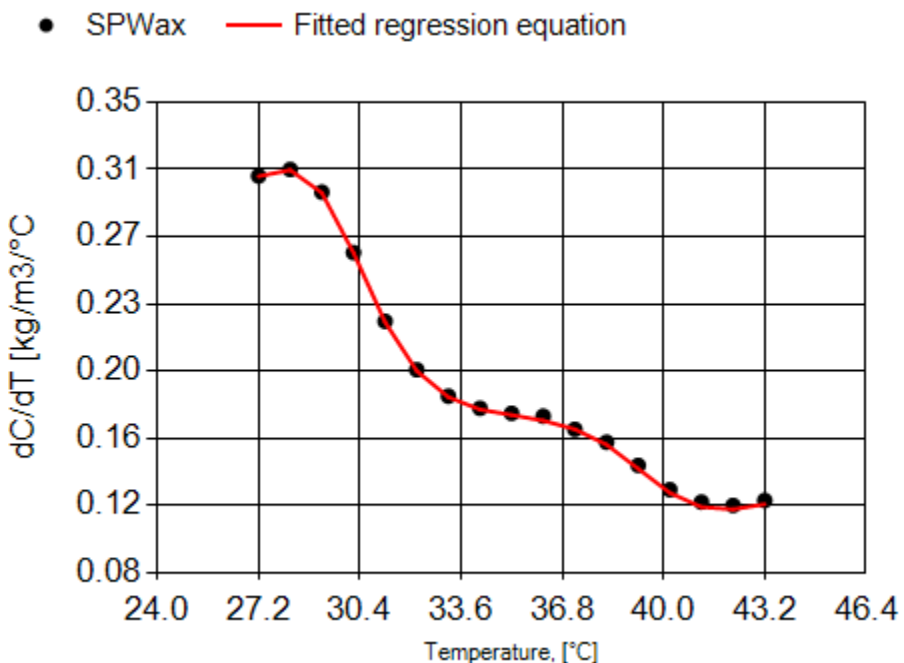


Figure 0-24: $\frac{\partial C}{\partial T}$ calculated from the SP-Wax thermodynamic model with fitted regression curve for South Pelto oil case

- SPWax — Fitted regression equation

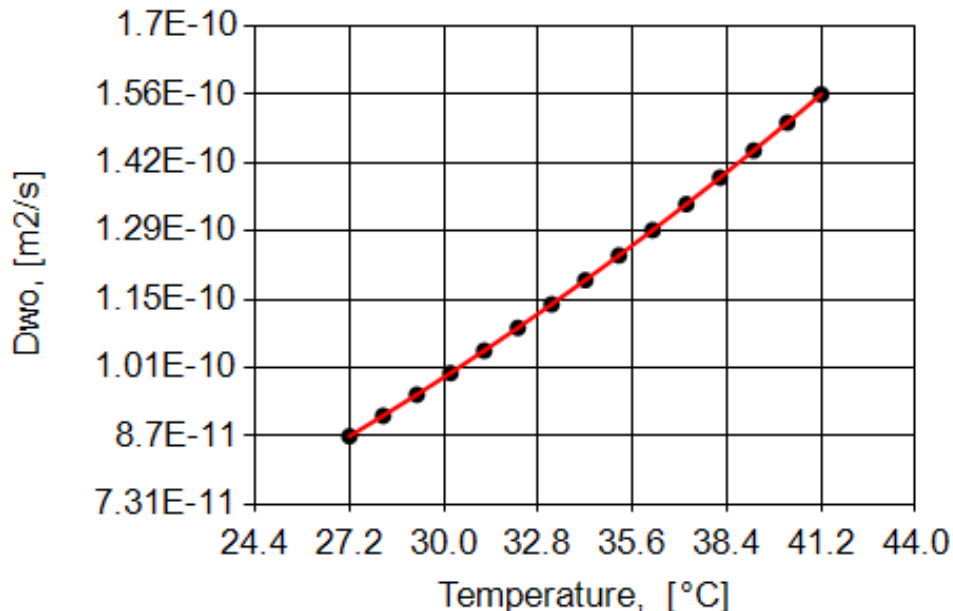


Figure 0-25: D_{wo} calculated from the SP-Wax thermodynamic model with fitted regression curve for South Pelto oil case

So, after reassuring about the thermodynamic model and the fitted regression equations, the software can be run. In SP-Depo, deposit's thickness, solid wax fraction and solid phase CND are predicted for each axial section. In the two following graphs, SP-Depo predicted thickness and F_w profiles are plotted using SP-Comp wax deposition model.

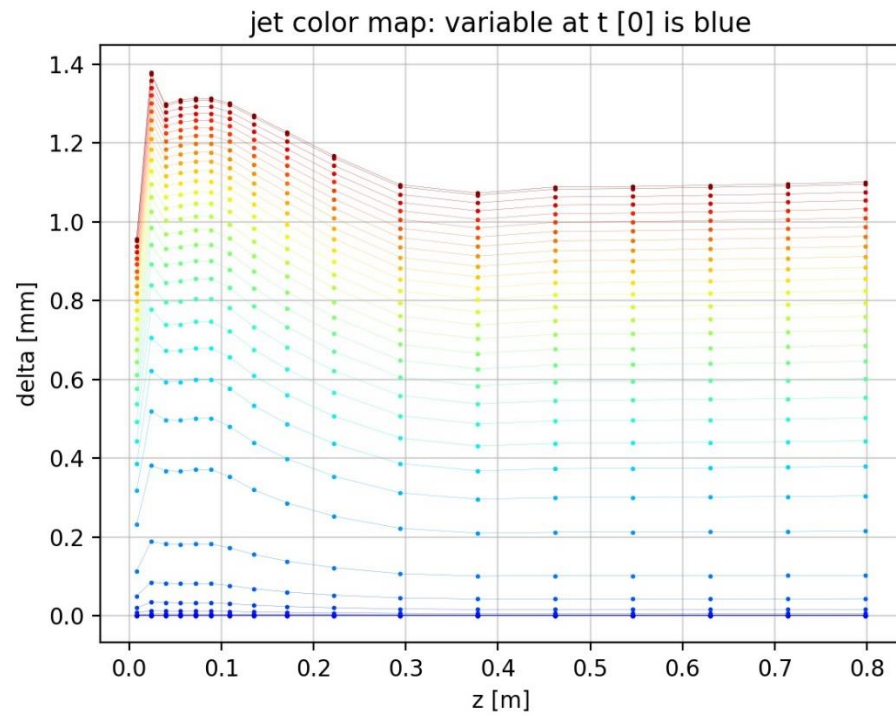


Figure 0-26: Deposit's thickness axial profile for Test #21 ($V_{oil} = 1.19 \text{ m/s}$)

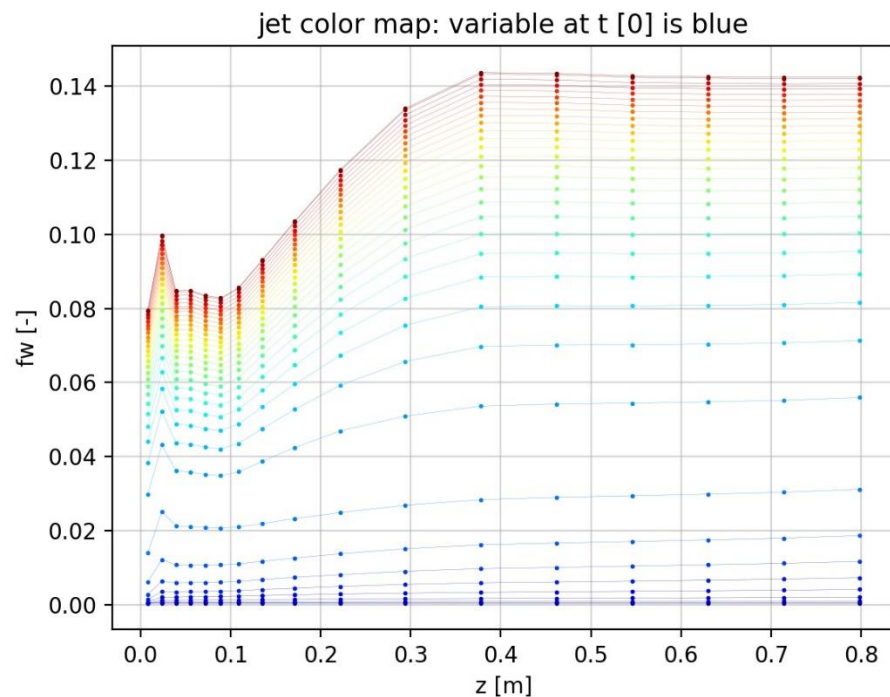


Figure 0-27: Deposit's solid wax fraction axial profile for Test #21 ($V_{oil} = 1.19 \text{ m/s}$)

And average deposit's thickness and solid wax fraction have been plotted against the experimental data in Figure 0-28, Figure 0-29 and Figure 0-30. Notably, SP-Depo successfully predicts thickness and solid phase wax fraction for all three flow conditions using SP-Compo wax deposition model. In SP-Depo, Dormand-Prince ODE solving method has been used which incorporates adaptive step size when rate of change is high. In the three following graphs, denser discretization is chosen at earlier times due to higher rate of change.

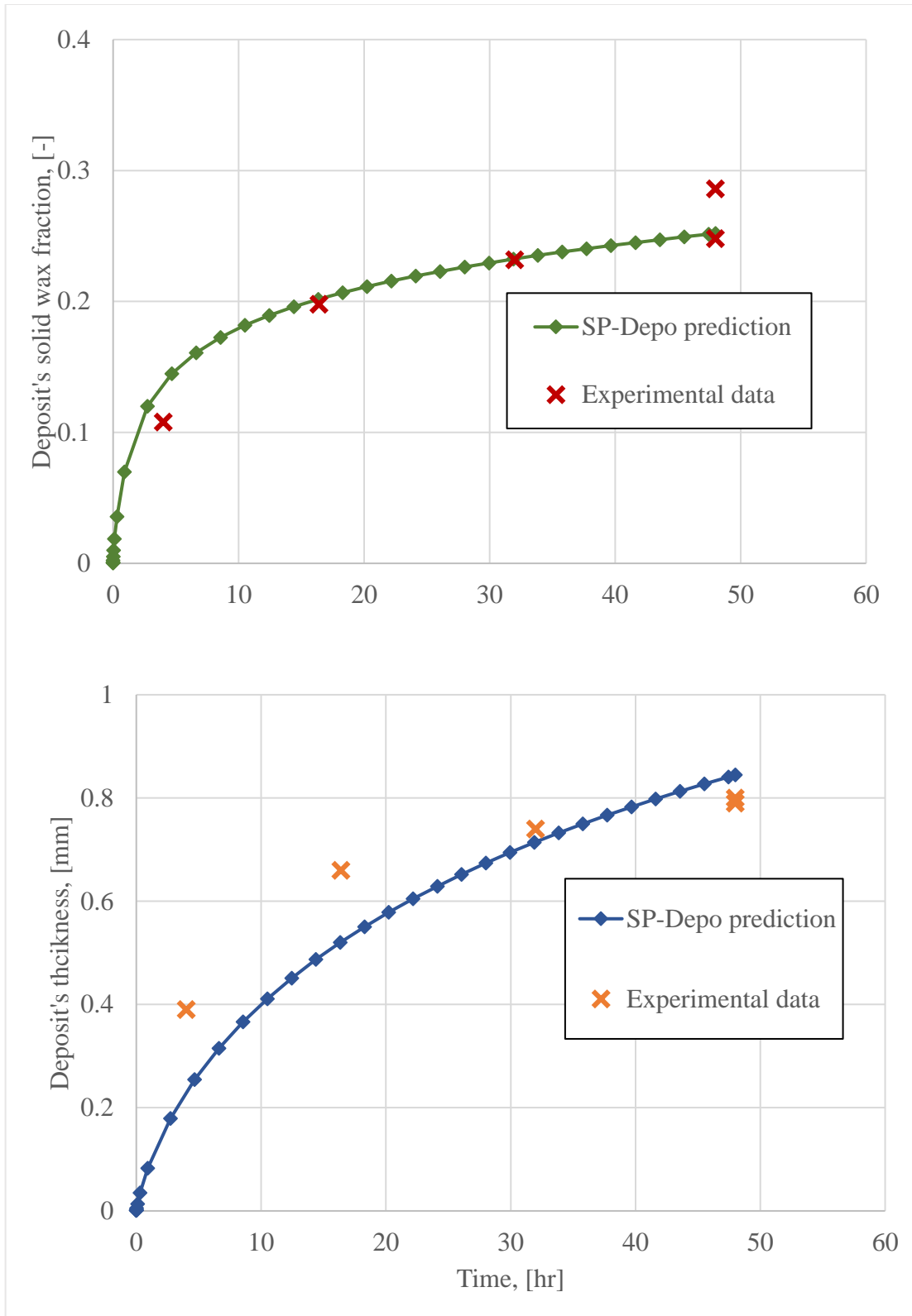


Figure 0-28: Average deposit's and solid wax fraction predictions versus experimental data for $V_{oil} = 2.24 \text{ m/s}$

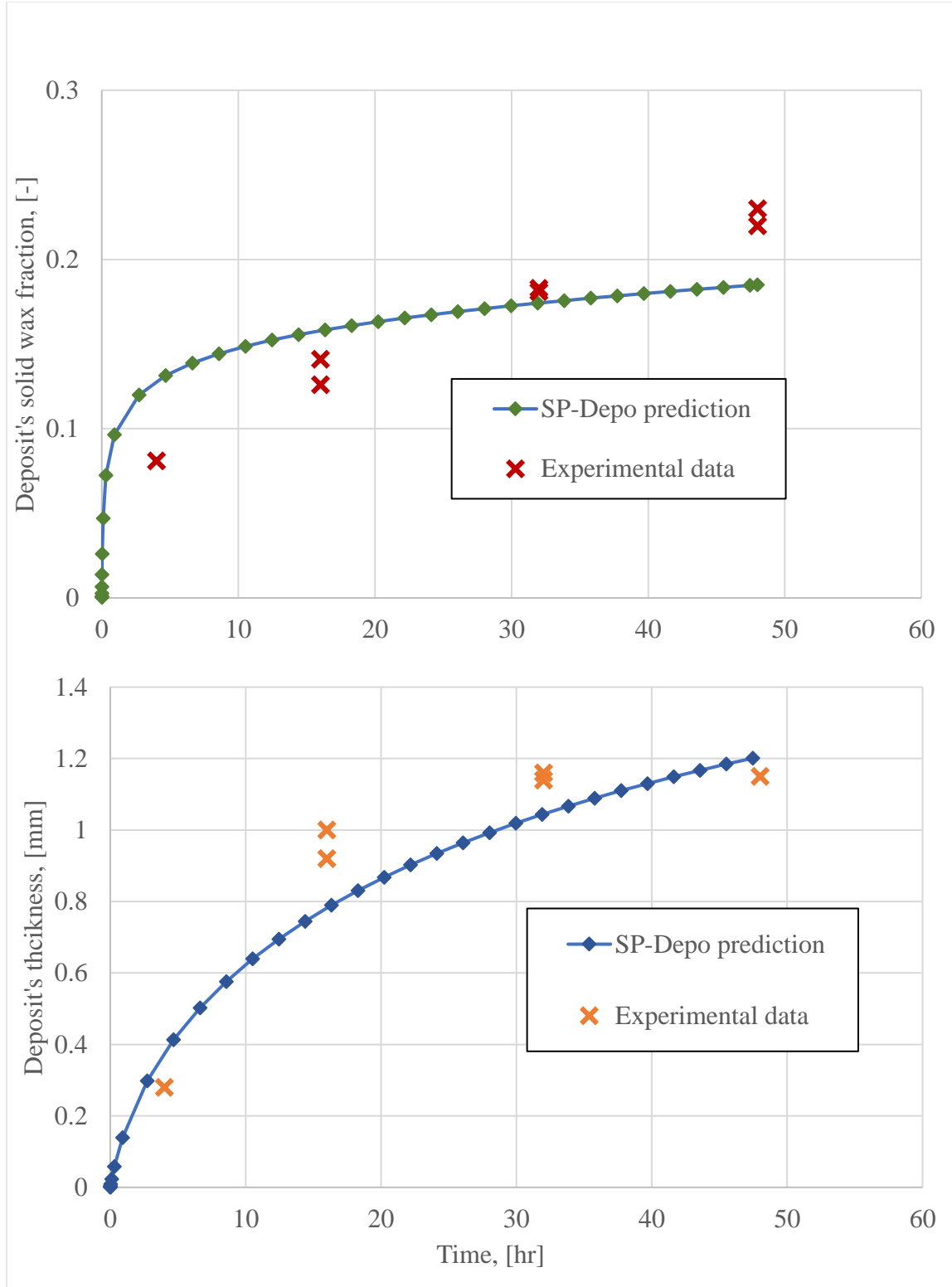


Figure 0-29: Average deposit's and solid wax fraction predictions versus experimental data for $V_{oil} = 1.83 \text{ m/s}$

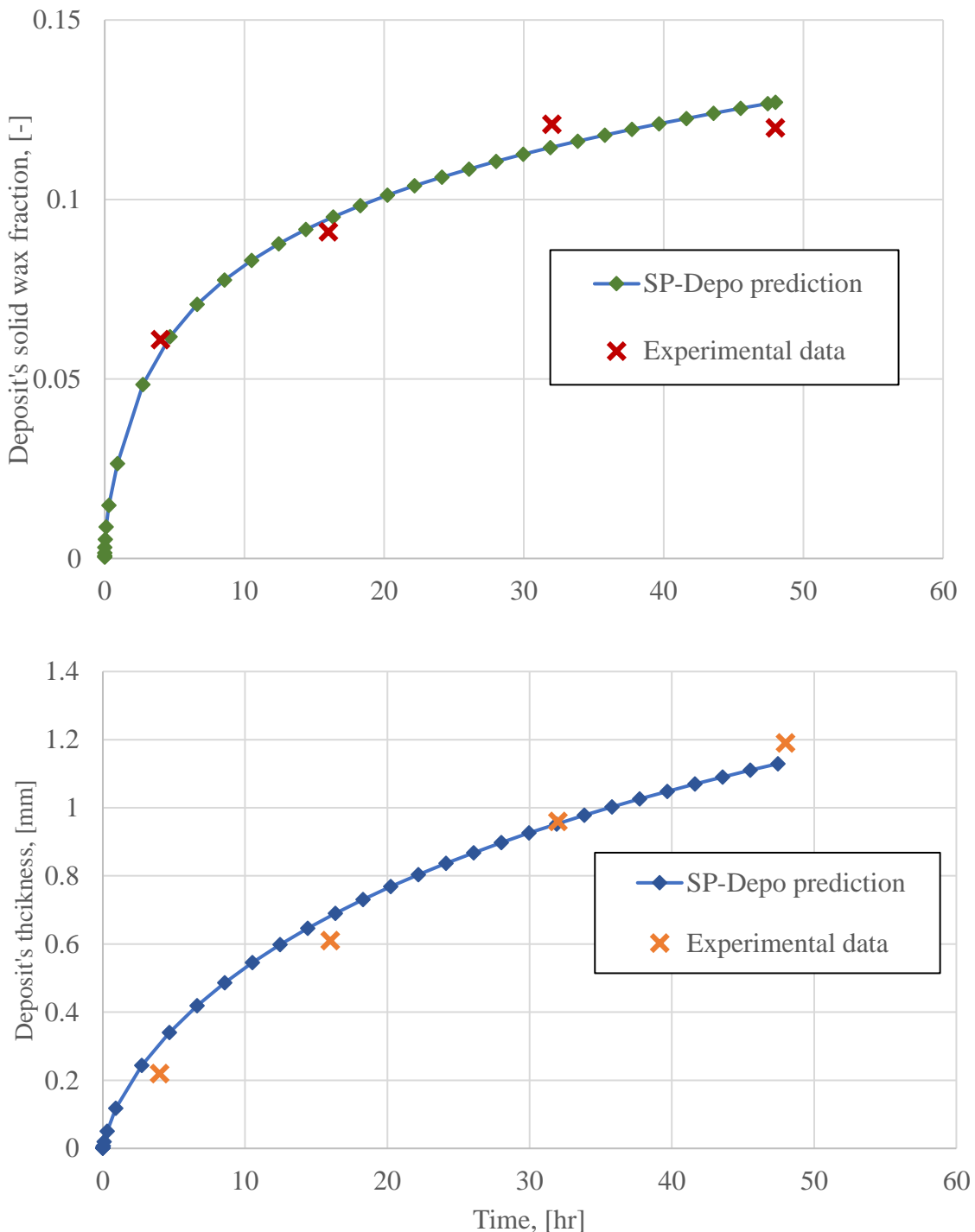


Figure 0-30: Average deposit's thickness and solid wax fraction predictions versus experimental data for $V_{oil} = 1.19 \text{ m/s}$

In SP-Compo wax deposition model, the governing equations from Panacharoensawad [10] have been used where no precipitation curve and $k_\alpha = 1$ have been assumed. Moreover, *msr1* and *msr2* fitting parameters were adjusted using Levenberg-Marquardt non-linear optimization tool which are coded in SP-Depo (Table 0-12).

Table 0-12:Determined fitting parameters in Eq.0-62 and Eq.0-63 by LM algorithm in SP-Depo

V_{oil} [m/s]	msr1	msr2
1.19	15.53	12.25
1.83	13.30	90.86
2.24	5.34	26.36

2.7.3 Deposit's solid phase composition

Carbon number distribution of the deposit is crucial for pigging frequency planning and chemical treatment design. Longer chain n-alkanes form stronger deposits which are harder to be removed from the pipe. So, it is important for a wax deposition software to predict deposit's solid phase composition. Fortunately, SP-Compo model predicts the deposit's solid phase average carbon number (ACN) and carbon number distribution (CND) in addition to thickness and solid wax fraction parameters. In SP-Depo software, the temperature terms (T_{wh} , T_{dep} and T_i) are calculated based on the estimated deposit's thickness and solid wax fraction. Then, the thermodynamic model is used to predict solid phase CNDs at the mentioned temperatures.

Waxy deposits can be characterized by three temperatures including interface temperature (T_i), average deposit temperature (T_{dep}) and pipe wall temperature (T_{wh}).

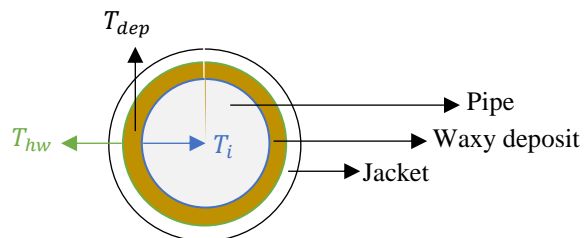


Figure 0-31: The deposit's surrounding temperatures

Right after the start of the experiment, a layer of waxy deposit is formed which mostly contains oil which is trapped in a 3D network of solidified wax molecules. In time, the oil content decreases and solid wax fraction increases through a counter-diffusion process (Figure 0-13). Also,

Due to concentration gradient within the deposit, some of the dissolved wax molecules (larger than CCN) move from the interface to the pipe's wall where much lower temperature exists. Even though it is nearly impossible to quantify such movement of wax molecules in the deposit, it is almost certain that the solidified molecules were precipitated at a temperature between T_{wh} and T_i . In Figure 0-32 and Figure 0-33, the predicted wall and interface temperatures are plotted. The temperature difference between the pipe's wall and the deposit's interface increases and reaches up to $\Delta T \cong 9^\circ\text{C}$.

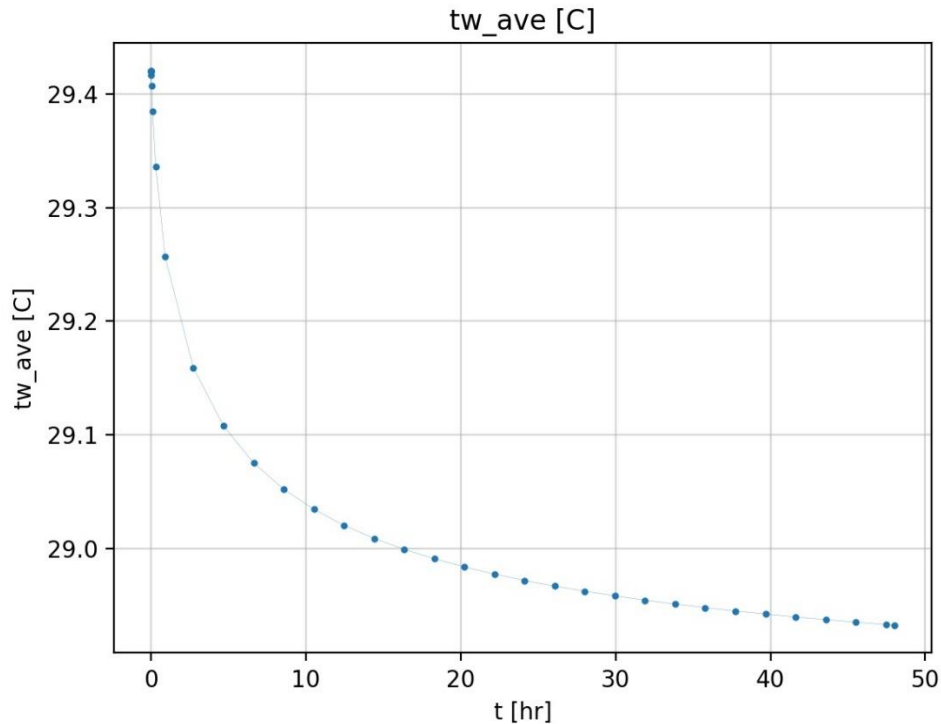


Figure 0-32: Pipe's inner wall temperature (T_{wh}) for Test #21

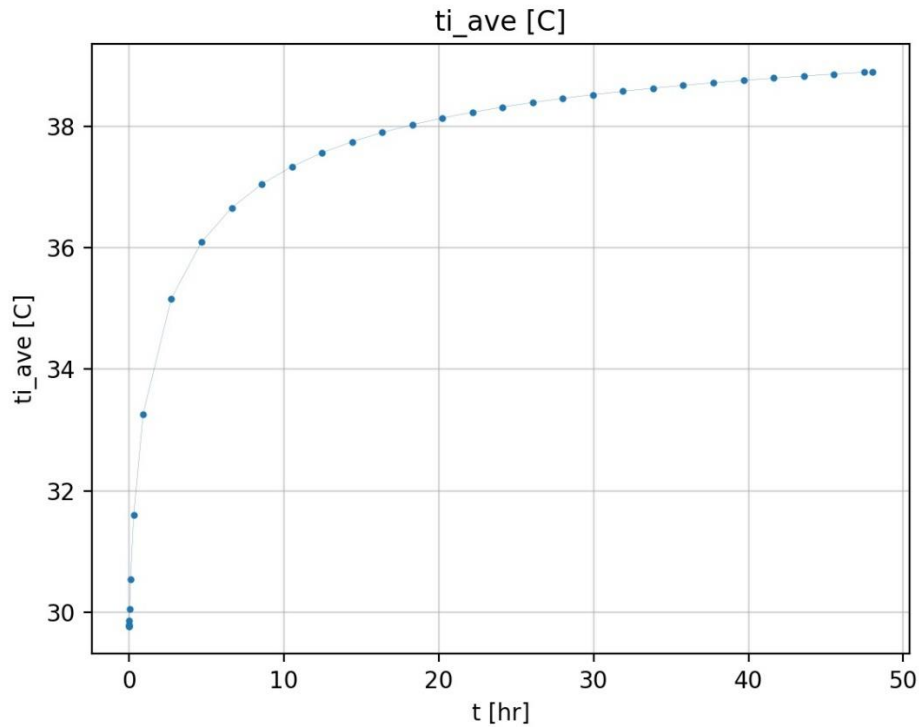


Figure 0-33: The deposit's interface temperature (T_i) for Test #21

Consequently, the deposit's solid phase carbon number distribution (CND) should also lay between the predicted CNDs at T_{wh} and T_i . In the following graph, the predicted ACN profile for test #21 is shown. Near inlet, ACN is predicted to be higher which is consistent with experimental data reported by Panacharoensawad [10]. He showed that experimental ACN is correlated with the local heat transfer coefficient where it is the highest near the inlet.

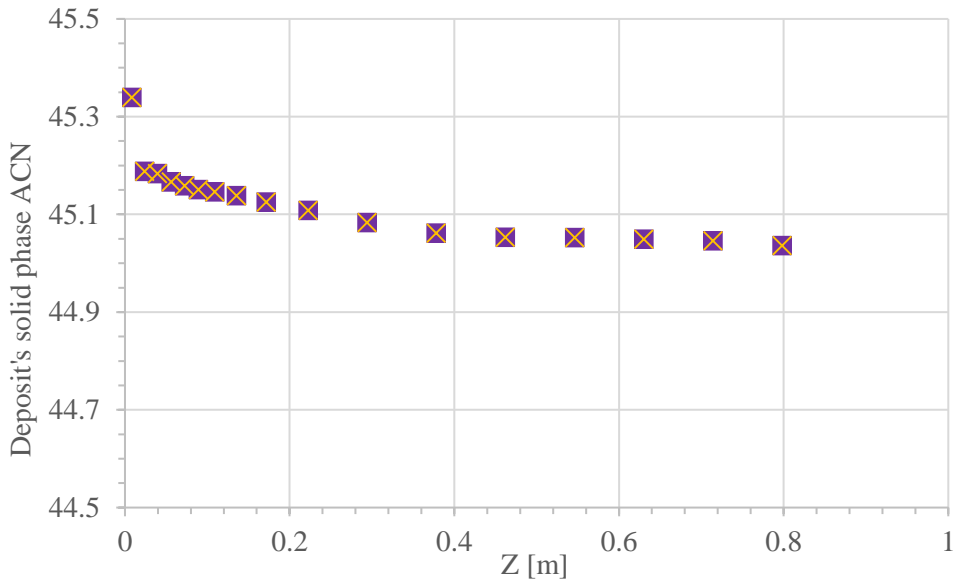


Figure 0-34: Predicted solid phase ACN in axial direction for test #21

In the following graph, experimental solid phase CND are plotted versus SP-Depo predictions at T_{wh} , T_i and $T_{dep} = \frac{T_i + T_{wh}}{2}$, for Test #32. In Figure 0-35, predicted CNDs at T_{wh} and T_i are considered as the lower and upper bounds for CND prediction, respectively. Furthermore, in, predictions for solid phase average carbon number (ACN) at T_{wh} , T_i and T_{dep} are plotted against the experimental data. In Figure 0-36, it is shown that the experimental ACN data are bounded within the two limiting ACN predictions which are predicted at deposit's interface and inner pipe's wall temperature. Please note that the same fitting parameters (*Table 0-12:Determined fitting parameters in Eq.0-62 and Eq.0-63 by LM algorithm in SP-DepoTable 0-12*), which are determined previously using thickness and solid wax fraction data, are used for solid phase composition predictions.

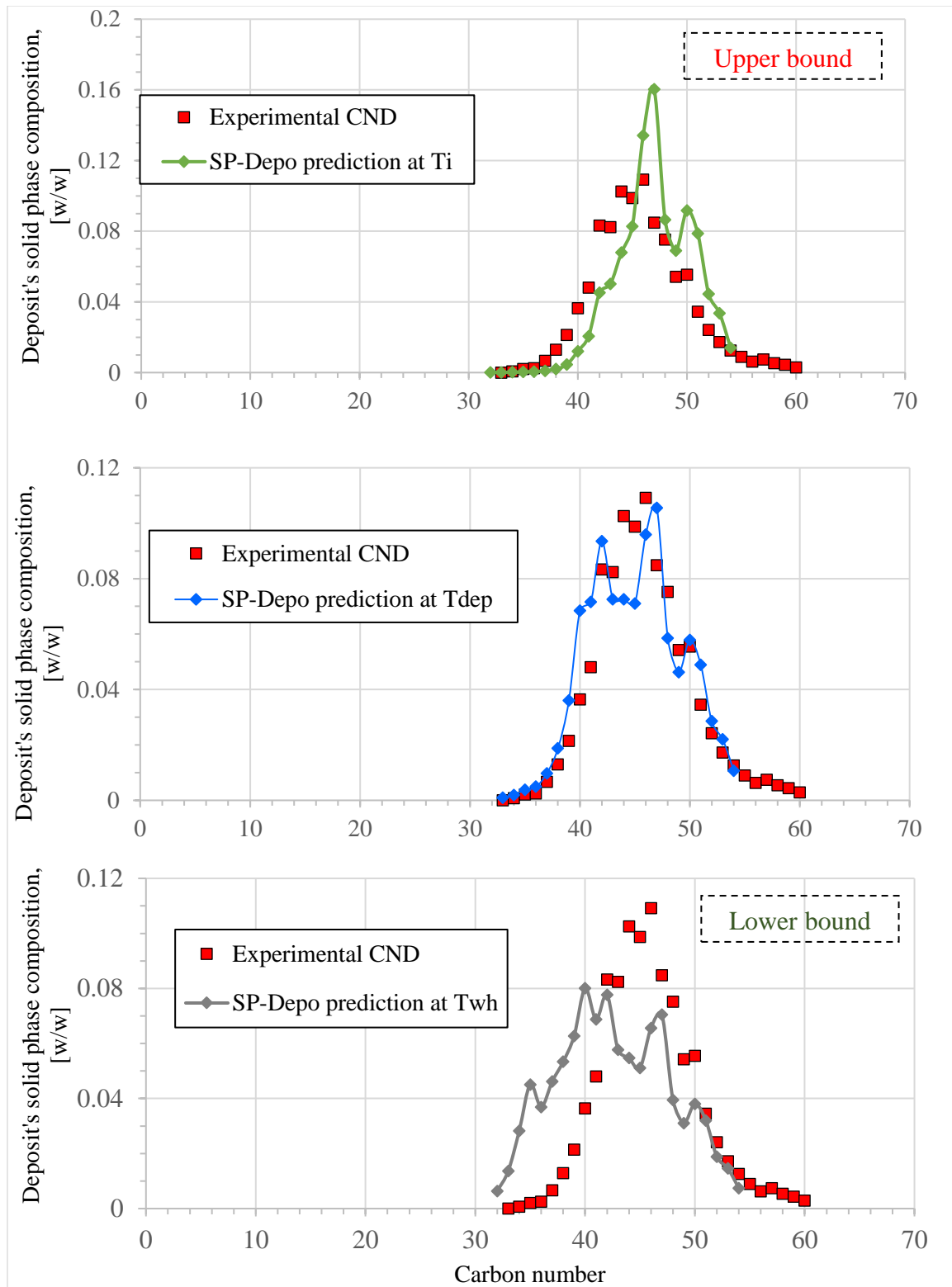


Figure 0-35: Experimental CND versus SP-Depo predictions at interface, average and wall temperatures, respectively for Test #32.

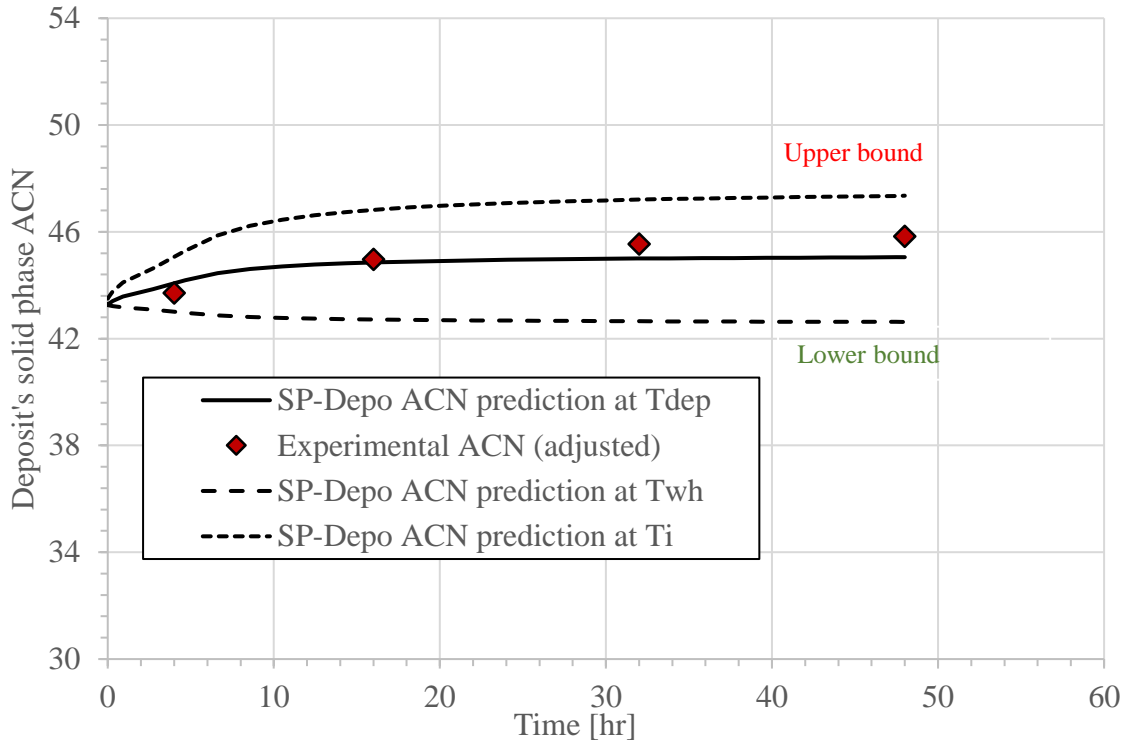


Figure 0-36: ACN prediction at T_{wh} , T_{dep} and T_i versus experimental data. ACN was adjusted and updated after subtracting the oil composition from the raw HTGC data for $V_{oil} = 1.83 \text{ m/s}$

- **Effect of shear stress on ACN prediction**

In the deposit, the lighter wax crystals are likely to break by the shear force which is exerted by the high velocity flow. Panacharoensawad [10] showed that the experimental solid phase ACN increases with initial shear stress. In our study, we estimated the solid phase ACN for three oil velocities (Table 0-10) and investigated the effect of shear stress on the carbon number distribution of the solidified phase using SP-Depo. We previously showed that SP-Depo accurately predict the thickness and solid wax fraction for the three flowing conditions through Figure 0-28 to Figure 0-30 using the adjusted fitting parameters shown in Table 0-12. By using the same fitting parameters, we plotted the predicted ACN versus the experimental data and showed that the average carbon number of the solidified phase increases with shear stress.

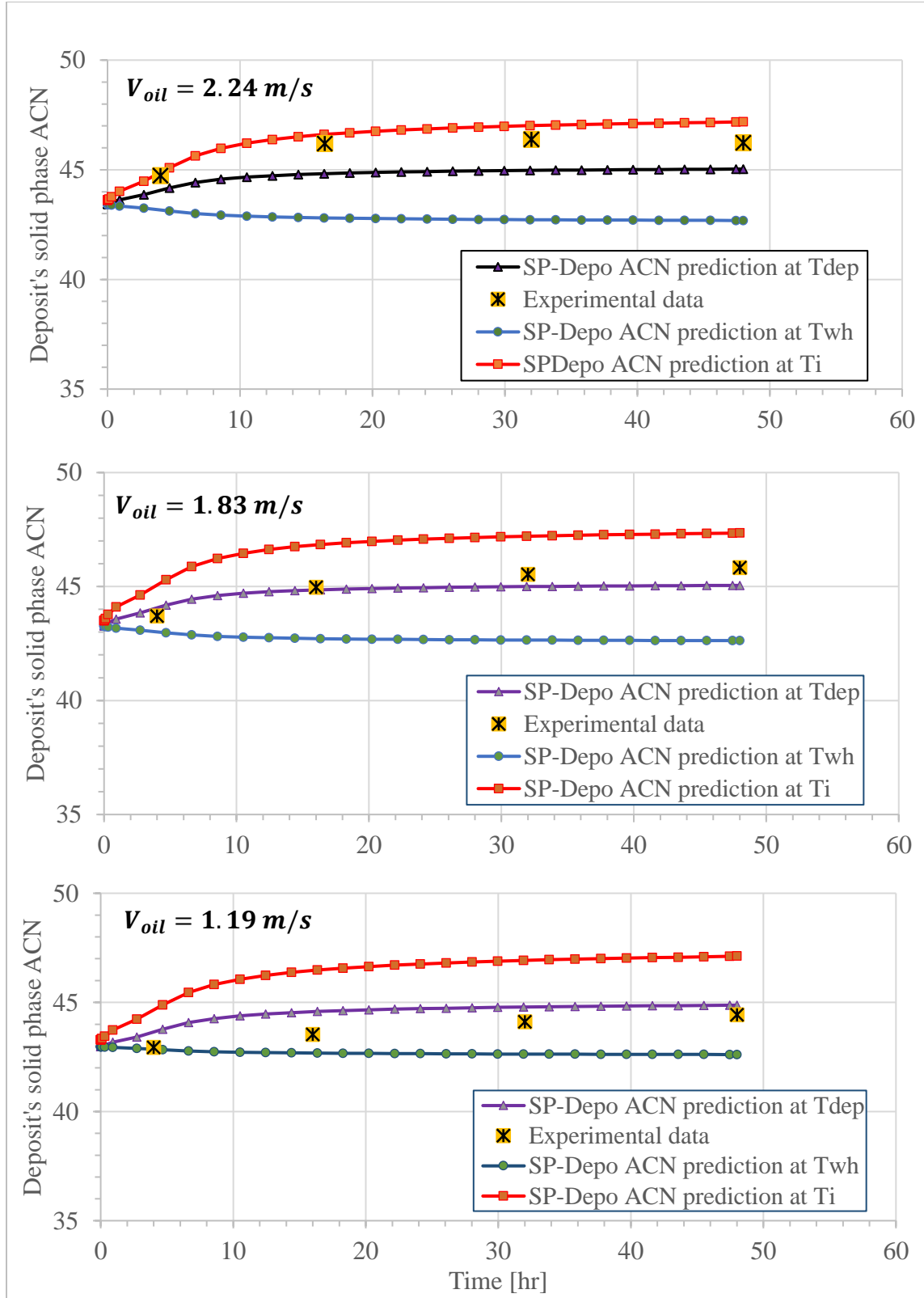


Figure 0-37: Predicted and experimental ACN for three oil velocities

In Figure 0-37, at the lower velocity ($V_{oil} = 1.19 \text{ m/s}$), the experimental ACN data are close to the lower bound prediction which gradually approach toward the upper limit as velocity increases. This behavior is mainly due to the shear effect which results in the breakage and removal of lighter n-alkane crystals. The following schematic illustrates the effect of shear stress on the deposit.

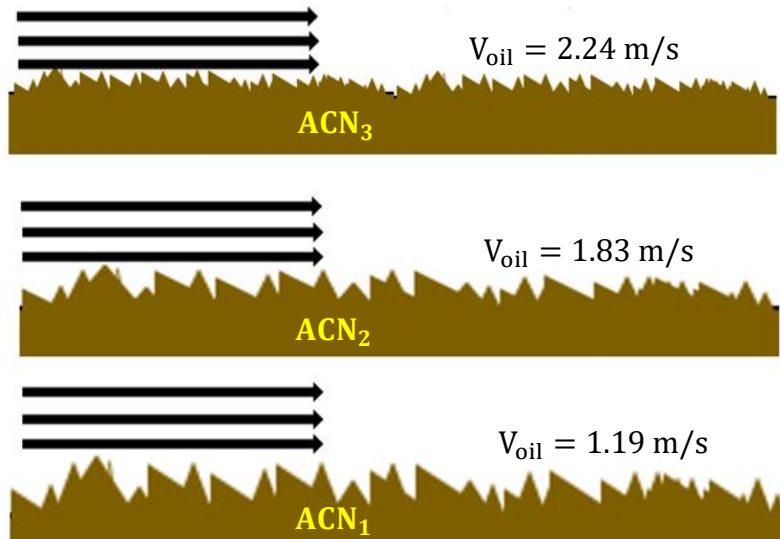


Figure 0-38: Effect of shear stress on the deposit. As oil velocity increases, shorter n-alkanes will be removed by the flow because of their low yield stress and ACN will increase ($\text{ACN}_3 > \text{ACN}_2 > \text{ACN}_1$).

In Figure 0-39, total solid mass is plotted versus time for different grouped components where groups C43-C46, C39-C42 and C47-C50 contain highest amount of solid wax in the deposit, respectively.

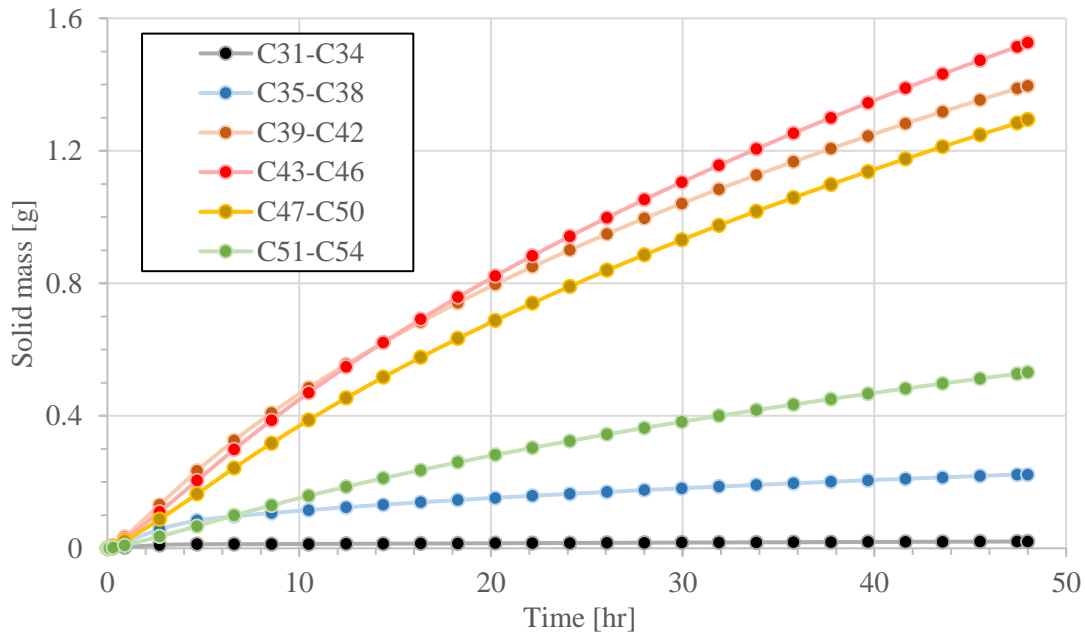


Figure 0-39: solid mass of grouped components versus time.

2.7.4 Sensitivity analysis

In this section, different input n-alkane compositions will be used, and the results will be shown. Then, different scenarios for longer and bigger pipes will be presented to investigate the applicability of SP-Depo for longer pipes and different conditions. For South Pelto showed three n-alkane compositions for

Effect of input n-alkane composition

SP-Depo is greatly dependent on the n-alkane composition of the oil which should be provided as an input for SP-Compo wax deposition model. Panacharoensawad [10] provided three n-alkane compositions for South Pelto oil which has been used in his experiments (Figure 0-19). So far, we have used the n-alkane composition reported by Bruno (2006) in our illustrative examples. Now, we will use the Weatherford n-alkane compositions and compare the results through the following graphs.

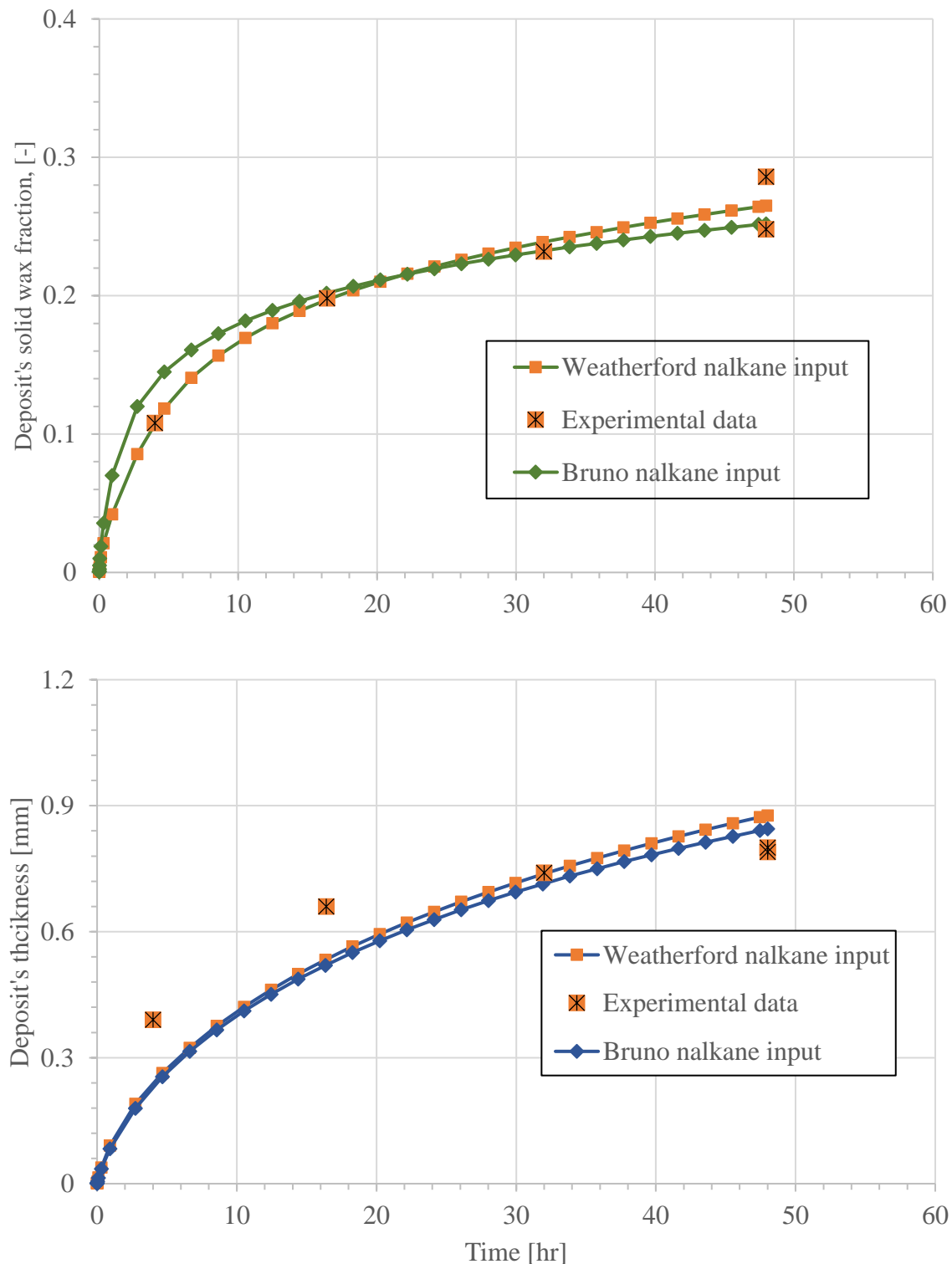


Figure 0-40: Average deposit's and solid wax fraction predictions from Bruno and Weatherford n-alkane compositions for $V_{oil} = 2.24 \text{ m/s}$

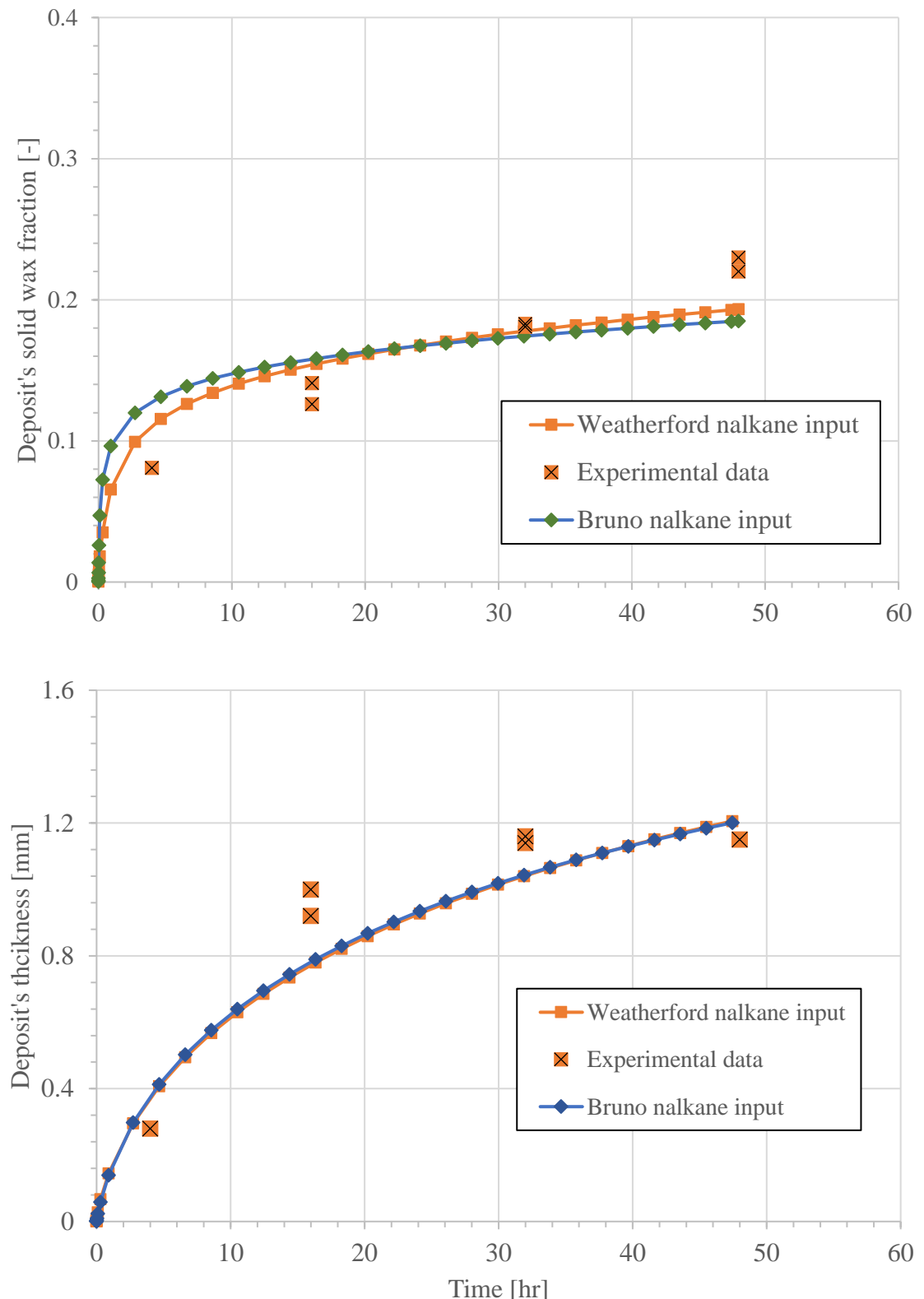


Figure 0-41: Average deposit's and solid wax fraction predictions from Bruno and Weatherford n-alkane compositions for $V_{oil} = 1.83 \text{ m/s}$

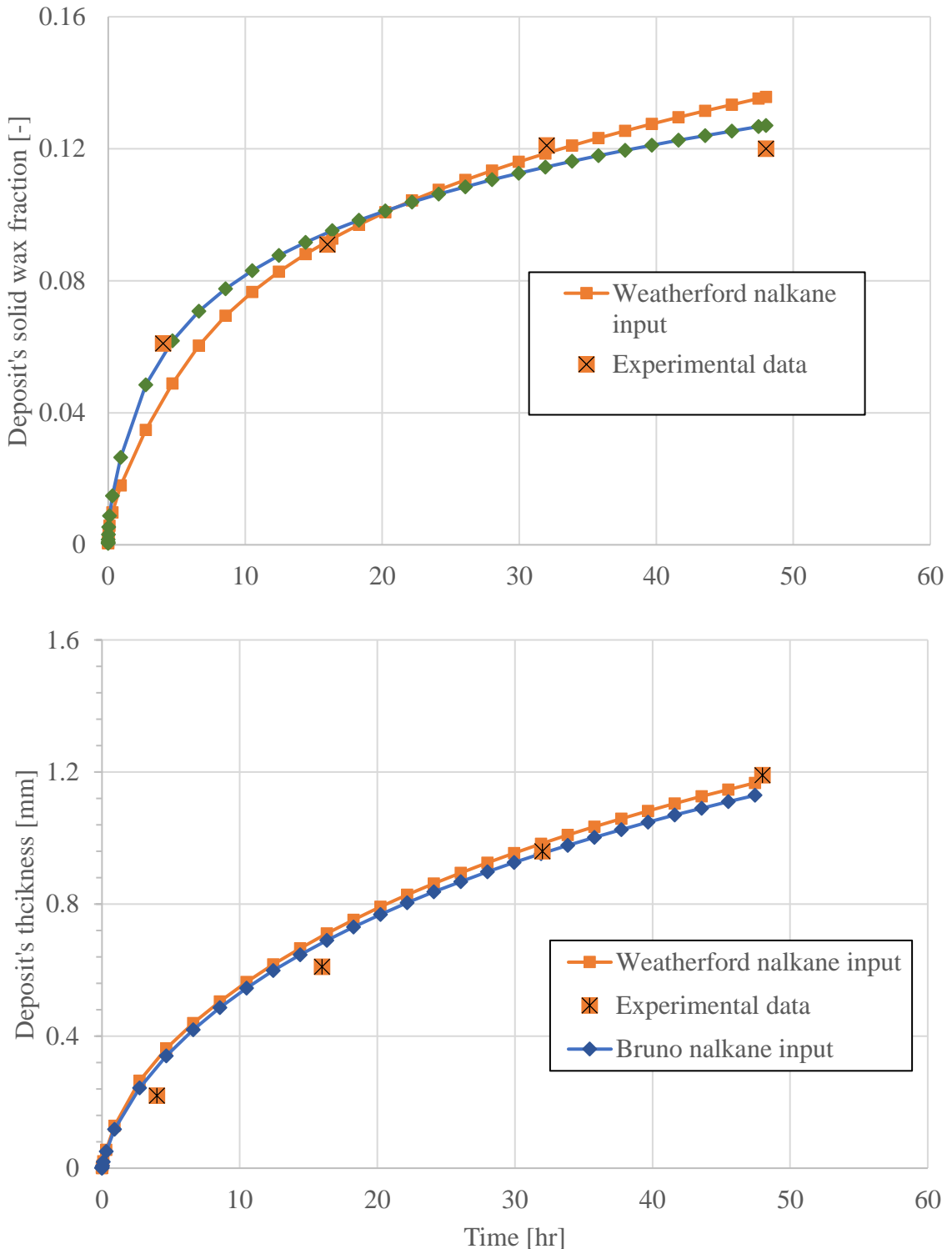


Figure 0-42: Average deposit's and solid wax fraction predictions from Bruno and Weatherford n-alkane compositions for $V_{oil} = 1.19 \text{ m/s}$

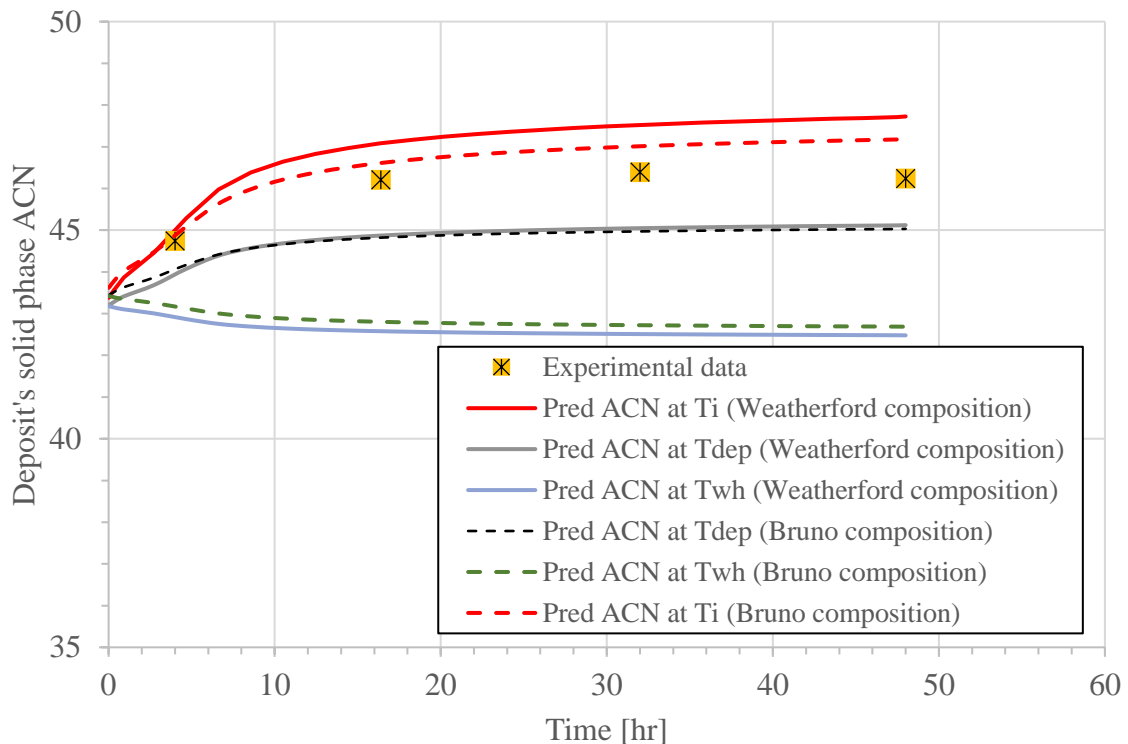


Figure 0-43: ACN predictions using Bruno and Weatherford n-alkane compositions

And the adjusted fitting parameters for both oil compositions are presented in the following table:

Table 0-13: Adjusted msr1 and msr2 for two n-alkane compositions

V_{oil} [m/s]	Weatherford n-alkane composition		Bruno n-alkane composition	
	msr1	msr2	msr1	msr2
1.19	12.29	5.33	15.53	12.25
1.83	9.43	22.48	13.30	90.86
2.24	4.19	9.80	5.34	26.36

The above graphs show how n-alkane composition variation could result in different predictions in different wax deposition characteristics. Therefore, it is suggested to use accurate n-alkane composition data for SP-Depo software.

Different operating conditions (pipe's diameter and length)

Although SP-Depo is verified by the experimental data of a lab-scale pipeline, it is important to show its applicability in different operating conditions. Ambient temperature, pipe's radius, oil velocity and pipe's length are the parameters whose effects will be investigated in this section. Some of the larger pipes similar in the field. In this section, we will run SP-Depo for different operating conditions and compare the results.

Pipe's Diameter Change Analysis Case Analysis

In this case, we want to explore the effect of pipe's diameter on the wax deposition prediction. In Table 0-14, the original and modified input parameters are included while the fitting parameters stay constant. In Figure 0-44, one can notice that increase in pipe's diameter result in slight decrease in deposit's thickness and solid wax fraction while deposit's solid phase carbon number composition remains almost unchanged.

Table 0-14: Original and new testing conditions for case 1. Every other parameter is the same

Parameters	Original	Changed
V_{oil} [m/s]	2.24	
$d_{in,pipe}$ [Inch]	0.651	1.3
$d_{out,pipe}$ [Inch]	0.75	1.5
$d_{in,cool}$ [Inch]	1	2

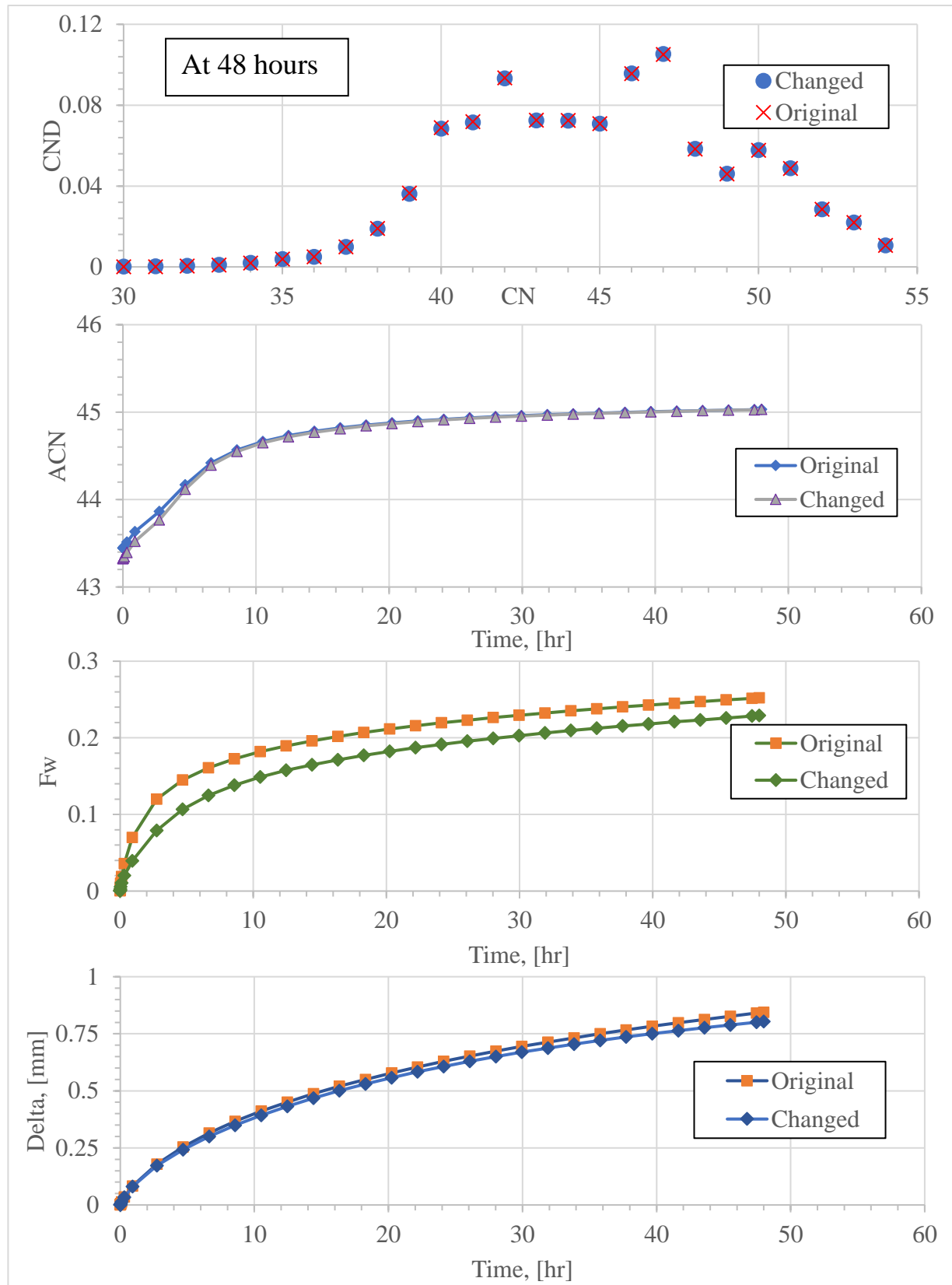


Figure 0-44: Simulation result comparison for case 1 sensitivity analysis with pipe's size variation

Ambient Temperature Change Case Analysis

Surrounding temperature is one of the most important parameters which could affect the wax deposition process massively. As ambient temperature decreases, more carbon number components will precipitate out of the solution and contribute to the deposition. Therefore, we investigated the effect of ambient temperature on different characteristics of the waxy deposit. In Figure 0-45, lowered ambient temperature resulted in more deposition as deposit's thickness and solid wax fraction are increased considerably. On the contrary, ACN is decreased since more lighter n-alkanes deposited due to the low coolant temperature.

Table 0-15: Original and new testing conditions for case 2. Other parameters are the same

Parameters	Original	Changed
v_{oil} [m/s]	2.24	
$T_{ambient}$ [°C]	28.78	20

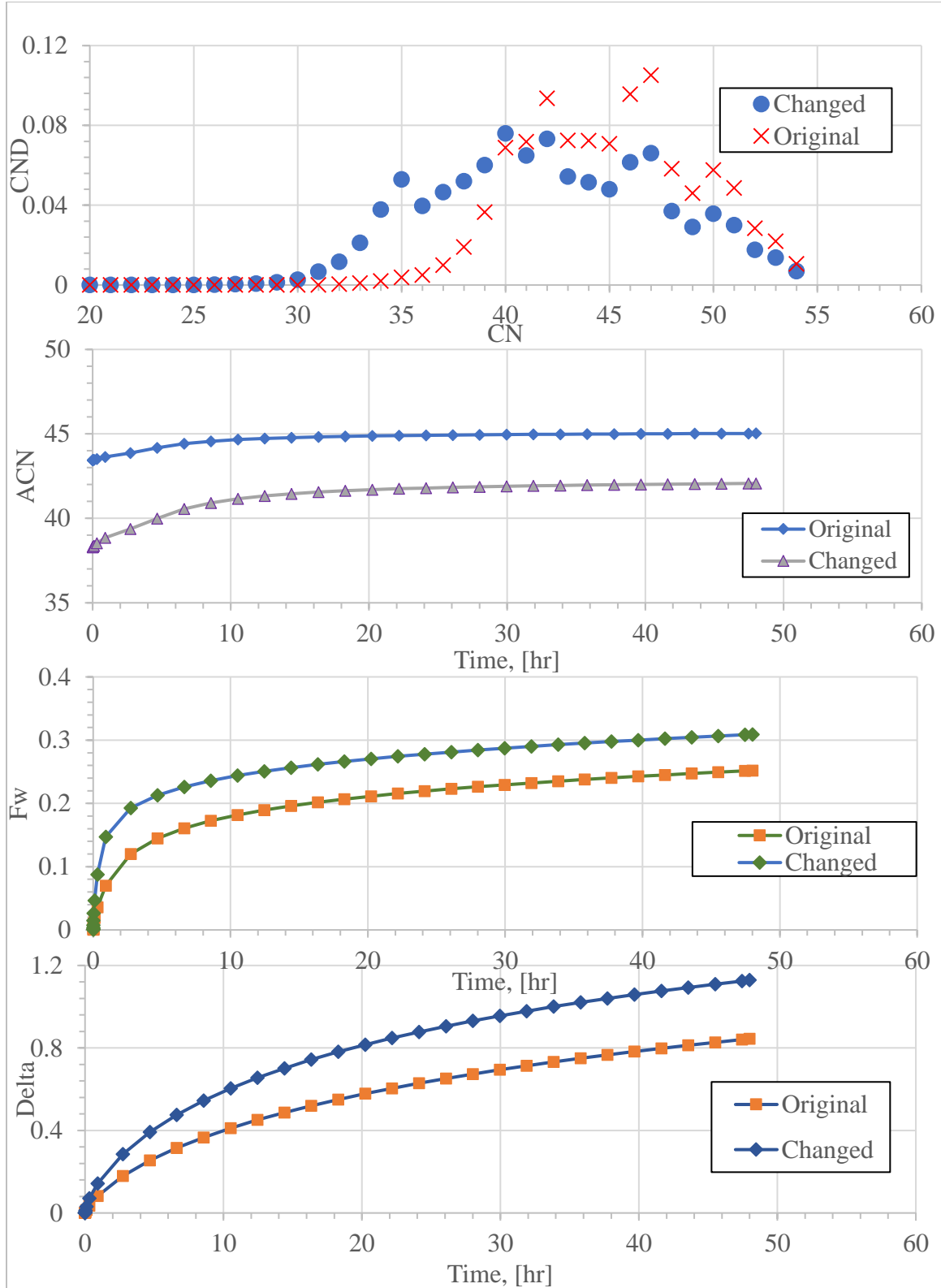


Figure 0-45: Simulation result comparison for case 2 sensitivity analysis with ambient temperature variation

Upscaled Case Analysis

In this case, we consider a larger and longer pipe for our case analysis. As we discussed previously, it is important to show that SP-Depo works in other operating conditions too. In the previous cases, we changed only one parameter (pipe's dimeter and ambient temperature) and showed the simulation results. However, in this sensitivity analysis case, pipe's dimeter, ambient temperature, pipe's length and coolant flow rate will vary and the results are illustrated.

Table 0-16: Original and changed parameters for upscaled sensitivity case analysis

Parameters	Original	Changed
V_{oil} [m/s]	2.24	
$d_{in,pipe}$ [Inch]	0.65	5.21
$d_{out,pipe}$ [Inch]	0.75	6
$d_{in,cool}$ [Inch]	1	7.95
$T_{ambient}$ [°C]	28.78	4
$Q_{coolant}$ [$\frac{gal}{s}$]	0.08	264.2
Pipe's Length,[m]	0.84	100.84

From Table 0-16, Pipe's dimeters are increased by eight times, the ambient temperature has been decreased to subsea conditions (4°C), coolant flow rate is increased considerably to make the inner pipe's wall temperature constant. Due to the importance of this sensitivity analysis case, we will include the plots of various parameters without comparing it to a base case.

Please note that in SP-Depo, heat transfer calculations are based on the counter-current pipe-in-pipe flow condition and it is different than subsea condition. However, the coolant flow rate has been increased considerably to make the inner pipe's wall temperature constant. In the following graph, wall temperature (T_{wh}) is plotted versus z and times,

respectively. As expected, high coolant flow rate has resulted in almost constant wall temperature.

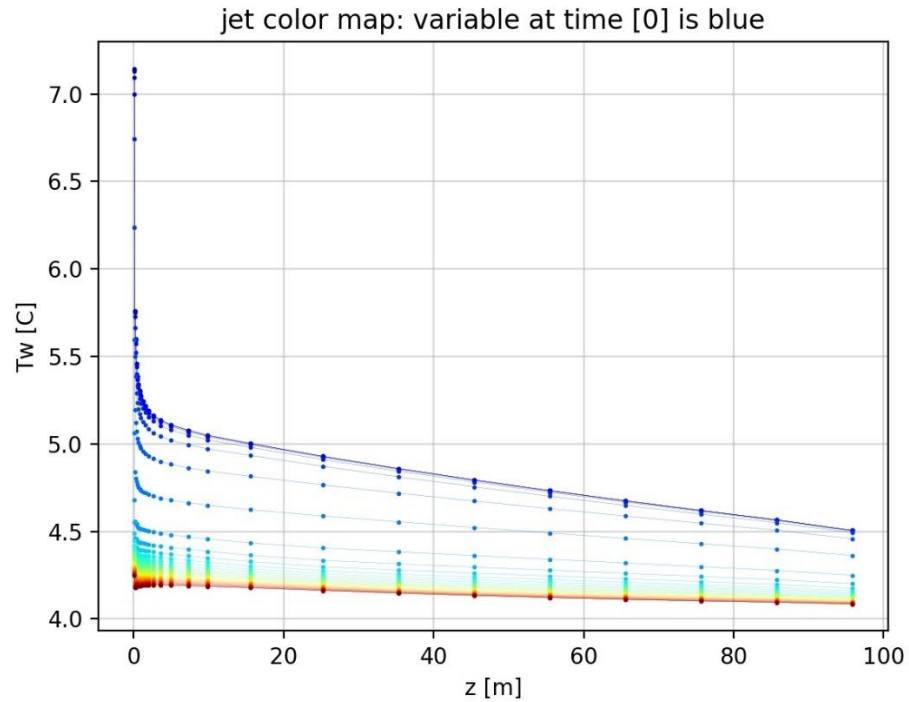


Figure 0-46: Inner pipe's wall temperature versus axial sections

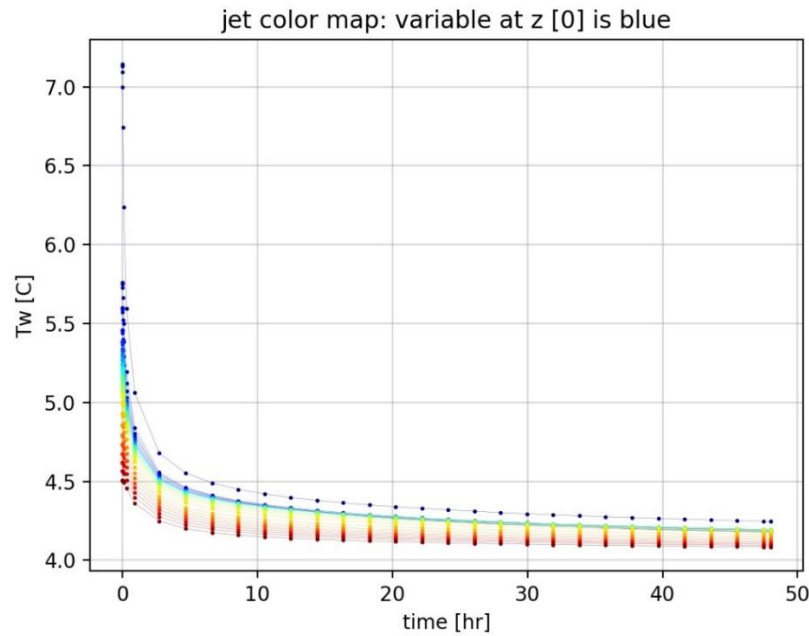


Figure 0-47: Pipe's inner wall temperature versus time

Then, the following graphs show the interface temperature (T_i). Even though T_i drops axially at early times, it does not vary at final time steps.

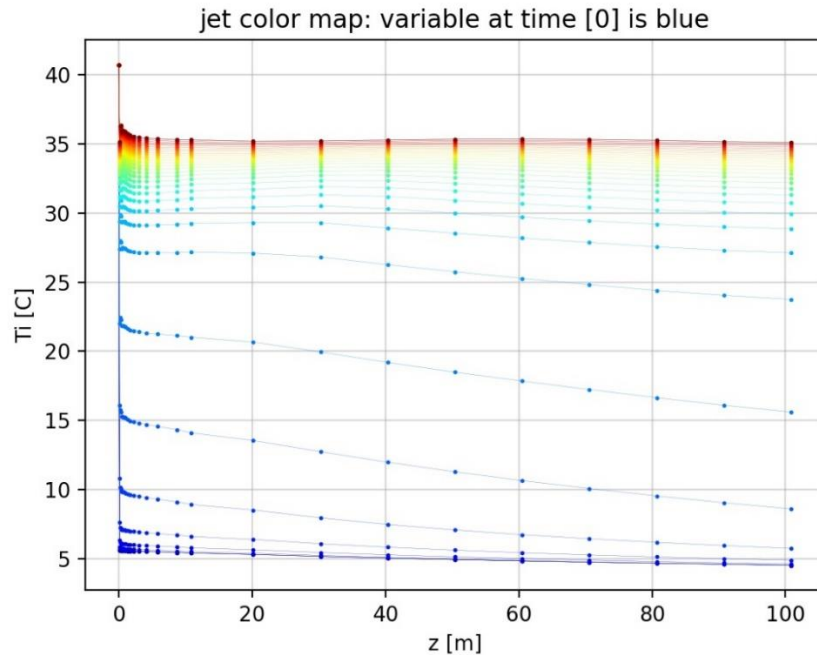


Figure 0-48: Deposit's interface temperature versus axial locations for different times

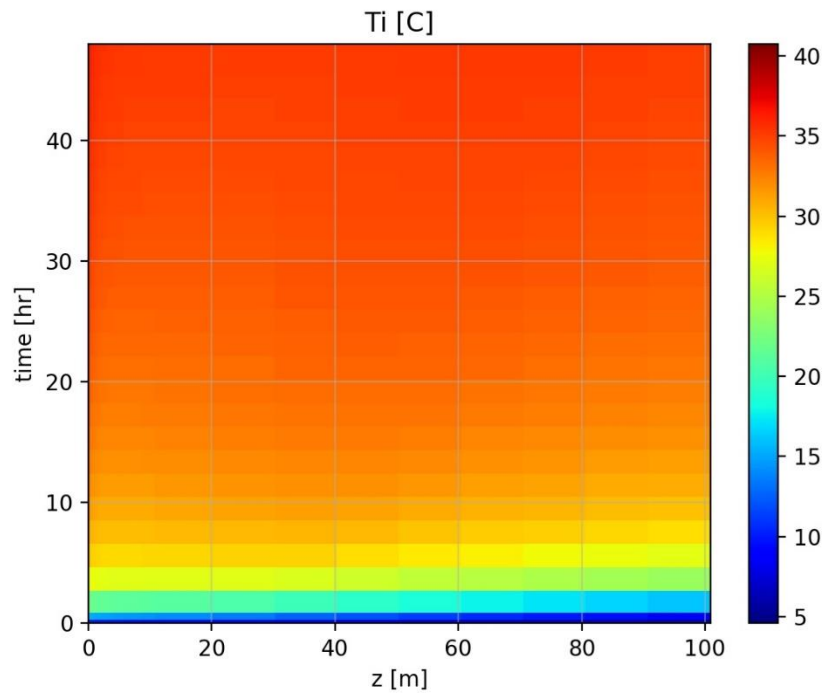


Figure 0-49: Deposit's interface temperature map (z vs time)

The final temperature parameter is the radial temperature profile which is illustrated through graphs at $t = 0$ [hr] and $t = 48$ [hr].

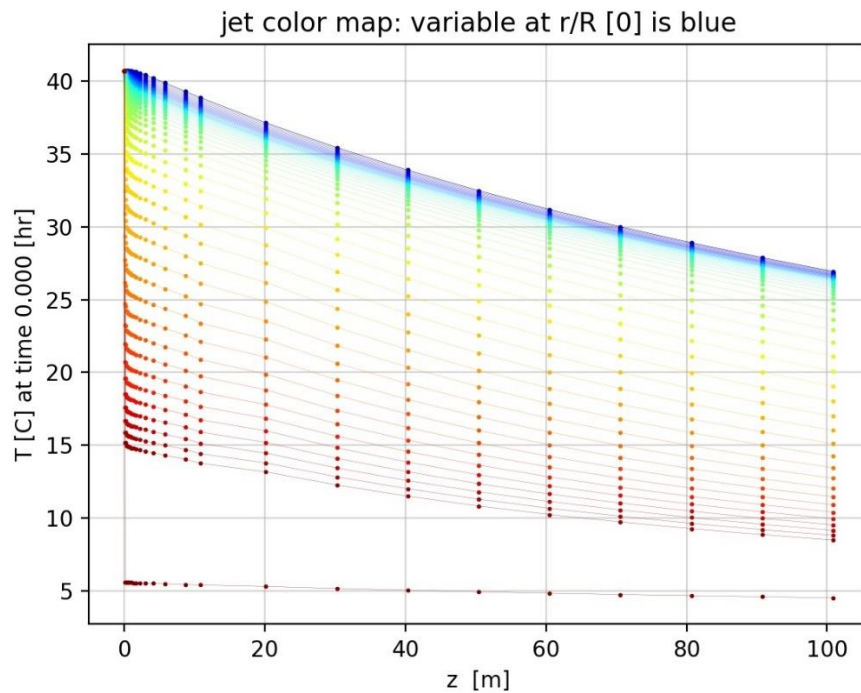


Figure 0-50: Radial temperature profile within the pipe at $t = 0$ [hr]

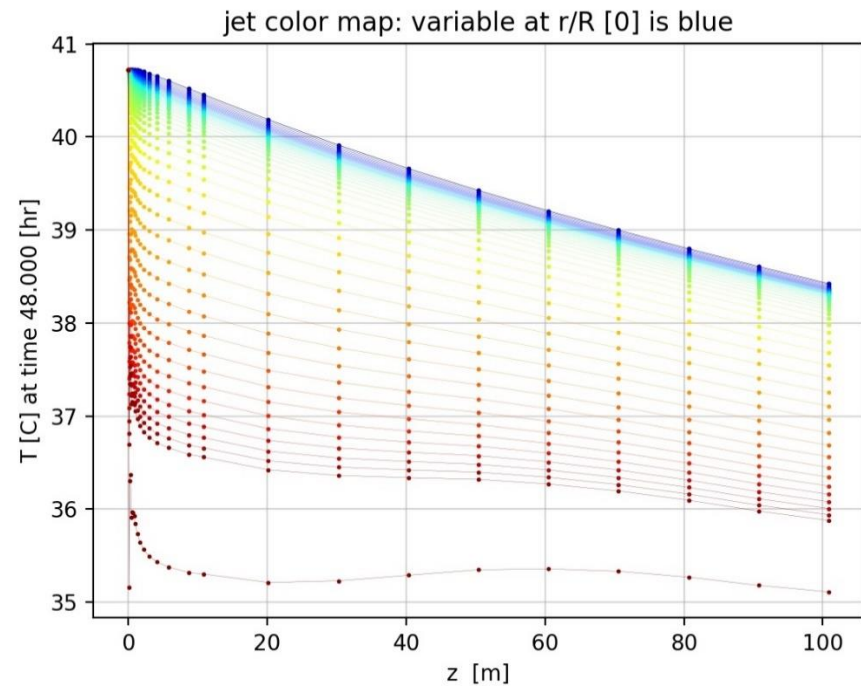


Figure 0-51: Radial temperature profile within the pipe at $t = 48$ [hr]

The next graphs are the radial concentration profile at $t = 0 [hr]$ and $t = 48 [hr]$. Concentration gradient near the deposit's interface is the main driving force in wax deposition phenomenon.

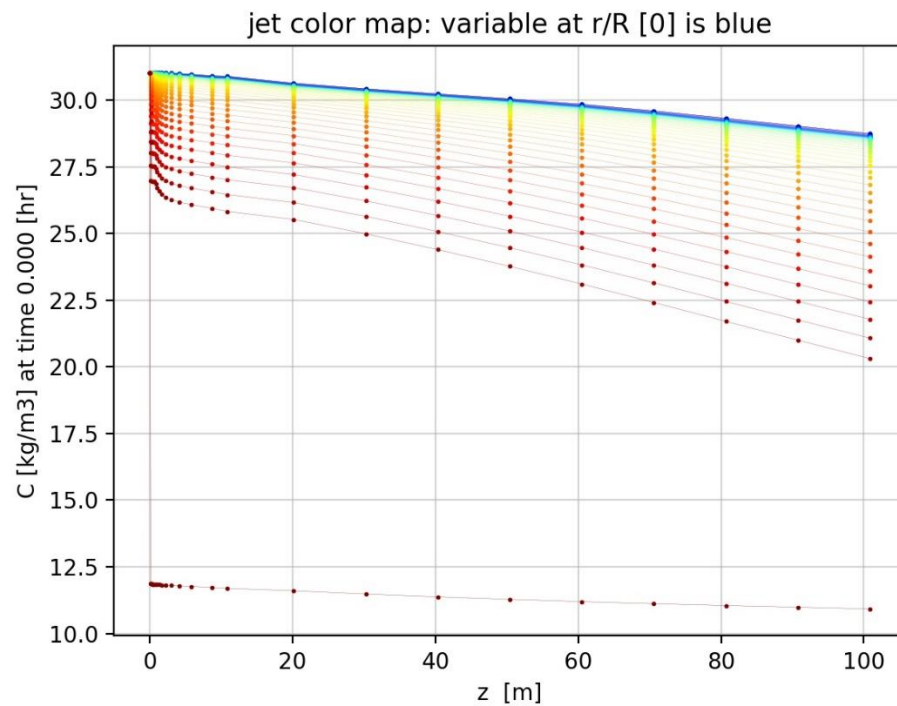


Figure 0-52: Radial concentration profile within the pipe at $t = 0 [hr]$

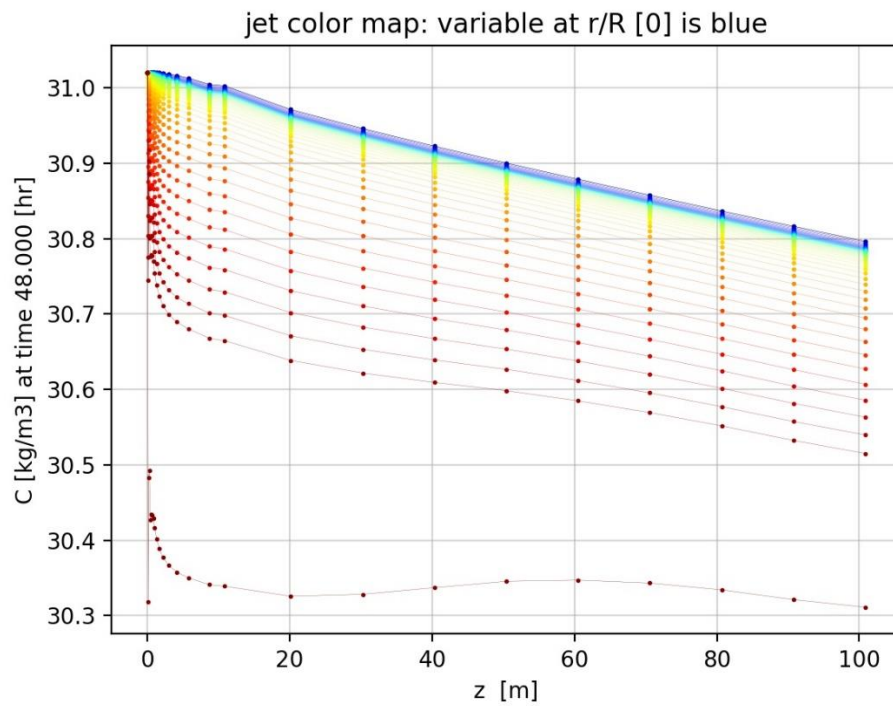


Figure 0-53: Radial temperature profile within the pipe at $t = 48$ [hr]

After presenting the temperature and concentration profiles, we will include the solid wax fraction and deposit's thickness plots

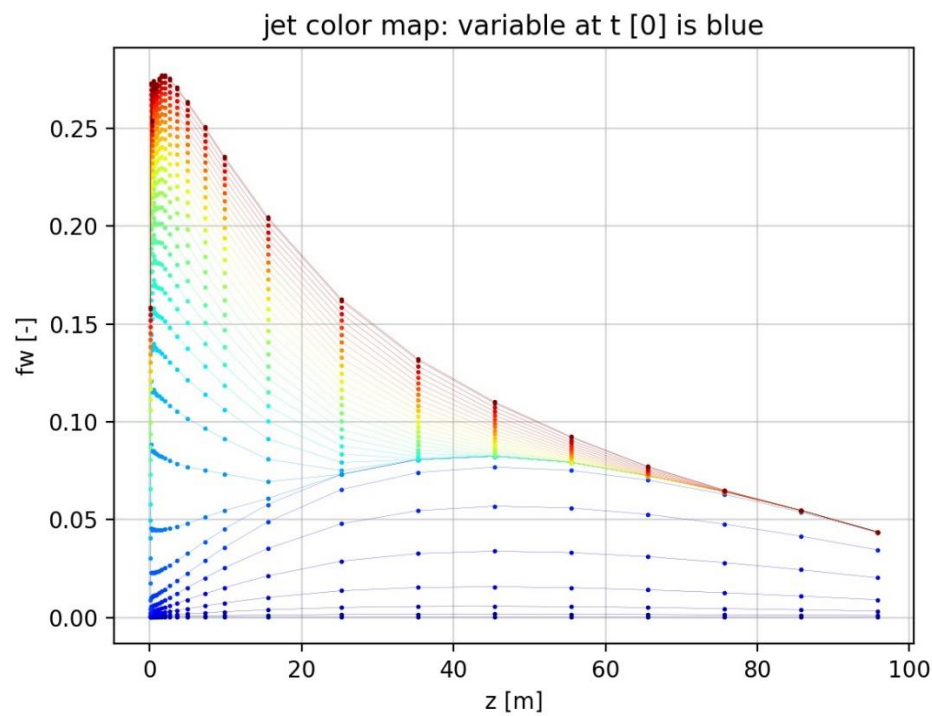


Figure 0-54: Axial solid wax fraction profile for different times

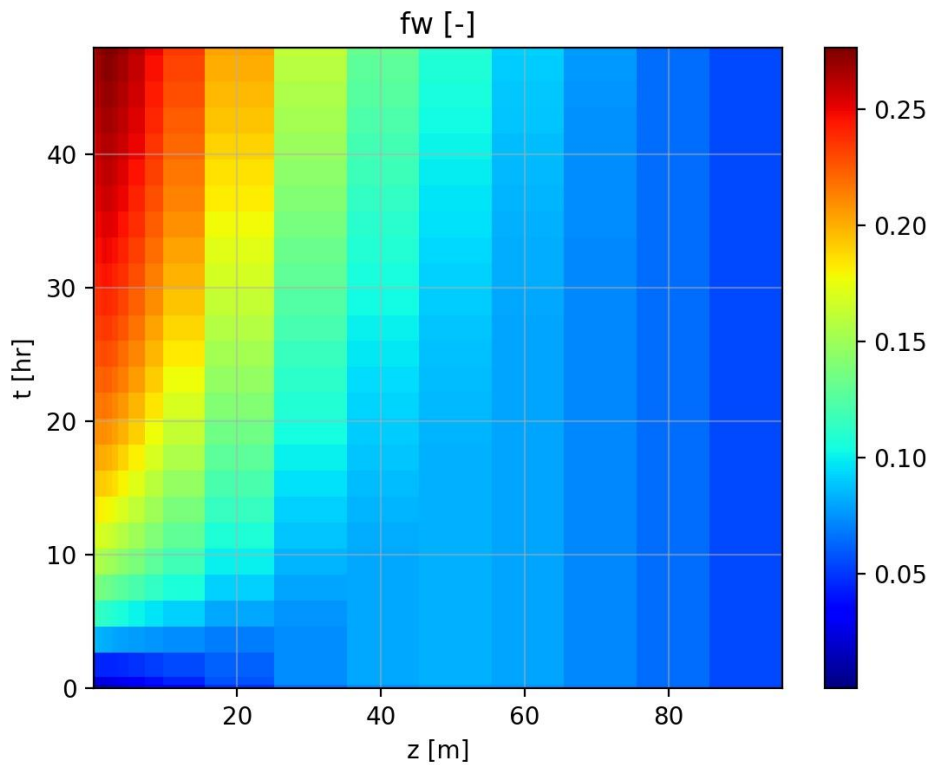


Figure 0-55: Solid wax fraction map (z vs time)

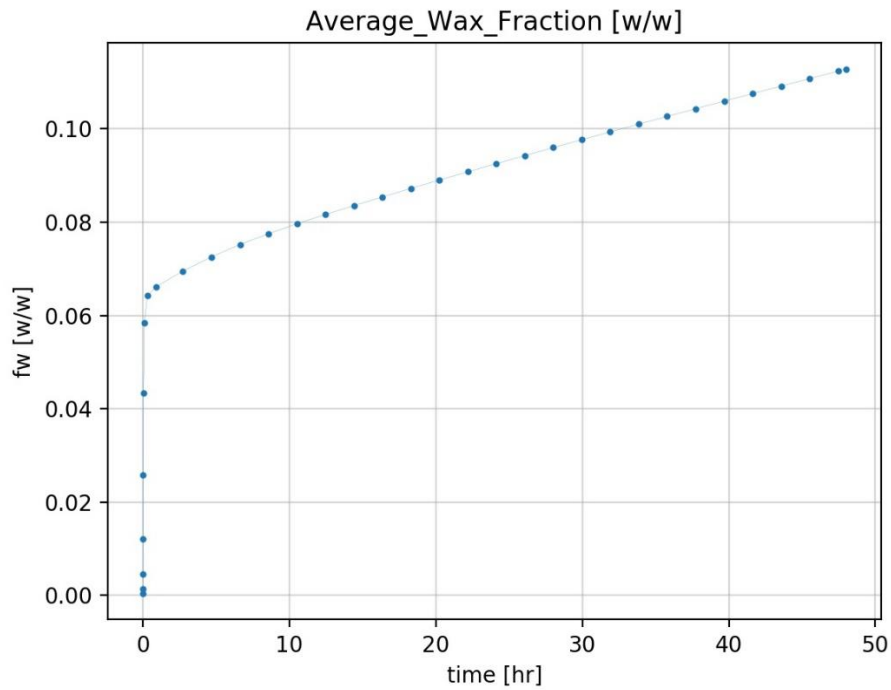


Figure 0-56: Average solid wax fraction versus time

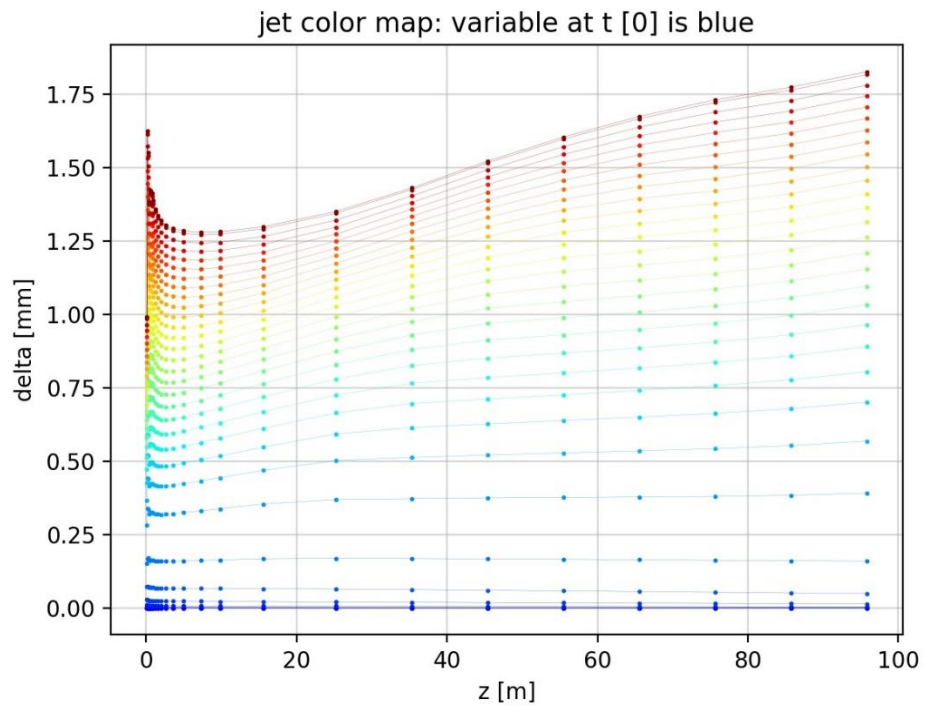


Figure 0-57: Axial deposit's thickness profile for different times

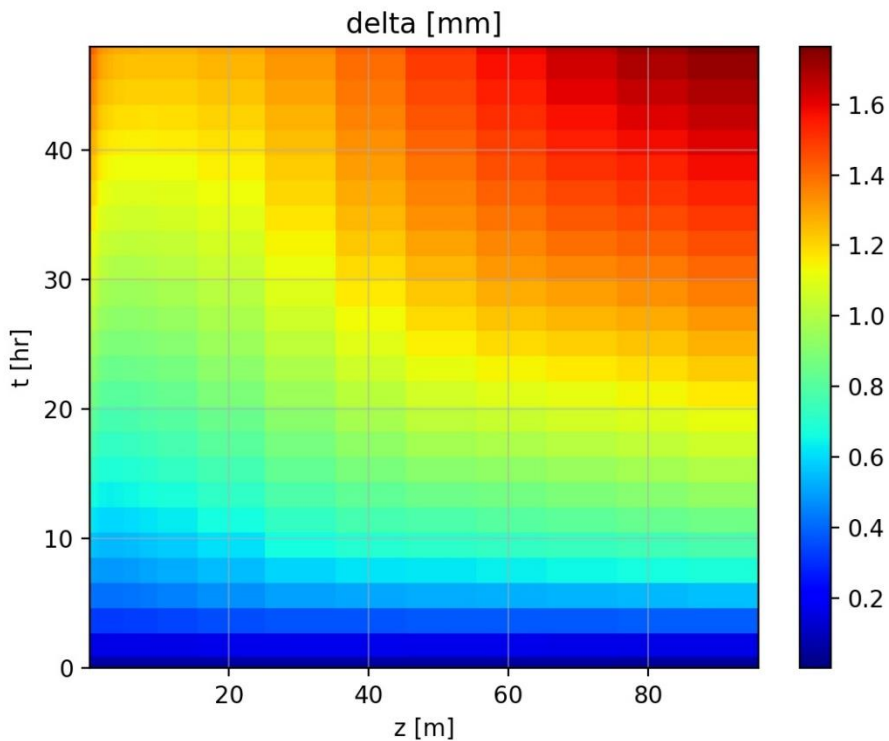


Figure 0-58: Deposit's thickness map (z vs time)

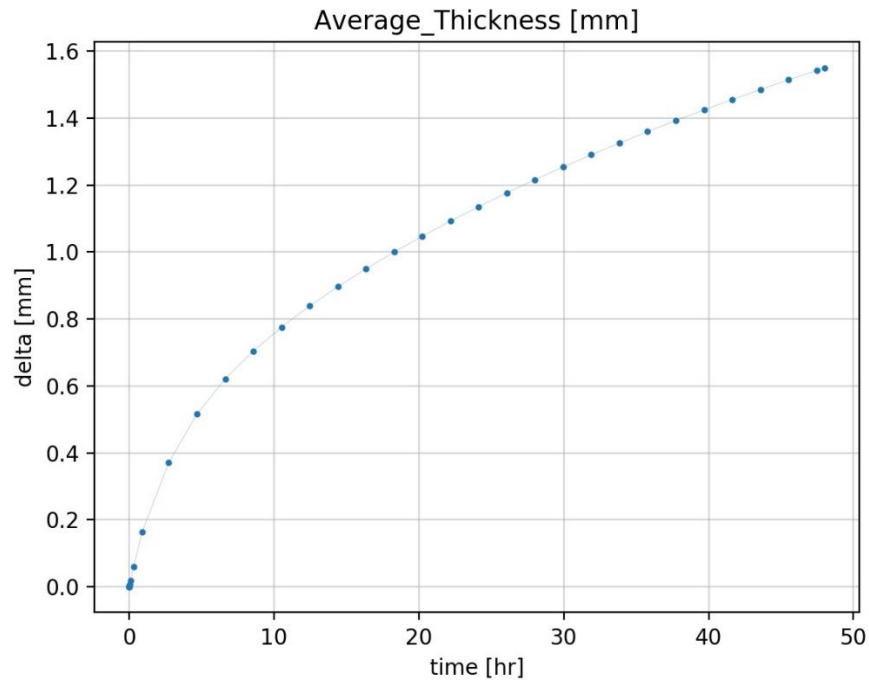


Figure 0-59: Average deposit's thickness versus time

Finally, the following graphs show ACN and CND of the deposit's solidified phase.

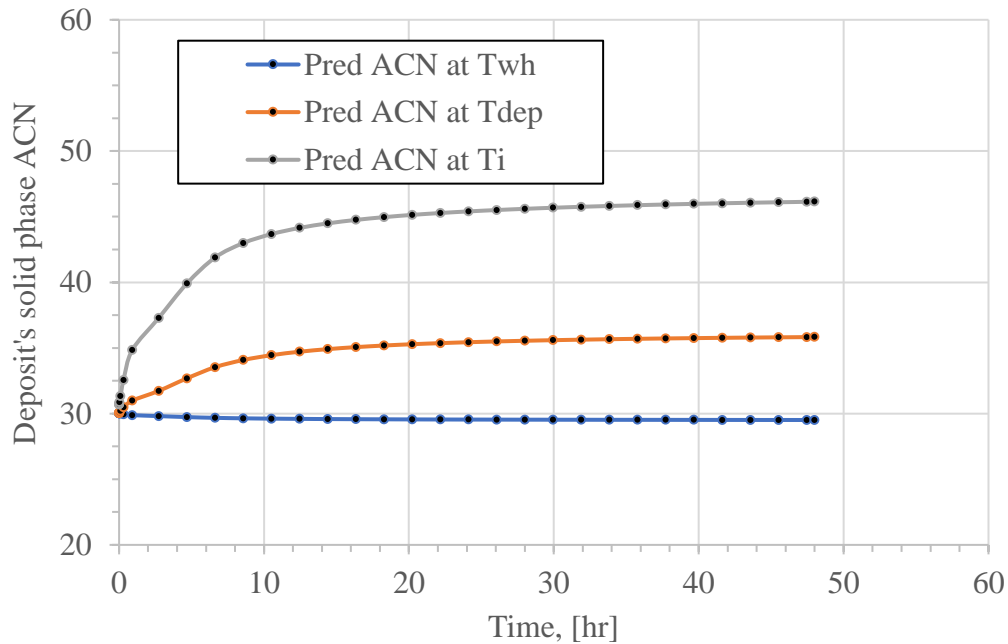


Figure 0-60: Deposit's solid phase ACN versus time at wall, deposit and interface temperature

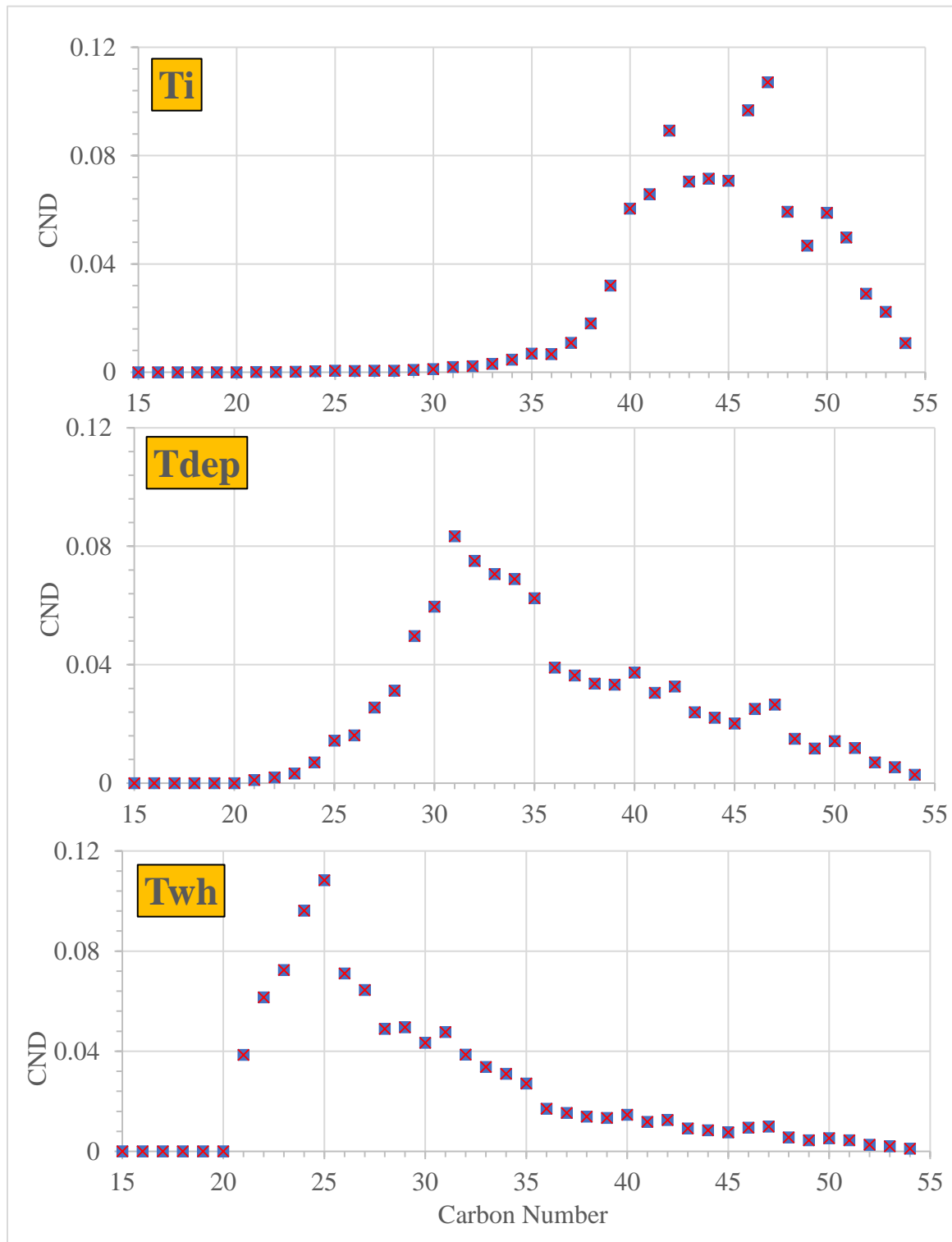


Figure 0-61: Deposit's solid phase carbon number distribution at wall, deposit and interface temperatures

CHAPTER 6

CONCLUSIONS

In wax deposition phenomenon, carbon number distribution (CND) of the deposit is a crucial factor to optimally design the pigging frequency and to correctly select the inhibiting chemicals. Despite its importance, wax deposit's composition prediction remains one of the missing pieces of nearly all commercialized wax deposition software (e.g., OLGA and LedaFlow). In our study, we solved this problem by developing a new wax deposition software (SP-Depo) to predict the deposit's solid phase CND in addition to thickness and solid wax fraction. In SP-Depo, a new thermodynamically-coupled wax deposition model has been used which is exclusively theorized for this study. For verification purposes, SP-Depo's simulation results were plotted against data from more than 12 flow-loop experiments. In all cases, SP-Depo's predictions were successfully matched with the experimental data. We also introduced a limiting prediction bound for solid phase ACN and showed that experimental data will lay within this bound. In addition, we used our newly developed software to elucidate the effect of shear stress on deposit's solid phase carbon number distribution (CND) and average carbon number (ACN). After comparing our simulation results to the experimental ACN data, it was found that short n-alkanes are more likely to be removed from the deposit due to their low yield stress as shear stress increases. On the contrary, in lower flow rates, experimental ACN data approached to the lower bound prediction. Moreover, in SP-Depo, SP-Wax thermodynamic simulation was incorporated with Panacharoensawad wax deposition model [10] to provide composition prediction of the deposit.

SP-Wax is our second software which is developed to predict various SLE characteristics of paraffin in binary and multicomponent systems. For the first time, a simplified CCN estimation method has been proposed via the use of SP-Wax thermodynamic tool without the need to fully solve the whole wax deposition equations. In SP-Wax, the SLE thermodynamic model from Coutinho and co-workers [14]–[21] and other literature [22]–[35] were simulated and verified by experimental data of five binary and seven multicomponent systems. In SP-Wax, a novel numerical technique has been invented to solve the convergence problem near WAT.

In both of our developed software, scientific modeling is coded through more than 17,000 lines of code in C++ and C# GUI (with more than 16,000 lines of code) has been used to make a user-friendly interface for technical and non-technical users. Performance was our top priority in our developed software. Therefore, we implemented OpenMp parallel programming technique to minimize the run-time. Moreover, in SP-Depo, fluid-flow transport equations are solved using various numerical methods (e.g., Dorman Prince-RKDP, Finite Difference Method-FDM, three-zone linear regression and Levenberg-Marquardt optimization algorithm).

Last but no least, we included three sensitivity analysis cases with varying operating conditions to make sure that SP-Depo works in different cases too. Even though we used experimental data from a lab-scale flow-loop for validation purposes, a hypothetical upscaled case was analyzed with one-hundred meter 5" pipe at subsea temperature of 4°C. SP-Depo successfully predicted different wax deposition characteristics without any problem. Nevertheless, reliable field data are required to further develop SP-Depo for multi-mile subsea pipelines.

NOMENCLATURE

Variables

a	Correction factor coefficient
C_p	Specific heat capacity, $\left[\frac{J}{^{\circ}K}\right]$
D	Diameter, [m]
D_{wo}	Molecular diffusivity of wax in oil, $\left[\frac{m^2}{s}\right]$
D_e	Effective diffusivity of wax in oil, $\left[\frac{m^2}{s}\right]$
C	Concentration, $\left[\frac{kg}{m^3}\right]$
CN	Carbon Number
F_w	Solid wax fraction, $\left[\frac{w}{w}\right]$
f	Friction factor, [-]
f	Fugacity, [psia]
f_{NA}^L	Ratio of n-alkane mass in liquid phase over total n-alkane mass in liquid and in solid phases, $\left[\frac{kg\ NA_L}{kg\ NA_{(S+L)}}\right]$
f_{NA}^S	Ratio of n-alkane mass in solid phase over total n-alkane mass in liquid and in solid phases, $\left[\frac{kg\ NA_S}{kg\ NA_{(S+L)}}\right]$
G_z	Graetz number, [-]
h	Heat transfer coefficient, $\left[\frac{W}{m^2 \cdot ^{\circ}K}\right]$
ΔH	Enthalpy, $\left[\frac{J}{mol}\right]$
J	Wax mass flux, $\left[\frac{kg}{m^2 s}\right]$
K	Equilibrium constant, [-]
k	Thermal conductivity, $\left[\frac{W}{m \cdot ^{\circ}K}\right]$
K^C	Equilibrium constant from previous iteration, [-]

k_l	Convective mass transfer coefficient, $\left[\frac{w}{m_K} \right]$
k_r	Precipitation rate in Lee model
k_α	Fitting parameter in wax crystal aspect ratio formula from Singh model, [-]
L	Length, [m]
\dot{m}	Mass flow rate, $\left[\frac{kg}{s} \right]$
\tilde{m}	Ratio of n-alkane mass in liquid phase over one-unit mass of oil, $\left[\frac{kg\ NA_{i,L}}{kg\ oil} \right]$
MSR_1, MSR_2	Fitting parameters from Panacharoensawad model
MW	Molecular weight, $\left[\frac{kg}{mole} \right]$
N	Number of carbon number components
NN	Total number of cases used to calculate the mean absolute relative error.
n_s	Solid mole fraction in n-alkane system (or [mole of solidified n-alkanes] / [total moles of all n-alkanes]), [-]
R	Pipe's radius, [m]
r_i	Effective pipe's radius, [m]
Sc	Schmidt number
S_f	Solidified weight fraction (from the thermodynamic model) $\left[\frac{w}{w} \right]$
SR_1, SR_2	Shear effect multiplier (Panacharoensawad model)
T	Temperature, $^{\circ}C$, $^{\circ}K$
t	time, [s], [hr]
T_c	Critical temperature, $^{\circ}K$
V	Volume, $[m^3]$
V	Velocity, $\left[\frac{m}{s} \right]$
V_z	Axial velocity, $\left[\frac{m}{s} \right]$
W_f	Mass of total n-alkanes in one-unit mass of oil, $\left[\frac{kg\ NA_{(S+L)}}{kg\ oil} \right]$
$x_{m,i}^S$	mole fraction of i th component in solid phase and in n-alkane system, $\left[\frac{mole\ NA_{i,S}}{mole\ NA_S} \right]$
$x_{m,i}^L$	mole fraction of i th component in liquid-phase and in n-alkane system, $\left[\frac{mole\ NA_{i,L}}{mole\ NA_L} \right]$

$x_{w,i}^L$	weight fraction of i^{th} component in liquid-phase and in n-alkane system, $\left[\frac{\text{kg NA}_{i,L}}{\text{kg NA}_L} \right]$
y	Sample parameter in relative error equation
z_i	Input mole composition of n-alkanes ($\sum z_i = 1$), $\left[\frac{\text{mole NA}_{i,(S+L)}}{\text{mole NA}_{(S+L)}} \right]$
z	Axial location, [m]
$\Delta_s^l C_{p_i}$	Difference between specific heat capacity of i^{th} component in liquid and in solid phase

Greek letters

α	Aspect ration of wax crystal, [-]
α	Thermal diffusivity, $\left[\frac{m^2}{s} \right]$
α	Correction factor, [-]
γ	Activity coefficient, [-]
ϵ	Relative error, [-]
ε	Eddy diffusivity
Λ	Major binary interaction energy parameter in Wilson equation, [-]
ρ	Density, $\left[\frac{\text{kg}}{\text{m}^3} \right]$
λ	Minor binary interaction energy parameter, $\left[\frac{\text{J}}{\text{mol}} \right]$
μ	Viscosity, [cp]
ν	Volume fraction for n-alkanes in total fluid, [-]
ξ	Volume fraction, [-]
Φ	Volume over one-mass of oil, $\left[\frac{\text{m}^3}{\text{kg oil}} \right]$
ϕ	Composition fraction, [-]
$\phi_i^{\circ L}$	Fugacity coefficient of i^{th} pure component in the liquid phase
γ_i^{comb}	Combinatorial contribution in liquid phase non-ideality
$\tau_{\max}, \tau_{\text{ini}}$	Maximum and initial shear stresses, [Pa]
τ_w	Wall shear stress, [Pa]
Ω	Heat resistance, $\left[\frac{\text{m}^\circ \text{K}}{\text{W}} \right]$

Subscripts

<i>b</i>	Bulk
<i>c</i>	Coolant
<i>dep</i>	Deposit
<i>exp</i>	Experimental
<i>i</i>	<i>i</i> th carbon number
<i>i</i>	Interface
<i>ii</i>	<i>ii</i> th cases used in the mean absolute relative error calculation.
<i>int</i>	Interface
<i>j</i>	<i>j</i> th carbon number
<i>k</i>	<i>k</i> th carbon number
<i>l</i>	Long
<i>m</i>	Mole
<i>MinC</i>	Minimum depositable carbon number
<i>N</i>	Last section or component
<i>NA</i>	Normal n-alkane
<i>s</i>	Short
<i>sol</i>	Solidified
<i>Sim</i>	Simulation
<i>w</i>	Weight
<i>VDW</i>	Van der Waals

Superscripts

<i>f</i>	Fusion
<i>L</i>	Liquid
<i>S</i>	Solid
<i>Sub</i>	Sublimation
<i>tot</i>	Total

tr Solid phase transition

vap Vaporization

BIBLIOGRAPHY

- [1] D. Stern, “The role of energy in economic growth,” *Ann. N. Y. Acad. Sci.*, 2011.
- [2] X. Zhao, Q. Shi, M. Gray, and C. Xu, “New vanadium compounds in venezuela heavy crude oil detected by positive-ion electrospray ionization fourier transform ion cyclotron resonance mass,” *Sci. Rep.*, 2014.
- [3] P. Singh, R. Venkatesan, H. S. Fogler, and N. Nagarajar, “Formation and aging of incipient thin film wax-oil gels,” *Am. Inst. Chem. Eng.*, vol. 46, no. 5, pp. 1059–1074, May 2000.
- [4] D. Jennings and K. Weispfennig, “Effect of shear on the performance of paraffin inhibitors: coldfinger investigation with Gulf of Mexico crude oils,” *Energy & fuels*, vol. 20, no. 6, pp. 2457–2464, 2006.
- [5] Y. Lu, Z. Huang, R. Hoffmann, L. Amundsen, and H. S. Fogler, “Counterintuitive effects of the oil flow rate on wax deposition,” *Energy & Fuels*, vol. 26, no. 7, pp. 4091–4097, 2012.
- [6] S. Zheng, F. Zhang, Z. Huang, and H. S. Fogler, “Effects of operating conditions on wax deposition carbon number distribution: Theory and experiment,” *Energy and Fuels*, vol. 27, no. 12, pp. 7379–7388, 2013.
- [7] Z. Huang, H. S. Lee, M. Senra, and H. Scott Fogler, “A fundamental model of wax deposition in subsea oil pipelines,” *Am. Inst. Chem. Eng.*, vol. 57, no. 11, pp. 2955–2964, Nov. 2011.
- [8] C. Labes-Carrier, H. Rønning, and J. Kolnes, “Wax deposition in North Sea gas condensate and oil systems: Comparison between operational experience and model prediction,” in *SPE Annual Technical Conference and Exhibition*, 2002.
- [9] E. Panacharoensawad, A. Rittirong, and C. Sarica, “A Self-Sufficient Wax Deposition Model for Horizontal Gas-Oil Slug Flow,” in *American Institute of Chemical Engineers (AIChE) Spring Meeting and Global Congress on Process Safety*, 2015.
- [10] E. Panacharoensawad, “Wax deposition under two-phase oil-water flowing conditions,” Ph.D. Dissertation, University of Tulsa, 2012.
- [11] R. Venkatesan, “The deposition and rheology of organic gels,” *Ph.D. Diss. Univ. Michigan*, 2004.
- [12] H. S. Lee, “Computational and Rheological Study of Wax Deposition and Gelation in Subsea Pipelines,” 2008.
- [13] A. Mehrotra and N. Bhat, “Modeling the effect of shear stress on deposition from ‘waxy’ mixtures under laminar flow with heat transfer,” *Energy & Fuels*, 2007.
- [14] J. A. P. Coutinho, B. Edmonds, T. Moorwood, R. Szczepanski, and X. Zhang, “Reliable Wax Predictions for Flow Assurance,” *Energy & Fuels*, vol. 20, no. 3, pp. 1081–1088,

May 2006.

- [15] J. Coutinho, C. Gonçalves, I. M. Marrucho, J. Pauly, and J. L. Daridon, “Paraffin crystallization in synthetic mixtures: Predictive local composition models revisited,” *Fluid Phase Equilib.*, vol. 233, no. 1, pp. 28–33, 2005.
- [16] J. Coutinho and E. H. Stenby, “Predictive Local Composition Models for Solid/Liquid Equilibrium in n-Alkane Systems: Wilson Equation for Multicomponent Systems,” *Ind. Eng. Chem. Res.*, vol. 35, no. 3, pp. 918–925, 1996.
- [17] J. Coutinho, S. Andersen, and E. Stenby, “Solid-liquid Equilibrium of N-alkanes Using the Chain Delta Lattice Parameter Model,” *Fluid Phase Equilib.*, vol. 117, no. 1–2, pp. 138–145, 1996.
- [18] J. Coutinho, K. Knudsen, and S. Andersen, “A local composition model for paraffinic solid solutions,” *Chem. Eng. Sci.*, vol. 51, no. 12, pp. 3273–3282, 1996.
- [19] J. Coutinho and J. Daridon, “Low-Pressure Modeling of Wax Formation in Crude Oils,” *Energy & Fuels*, vol. 15, no. 6, pp. 1454–1460, Nov. 2001.
- [20] J. A. P. Coutinho, “Predictive UNIQUAC: A New Model for the Description of Multiphase Solid–Liquid Equilibria in Complex Hydrocarbon Mixtures,” *Ind. Eng. Chem. Res.*, vol. 37, no. 12, pp. 4870–4875, Dec. 1998.
- [21] J. Coutinho, S. Andersen, and E. Stenby, “Evaluation of Activity Coefficient Models in Prediction of Alkane Solid-liquid Equilibria,” *Fluid Phase Equilib.*, vol. 103, no. 1, pp. 23–39, 1995.
- [22] R. Hutchings, “Molar volumes in the homologous series of normal alkanes at two temperatures,” *Fluid Phase Equilib.*, vol. 21, no. 1–2, pp. 165–170, 1985.
- [23] H. S. Elbro, A. Fredenslund, and P. Rasmussen, “A new simple equation for the prediction of solvent activities in polymer solutions,” *Macromolecules*, vol. 23, no. 21, pp. 4707–4714, Oct. 1990.
- [24] T. Daubert and R. Danner, “Physical and thermodynamic properties of pure compounds: data compilation,” *Hemisph. Publ. Corp.*, 1989.
- [25] A. Bondi, *Physical Properties of Molecular Crystals Liquids, and Glasses*. NY Wiley, 1968.
- [26] H. S. Elbro, A. Fredenslund, and P. Rasmussen, “Group Contribution Method for The Prediction of Liquid Densities as a Function of Temperature for Solvents, Oligomers, and Polymers,” *Ind. Eng. Chem. Res.*, vol. 30, no. 12, pp. 2576–2582, 1991.
- [27] K. Pedersen, P. Christensen, and J. Shaikh, “Phase behavior of petroleum reservoir fluids,” *CRC Press*, 2006.
- [28] P. J. Flory, “Fifteenth spiers memorial lecture. Thermodynamics of polymer solutions,” *Discuss. Faraday Soc.*, vol. 49, pp. 7–29, 1970.
- [29] F. Fleming, J. Daridon, L. Azevedo, J. P.-F. P. Equilibria, and U. 2017, “Direct Adjustment of Wax Thermodynamic Model Parameter to Micro Differential Scanning Calorimetry Thermograms,” *Fluid Phase Equilib.*, vol. 436, pp. 20–29, 2017.
- [30] H. Madsen, R. B.-J. of the C. Society, U. Faraday, and U. 1979, “Solubility of Octacosane and Hexatriacontane in Different N-alkane Solvents,” *J. Chem. Soc. Faraday Trans.*, vol.

- 75, pp. 1254–1258, 1979.
- [31] J. Yang, W. Wang, B. Shi, Q. Ma, P. Song, and J. Gong, “Prediction of wax precipitation with new modified regular solution model,” *Fluid Phase Equilib.*, vol. 423, pp. 128–37, 2016.
 - [32] D. L. Morgan and R. Kobayashi, “Extension of Pitzer CSP Models for Vapor Pressures and Heats of Vaporization to Long-chain Hydrocarbons,” *Fluid Phase Equilib.*, vol. 94, pp. 51–87, 1994.
 - [33] J. M. Prausnitz, R. N. Lichtenthaler, and E. G. de Azevedo, “Molecular thermodynamics of fluid-phase equilibria,” *Pearson Educ.*, 1998.
 - [34] J. J. Marano and G. D. Holder, “General Equation for Correlating the Thermophysical Properties of n-Paraffins, n-Olefins, and Other Homologous Series. 2. Asymptotic Behavior Correlations for PVT Properties,” *Ind. Eng. Chem. Res.*, vol. 36, no. 5, pp. 1895–1907, May 1997.
 - [35] M. G. Broadhurst, “An Analysis of The Solid Phase Behavior of The Normal Paraffins,” *J. Res. Natl. Bur. Stand. (1934)*, pp. 241–249, 1962.
 - [36] K. Pedersen and P. Christensen, “Flash and phase envelope calculations,” *Phase Behav. Pet. Reserv. Fluids, 1st ed.; CRC Press Taylor Fr. Gr.*, 2006.
 - [37] T. Zhu, J. Walker, and J. Liang, “Evaluation of wax deposition and its control during production of Alaska north slope oils,” *Scitech Connect*, 2008.
 - [38] A. Rittirong, “Paraffin Deposition Under Two-Phase Gas-oil Slug Flow in Horizontal Pipes,” *Ph.D. Diss. Univ. Tulsa*, 2014.
 - [39] T. Brown, V. Niesen, and D. Erickson, “Measurement and prediction of the kinetics of paraffin deposition,” in *SPE Annual Technical Conference and Exhibition*, 1993.
 - [40] E. Burger, T. Perkins, and J. Striegler, “Studies of wax deposition in the trans Alaska pipeline,” *J. Pet.*, 1981.
 - [41] P. Bern, V. Withers, and R. Cairns, “Wax deposition in crude oil pipelines,” in *European Offshore Technology Conference and Exhibition*, 1980.
 - [42] R. Venkatesan and H. Fogler, “Comments on analogies for correlated heat and mass transfer in turbulent flow,” *AIChE J.*, vol. 50, pp. 1623–1626, 2004.
 - [43] E. Panacharoensawad and C. Sarica, “Experimental Study of Single-Phase and Two-Phase Water-in-Crude-Oil Dispersed Flow Wax Deposition in a Mini Pilot-Scale Flow Loop,” *Energy & Fuels*, vol. 27, no. 9, pp. 5036–5053, 2013.
 - [44] A. Matzain, “Multiphase flow paraffin deposition modeling.,” Ph.D. Dissertation, University of Tulsa, 2002.
 - [45] M. Senra and E. Panacharoensawad, “Role of n-alkane polydispersity on the crystallization of n-alkanes from solution,” *Energy & Fuels*, vol. 22, no. 1, pp. 545–555, 2007.
 - [46] K. W. Won, “Thermodynamics for solid solution-liquid-vapor equilibria: wax phase formation from heavy hydrocarbon mixtures,” *Fluid Phase Equilib.*, vol. 30, pp. 265–279, 1986.

- [47] K. . Won, “Thermodynamic calculation of cloud point temperatures and wax phase compositions of refined hydrocarbon mixtures,” *Fluid Phase Equilib.*, vol. 53, pp. 377–396, 1989.
- [48] J. H. Hansen, A. Fredenslund, K. S. Pedersen, and H. P. Rønningse, “A thermodynamic model for predicting wax formation in crude oils,” *AIChE*, vol. 34, no. 12, pp. 1937–1942, Dec. 1988.
- [49] W. B. Pedersen, A. B. Hansen, E. Larsen, and A. B. Nielsen, “Wax precipitation from North Sea crude oils. 2. Solid phase content as function of temperature determined by pulsed NMR,” *Energy & Fuels*, vol. 5, no. 6, pp. 908–913, 1991.
- [50] V. Ruffier-Meray, F. Brucy, and E. Behar, “Multiphase transport of waxy crudes: influence of dissolved gases on the Wax Appearance Temperature,” *Proc. Multiph.*, pp. 553–564, 1997.
- [51] D. D. Erickson, V. G. Niesen, and T. S. Brown, “Thermodynamic measurement and prediction of paraffin precipitation in crude oil,” in *SPE Annual Technical Conference and Exhibition*, 1993.
- [52] H. Rønningse, B. . Sømme, and K. . Pedersen, “An improved thermodynamic model for wax precipitation,” *BHR Gr. Conf. Ser. Publ.*, vol. 24, pp. 149–170, 1997.
- [53] A. Hansen, E. Larsen, W. Pedersen, and A. Nielsen, “Wax precipitation from North Sea crude oils. 3. Precipitation and dissolution of wax studied by differential scanning calorimetry,” *Energy & Fuels*, vol. 5, no. 6, pp. 914–923, 1991.
- [54] C. Lira-Galeana, A. Firoozabadi, and J. M. Prausnitz, “Thermodynamics of wax precipitation in petroleum mixtures,” *AIChE J.*, vol. 42, no. 1, pp. 239–248, 1996.
- [55] H. Pan, A. Firoozabadi, and P. Fotland, “Pressure and composition effect on wax precipitation: experimental data and model results,” *SPE Prod. Facil.*, vol. 12, no. 4, pp. 250–258, 1997.
- [56] E. Ghanaei, F. Esmaeilzadeh, and J. F. Kaljahi, “A new predictive thermodynamic model in the wax formation phenomena at high pressure condition,” *Fluid Phase Equilib.*, vol. 254, no. 1, pp. 126–137, 2007.
- [57] H. Rackett, “Equation of state for saturated liquids,” *J. Chem. Eng. Data*, vol. 15, no. 4, pp. 514–517, 1970.
- [58] D. Nichita, L. Goual, and A. Firoozabadi, “Wax precipitation in gas condensate mixtures,” *SPE Prod. Facil.*, vol. 16, no. 4, pp. 250–259, 2001.
- [59] J. Coutinho, “A thermodynamic model for predicting wax formation in jet and diesel fuels,” *Energy & Fuels*, vol. 14, no. 3, pp. 625–631, 2000.
- [60] M. Vafaie-Sefti, S. Mousavi-Dehghani, and M. Bahar, “Modification of multisolid phase model for prediction of wax precipitation: a new and effective solution method,” *Fluid Phase Equilib.*, 2000.
- [61] F. Esmaeilzadeh, J. F. Kaljahi, and E. Ghanaei, “Investigation of different activity coefficient models in thermodynamic modeling of wax precipitation,” *Fluid Phase Equilib.*, vol. 248, no. 1, pp. 7–18, 2006.
- [62] H.-Y. Ji, B. Tohidi, A. Danesh, and A. C. Todd, “Wax phase equilibria: developing a

- thermodynamic model using a systematic approach," *Fluid Phase Equilib.*, vol. 216, no. 2, pp. 201–217, 2004.
- [63] A. Shahdi and E. Panacharoensawad, "SP-Wax: Solid–liquid equilibrium thermodynamic modeling software for paraffinic systems," *SoftwareX*, vol. 9, pp. 145–153, 2019.
 - [64] P. Singh, R. Venkatesan, H. S. Fogler, and N. R. Nagarajan, "Morphological evolution of thick wax deposits during aging," *AICHE J.*, vol. 47, no. 1, pp. 6–18, 2001.
 - [65] A. Rittirong, E. Panacharoensawad, and C. Sarica, "An Experimental Study of Paraffin Deposition under Two-Phase Gas-Oil Slug Flow in Horizontal Pipes," in *Offshore Technology Conference*, 2015.
 - [66] W. Hayduk and B. Minhas, "Correlations for prediction of molecular diffusivities in liquids," in *30th Canadian Chemical Engineering Conference*, 1982.
 - [67] E. Cussler, S. Hughes, W. Ward, and R. Aris, "Barrier membranes," *J. Memb. Sci.*, vol. 38, no. 2, pp. 161–174, 1988.
 - [68] J. Dormand and P. Prince, "A family of embedded Runge-Kutta formulae," *J. Comput. Appl. Math.*, vol. 6, no. 1, pp. 19–26, 1980.
 - [69] D. W. Marquardt, "An Algorithm for Least-Squares Estimation of Nonlinear Parameters," *J. Soc. Ind. Appl. Math.*, vol. 11, no. 2, pp. 431–441, Jun. 1963.
 - [70] A. Shahdi, M. Yermekova, and E. Panacharoensawad, "Wax Deposition Model Analysis," *Southwest. Pet. Short Course*, pp. 411–425, 2016.
 - [71] H. Hausen, "Darstellung des Wärmeüberganges in Rohren durch verallgemeinerte Potenzbeziehungen," *Z. VDI Beih. Verfahrenstechnik*, vol. 4, no. 91, 1943.
 - [72] E. N. Sieder and G. E. Tate, "Heat Transfer and Pressure Drop of Liquids in Tubes," *Ind. Eng. Chem.*, vol. 28, no. 12, pp. 1429–1435, Dec. 1936.
 - [73] J. Chickos, W. H.-J. of C. & Engineering, and U. 2004, "Vapor Pressures and Vaporization Enthalpies of the n-Alkanes from C₃₁ to C₃₈ at T = 298.15 K by Correlation Gas Chromatography," *ACS Publ.*, vol. 49, no. 1, pp. 77–85, 2004.
 - [74] E. Morawetz, "Enthalpies of vaporization of n-alkanes from C₁₂ to C₂₀," *J. Chem. Thermodyn.*, vol. 1, no. 2, pp. 139–144, Apr. 1994.
 - [75] E. Provost, V. Chevallier, M. Bouroukba, D. Petitjean, and M. Dirand, "Solubility of Some n -Alkanes (C₂₃ , C₂₅ , C₂₆ , C₂₈) in Heptane, Methylcyclohexane, and Toluene," *J. Chem. Eng. Data*, vol. 43, no. 5, pp. 745–749, 1998.
 - [76] C. Sarica and E. Panacharoensawad, "Review of paraffin deposition research under multiphase flow conditions," *Energy & Fuels*, vol. 26, no. 7, pp. 3968–3978, 2012.
 - [77] C. Dauphin, J. Daridon, J. Coutinho, p Baylere, and M. Potin-Gautier, "Wax content measurements in partially frozen paraffinic systems," *Fluid Phase Equilib.*, vol. 161, no. 1, pp. 135–151, 1991.
 - [78] A. Singh, E. Panacharoensawad, and C. Sarica, "A Mini Pilot-Scale Flow Loop Experimental Study of Turbulent Flow Wax Deposition by Using a Natural Gas Condensate," *Energy & Fuels*, vol. 31, no. 3, pp. 2457–2478, 2017.

